

Enabling Membrane Reactor Technology Using Polymeric Membranes for Efficient Energy and  
Chemical Production

by

Yixiao Li

B.E., Tianjin University, 2013

AN ABSTRACT OF A DISSERTATION

submitted in partial fulfillment of the requirements for the degree

DOCTOR OF PHILOSOPHY

Department of Chemical Engineering  
College of Engineering

KANSAS STATE UNIVERSITY  
Manhattan, Kansas

2018

## Abstract

Membrane reactor is a device that simultaneously carrying out reaction and membrane-based separation. The advantageous transport properties of the membranes can be employed to selectively remove undesired products or by-products from the reaction mixture, to break the thermodynamic barrier, and to selectively supply the reactant. In this work, membrane reactor technology has been exploited with robust H<sub>2</sub> selective polymeric membranes in the process of hydrogenation and dehydrogenation.

A state-of-the-art 3-phase catalytic membrane contactor is utilized in the processes of soybean hydrogenation and bio-oil hydro-deoxygenation, where the membrane functions as phase contactor, H<sub>2</sub> supplier, and catalytic support. Intrinsically skinned asymmetric Polyetherimide (PEI) membranes demonstrated predominant H<sub>2</sub> permeance and selectivity. By using the PEI membrane in the membrane contactor, soybean oil is partially hydrogenated efficiently at relatively mild reaction conditions compared with a conventional slurry reactor. In the hydroprocessing of bio-oil using the same system, the membrane successfully removed water, an undesired component from bio-oil by pervaporation.

The more industrially feasible membrane-assisted reactor is studied in the alkane dehydrogenation process. Viable polymeric materials and their stability in elevated temperatures and organic environment are examined. The blend polymeric material of Matrimid<sup>®</sup> 5218 and Polybenzimidazole (PBI) remained H<sub>2</sub> permeable and stable with the presence of hydrocarbons, and displayed consistent selectivity of H<sub>2</sub>/hydrocarbon, which indicated the feasibility of using the material to fabricate thermally stable membrane for separation.

The impact of membrane-assisted reactor is evaluated using finite parameter process simulation in the model reaction of the dehydrogenation of methylcyclohexane (MCH). By combining

tested catalyst performance, measured transport properties of the material and hypothetical membrane configuration, by using a membrane assisted packed-bed reactor, the thermodynamic barrier of the reaction is predicted to be broken by the removal of  $H_2$ . The overall dehydrogenation conversion can be increased by up to 20% beyond equilibrium.

The predicted results are justified by preliminary experimental validation using intrinsically skinned asymmetric Matrimid/PBI blend membrane. The conversions at varied temperatures partially exceeded equilibrium, indicating successful removal of  $H_2$  by the blend membrane as well as decent thermal stability of the membrane at elevated temperatures with the presence of hydrocarbons.

The successful outcome of membrane contactor and membrane-assisted reactor using robust polymeric membranes shows the effectiveness and efficiency of membrane reactors in varied application. The future work should be focusing on two direction, to further develop durable and efficient membranes with desired properties; and to improve the reactor system with better catalytic performance, more precise control in order to harvest preferable product and greater yield.

Enabling Membrane Reactor Technology Using Polymeric Membranes for Efficient Energy and  
Chemical Production

by

Yixiao Li

B.E., Tianjin University, 2013

A DISSERTATION

submitted in partial fulfillment of the requirements for the degree

DOCTOR OF PHILOSOPHY

Department of Chemical Engineering  
College of Engineering

KANSAS STATE UNIVERSITY  
Manhattan, Kansas

2018

Approved by:

Major Professor  
Mary E. Rezac

# Copyright

© Yixiao Li 2018.

## Abstract

Membrane reactor is a device that simultaneously carrying out reaction and membrane-based separation. The advantageous transport properties of the membranes can be employed to selectively remove undesired products or by-products from the reaction mixture, to break the thermodynamic barrier, and to selectively supply the reactant. In this work, membrane reactor technology has been exploited with robust H<sub>2</sub> selective polymeric membranes in the process of hydrogenation and dehydrogenation.

A state-of-the-art 3-phase catalytic membrane contactor is utilized in the processes of soybean hydrogenation and bio-oil hydro-deoxygenation, where the membrane functions as phase contactor, H<sub>2</sub> supplier, and catalytic support. Intrinsically skinned asymmetric Polyetherimide (PEI) membranes demonstrated predominant H<sub>2</sub> permeance and selectivity. By using the PEI membrane in the membrane contactor, soybean oil is partially hydrogenated efficiently at relatively mild reaction conditions compared with a conventional slurry reactor. In the hydroprocessing of bio-oil using the same system, the membrane successfully removed water, an undesired component from bio-oil by pervaporation.

The more industrially feasible membrane-assisted reactor is studied in the alkane dehydrogenation process. Viable polymeric materials and their stability in elevated temperatures and organic environment are examined. The blend polymeric material of Matrimid<sup>®</sup> 5218 and Polybenzimidazole (PBI) remained H<sub>2</sub> permeable and stable with the presence of hydrocarbons, and displayed consistent selectivity of H<sub>2</sub>/hydrocarbon, which indicated the feasibility of using the material to fabricate thermally stable membrane for separation.

The impact of membrane-assisted reactor is evaluated using finite parameter process simulation in the model reaction of the dehydrogenation of methylcyclohexane (MCH). By combining

tested catalyst performance, measured transport properties of the material and hypothetical membrane configuration, by using a membrane assisted packed-bed reactor, the thermodynamic barrier of the reaction is predicted to be broken by the removal of  $H_2$ . The overall dehydrogenation conversion can be increased by up to 20% beyond equilibrium.

The predicted results are justified by preliminary experimental validation using intrinsically skinned asymmetric Matrimid/PBI blend membrane. The conversions at varied temperatures partially exceeded equilibrium, indicating successful removal of  $H_2$  by the blend membrane as well as decent thermal stability of the membrane at elevated temperatures with the presence of hydrocarbons.

The successful outcome of membrane contactor and membrane-assisted reactor using robust polymeric membranes shows the effectiveness and efficiency of membrane reactors in varied application. The future work should be focusing on two direction, to further develop durable and efficient membranes with desired properties; and to improve the reactor system with better catalytic performance, more precise control in order to harvest preferable product and greater yield.

# Table of Contents

Table of Contents .....	viii
List of Figures .....	xiv
List of Tables .....	xviii
Acknowledgements .....	xix
Dedication .....	xx
Chapter 1 Introduction to Membrane Reactors .....	1
1.1 Types of Membrane Reactors .....	1
1.2 Transport Mechanism in Polymeric Membranes .....	4
Chapter 2 Background on Bio-oil Hydroprocessing in a Membrane Contactor .....	7
2.1 Bio-oil Hydroprocessing .....	7
2.2 Membrane Contactors .....	11
Chapter 3 Fabrication and Characterization of Asymmetric Polyetherimide Membranes .....	13
3.1 Introduction .....	13
3.1.1 Polyetherimide .....	13
3.1.2 Asymmetric Membranes and Phase Immersion .....	14
3.2 Experimental .....	15
3.2.1 Material .....	15
3.2.2 PEI Membrane Fabrication .....	15
3.2.3 Membrane Characterization .....	15
3.2.4 Catalyst Loading .....	16



3.3 Results and Discussion.....	17
Chapter 4 Soybean Hydrogenation and Bio-oil Hydroprocessing using 3-Phase Membrane	
Contactora.....	20
4.1 Soybean Hydrogenation .....	20
4.1.1 Introduction .....	20
4.1.2 Experimental.....	21
4.1.2.1 Material .....	21
4.1.2.2 Apparatus .....	21
4.1.2.3 Reaction Procedure .....	22
4.1.3 Results and Discussion .....	24
4.2 Preliminary Bio-oil Hydro-deoxygenation.....	27
4.2.1 Introduction .....	27
4.2.2 Experimental.....	28
4.2.2.1 Materials .....	28
4.2.2.2 Analytical.....	29
4.2.2.3 Apparatus .....	29
4.2.2.4 Reaction Procedure .....	29
4.2.3 Results and Discussion .....	30
4.2.3.1 Hydro-deoxygenation of Bio-oil.....	30
4.2.3.2 Effect on Water Removal .....	31

Chapter 5 Background on Alkane Dehydrogenation in a Membrane-assisted Reactor.....	33
5.1 Introduction .....	33
5.2 Research Objective.....	36
Chapter 6 Transport Properties and Thermal Stability of Matrimid/PBI Blend Materials .....	37
6.1 Introduction .....	37
6.1.1 Thermal Properties of Polymeric Materials .....	37
6.1.2 Effect of Temperature on Permeability of Polymeric Materials .....	38
6.1.3 Thermal Stability of Matrimid 5218, Polybenzimidazole (PBI) and Their Blend .....	40
6.2 Experimental .....	45
6.2.1 Materials .....	45
6.2.2 Apparatus.....	45
6.2.3 Fabrication of Dense Films .....	46
6.2.4 Permeability Measurement of the Dense Films.....	47
6.3 Results and Discussion.....	48
6.3.1 Physical Appearance .....	48
6.3.2 Transport Properties of 50/50 Films.....	49
6.3.3 Transport Properties of 90/10 Films.....	54
Chapter 7 Dehydrogenation of Methylcyclohexane in Membrane-Assisted Packed-Bed Reactor:	
Finite Parameter Process Simulation .....	59
7.1 Introduction .....	59
7.1.1 Alkane Dehydrogenation.....	59

7.1.2 Model Reaction .....	62
7.2 Thermodynamic Computation.....	64
7.2.1 Breaking the Thermodynamic Barrier.....	66
7.2.2.1 Dilution .....	66
7.2.2.2 Selective Removal of Product.....	67
7.2.3 Literature Review on Selective H <sub>2</sub> Removal in Methylcyclohexane Dehydrogenation .....	69
7.2.4 Ideal Impact of Selective H <sub>2</sub> Removal in Methylcyclohexane Dehydrogenation by Membrane.....	71
7.3 Finite Parameter Process Simulation.....	74
7.3.1 Hypothesis .....	74
7.3.2 Experimental.....	75
7.3.2.1 Materials .....	75
7.3.2.1.1 Hydrocarbons and Gas .....	75
7.3.2.1.2 Catalyst .....	75
7.3.2.2 Apparatus .....	75
7.2.2.3 Catalyst .....	77
7.2.3 Results and Discussion .....	78
7.2.3.1 Catalytic Performance.....	78
7.2.3.2 Predicted Membrane Performance.....	80

7.2.3.2.1 Pressure at 1 bar .....	84
7.2.3.2.2 Pressure at 2 bar .....	88
Chapter 8 Dehydrogenation of Methylcyclohexane in Membrane-Assisted Packed-Bed Reactor:	
Experimental Validation .....	94
8.1 Introduction .....	94
8.2 Experimental .....	97
8.2.1 Materials .....	97
8.2.1.1 Membrane Materials .....	97
8.2.2 Apparatus.....	97
8.2.3 Preparation of the Membrane .....	97
8.2.4 Characterization of Membrane .....	98
8.2.5 Reaction and Separation Procedure.....	98
8.3 Results and Discussion.....	100
8.3.1 Transport Properties of the Membrane.....	100
8.3.2 Effect of the Membrane on the Dehydrogenation of Methylcyclohexane .....	100
8.3.2.1 Mechanical Stability of the Membrane at Elevated Temperature .....	102
Chapter 9 Conclusion and Future Work .....	105
9.1 Conclusion.....	105
9.1.1 Hydrogenation in 3-Phase Membrane Contactor .....	105
9.1.2 Alkane Dehydrogenation.....	106
9.2 Future Work .....	109

References .....	113
Appendix A - Spin Coated PEI Membranes .....	121
Appendix B - Calibration Curve .....	123
Appendix C - GC Spectra of Typical Product Composition in the Dehydrogenation of Methylcyclohexane .....	124
Appendix D – Conversion Factors for Gas Permeance .....	125
Appendix E - Water Accumulation Rate during Bio-oil HDO Run .....	126

## List of Figures

Figure 1 Classification of Membrane Reactors .....	1
Figure 2 (a) Schematic of an Inert Membrane Reactor (b) Catalytic Membrane Reactor in Hydrogen Production .....	2
Figure 3 Schematic of Membrane-assisted Reactor.....	3
Figure 4 Different Types of Mechanisms of Gas Permeation .....	4
Figure 5 Detailed Schematic of Solution Diffusion Mechanism Over a Dense Film <sup>7</sup> .....	5
Figure 6 Primary Energy Production by Source since 2000 <sup>10</sup> .....	7
Figure 7 U.S. Renewable Energy Production and Consumption from 2007-2017 <sup>11</sup> .....	8
Figure 8 Ways of upgrade bio-oil to biofuels and chemicals <sup>20</sup> .....	10
Figure 9 Mechanism of the Gas Supply in a Membrane Contactor <sup>26</sup> .....	11
Figure 10 General Structure of Polyimides .....	13
Figure 11 Chemical Structure of Polyetherimide <sup>30</sup> .....	13
Figure 12 PEI Membrane Sputter Coated with Pd.....	17
Figure 13 Membranes used in Soybean Hydrogenation Runs. Each shape represents one particular membrane. Different colors represent different stages of the membrane. Blue: nascent; grey: sputter-coated with catalyst Pd; red: Reduced in H <sub>2</sub> after coated with catalyst. ....	18
Figure 14 Permeance and Selectivity of One Particular Membrane before Coated with Catalyst, after Sputter-coated with Pd and after Reduction with H <sub>2</sub> .....	18
Figure 15 Chemical Structure of a triglyceride, which consists of one glycerol backbone and three fatty acids .....	20
Figure 16 Schematic of Soybean Oil Hydrogenation in a 3-Phase Membrane Contactor <sup>38</sup> .....	22
Figure 17 Schematic of the Parr Reactor .....	22

Figure 18 Iodine Value of Soybean Oil after Dehydrogenation. Each shape represents each individual run. ....	24
Figure 19 PEI Membrane after 72 hours of Reaction Run .....	25
Figure 20 Schematic of the Membrane Reactor .....	28
Figure 21 Bio-oil HDO at 90°C .....	31
Figure 22 Water Removal by pervaporation via the PEI membrane .....	32
Figure 23 Concept of Product Selectively Removed by Membrane Separation .....	34
Figure 24 The Methylcyclohexane, Toluene and H <sub>2</sub> Cycle in the Novel Hydrogen Storage Project by Using Methylcyclohexane as Hydrogen Carrier <sup>102</sup> .....	35
Figure 25 Change of Yield, Selectivity and Conversion versus Temperature. Yield = Selectivity * Conversion. ....	36
Figure 26 Glass Transition Temperature .....	37
Figure 27 Schematic of Permeability, Diffusion Coefficient, Sorption Coefficient against Temperature .....	40
Figure 28 Where PBI and Matrimid Stand in the Upper Bound Plot <sup>60</sup> .....	41
Figure 29 a) Single Gas Permeabilities and b) Ideal selectivities for several industrially important separations of blended dense 50/50 PBI/Matrimid films <sup>50</sup> .....	43
Figure 30 Thermal Gravimetric Analysis of Matrimid Film, Matrimid/PBI Blend Films and PBI Film in a) N <sub>2</sub> , b) Air up to 600 °C <sup>50</sup> . Despite the mass loss in the high temperature region, all films performed similarly and until 300 °C. The retention of mass in the 100 °C to 300 °C region indicates its optimal utilization in the dehydrogenation application. ....	44
Figure 31 Detailed Setup in the Membrane Cell <sup>61</sup> .....	45
Figure 32 Schematic of Constant-Volume Variable-Pressure Gas Flux Measurement System...	46
Figure 33 Left: Sheet of Dense Film; Right: Dense Film Stamp.....	48

Figure 34 Permeabilities of Single Gases of 50/50 Matrimid/PBI Material.....	50
Figure 35 Permeabilities of Dehydrogenation Components of 50/50 Matrimid/PBI Material ....	51
Figure 36 Selectivities of Single Gases of 50/50 Matrimid/PBI Material .....	51
Figure 37 Selectivities of Dehydrogenation Components of 50/50 Matrimid/PBI material .....	52
Figure 38 Picture of a Cracked Film after Test at above 275°C .....	54
Figure 39 Permeabilities of Single Gases of 90/10 Matrimid/PBI Material.....	56
Figure 40 Permeabilities of Dehydrogenation Components of 90/10 Matrimid/PBI Material ....	57
Figure 41 Selectivities of Single Gases of 90/10 Matrimid/PBI Material .....	57
Figure 42 Selectivities of Dehydrogenation Components of 90/10 Matrimid/PBI material .....	58
Figure 43 Equilibrium Conversion of Alkane Dehydrogenation at Atmosphere Pressure <sup>44</sup> .....	60
Figure 44 Qualitative Profiles of Reactor Temperature-Conversion in Isobutene Dehydrogenation <sup>44</sup> .....	61
Figure 45 Schematic Diagram for the Implementation of the MTH Cycle in Mobile and Stationary Application <sup>74</sup> .....	64
Figure 46 Thermodynamics of Dehydrogenation of Methylcyclohexane .....	66
Figure 47 Dehydrogenation of n-Butane with Hydrocarbon: Diluent Ratio 0:1 to 10:1 under Various Temperatures .....	67
Figure 48 Schematic of Multi-Stage Membrane-Assisted PBRs.....	71
Figure 49 Increase of Conversion Comparing Equilibrium and Membrane Assisted PBR .....	72
Figure 50 Increase of Conversion in Multiple-stage Membrane-Assisted PBRs .....	73
Figure 51 Schematic of the Membrane-assisted Packed-bed Reactor System .....	75
Figure 52 Membrane-assisted Packed-bed Reactor System .....	76
Figure 53 Dehydrogenation of MCH in PBR .....	78
Figure 54 Picture of catalyst coking after reaction run at 400 °C.....	80



Figure 55 Temperature Range Selected.....	81
Figure 56 Impact of Utilizing Membrane-assisted Packed-bed Reactor Comparing to Conventional PBR at 1 bar .....	86
Figure 57 H <sub>2</sub> Removal Performance at 1 bar .....	87
Figure 58 Increase of Conversion in an Intuitive Illustration at 1 bar .....	88
Figure 59 Equilibrium Conversion of Dehydrogenation of MCH at 1 bar and 2 bar. ....	89
Figure 60 Impact of Utilizing Membrane-assisted Packed-bed Reactor Comparing to Conventional PBR at 2 bar .....	90
Figure 61 Increase of Conversion in an Intuitive Illustration at 2 bar .....	91
Figure 62 Comparison on the Impact of System Pressure .....	92
Figure 63 A Schematic of Intrinsically Skinned Asymmetric Polymeric Membrane. It Consists of a Porous Substructure and a Thin Dense Separation Layer. ....	94
Figure 64 SEM Images of Cross-section of 50/50 Matrimid/PBI Blend Membrane .....	95
Figure 65 Schematic of the Membrane-assisted Packed-bed Reactor .....	96
Figure 66 Effect of the Membrane in the Dehydrogenation of Methylcyclohexane by Selective Removal of Hydrogen.....	102
Figure 67 Schematic of a Composite Membrane.....	103

## List of Tables

Table 1 Comparison between bio-oil and crude oil <sup>17</sup> .....	9
Table 2 Permeance of Gases and Selectivity .....	19
Table 3 Chemical Structure of Matrimid and PBI.....	41
Table 4 Single Gas Permeabilities of Matrimid and Matrimid/PBI dense films at Room Temperature; Reference and Measured data.....	42
Table 5 Annual Consumption of Typical Chemicals Produced from Dehydrogenation .....	59
Table 6 Physical Properties of MCH and Toluene <sup>45</sup> .....	63
Table 7 Summary of Reaction Conditions.....	77
Table 8 Side Product at 350/400 °C.....	79
Table 9 Membrane Configuration.....	81
Table 10 Permeability of 90/10 Blend Material at 202 °C .....	83
Table 11 Membrane Separation Performance at 202 °C, $\Delta P=1.0$ bar .....	84
Table 12 Summary of System.....	99
Table 13 MCH Dehydrogenations with Membrane Assistance .....	101

## Acknowledgements

I would like to first acknowledge my advisors Dr. Rezac and Dr. Pfromm for their guidance and support as a graduate student. I truly appreciate the opportunity to have learned from their impeccable knowledge and broad vision; as well as their scrupulous attitude and endless passion. The research and learning experience in the Rezac-Pfromm research group is a priceless fortune for me in my path to further discover the world of science and engineering.

I would like to appreciate Dr. Wang, Dr. Schlup and Dr. Zolkiewska for serving on my committee.

I would also like to acknowledge former research group members, namely Dr. Schulte, Dr. Stanford, Dr. Wales, Dr. Young, Dr. Heidlage, Dr. Carson and Shuzhen Qiu. Thank you for your help with my research. I also enjoyed the time with you together outside the labs.

Special thanks to current and former staff members in the Department of Chemical Engineering: Karen Strathman, Danita Deters, Debi Wahl, Dave Threewit, Cynthia Brott, Karey DeBardeleben, Pat Nelson and Florence Sperman, as well as Department of Chemistry senior glassblower James Hodgson.

Finally, I would like to express my deepest gratitude and love to my parents, my wife and my son for their unconditional support.

This material is based upon work supported by U.S. Department of Agriculture and Phillips  
66.

## **Dedication**

*To the sacrifice, to the regrets, to the support, and to love.*

# Chapter 1 Introduction to Membrane Reactors

Membrane science and technology have been vastly applied in industrial processes. From the initial utilization in water desalination using reverse osmosis, to the potential of the integration of membrane (separation unit) with catalytic reactor. The latter, is generally a membrane reactor. A membrane reactor is a device for simultaneously carrying out a reaction and membrane-based separation in the same physical enclosure<sup>1</sup>. Novel applications of membrane reactors are being excessively exploited. The application of membrane reactors in various processes have been studied, such as hydrogen production, dehydrogenation, steam reforming of methane, and the water gas shift reaction. With respect to conventional reactors, a membrane reactor permits the improvement of the performances in terms of reaction conversion, products selectivity, etc<sup>2</sup>.

## 1.1 Types of Membrane Reactors

Generally, membrane reactors can be classified into two categories, catalytic membrane reactors and inert membrane reactors<sup>3</sup>. The following chart demonstrates the types of membrane reactors.

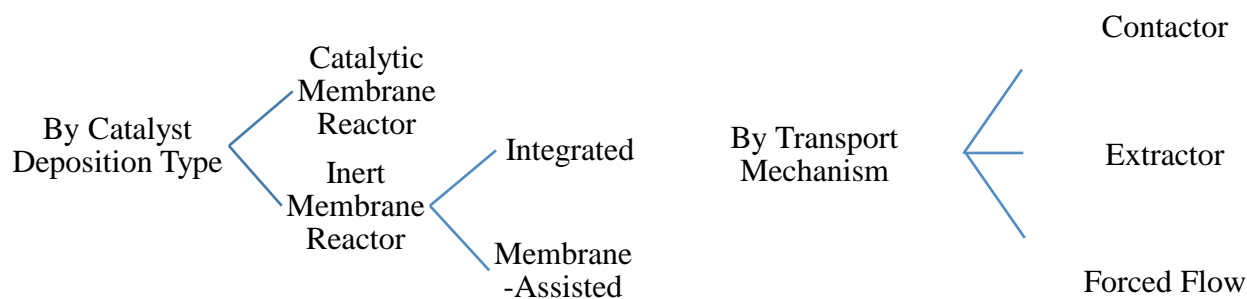


**Figure 1 Classification of Membrane Reactors**

In catalytic membrane reactors, the membrane itself is catalytic active; while in an inert membrane reactor, the membrane functions exclusively as a separation unit<sup>4</sup>.

Furthermore, membrane reactors can also be classified to contactor, extractor and forced-flow according to the transport mechanism.

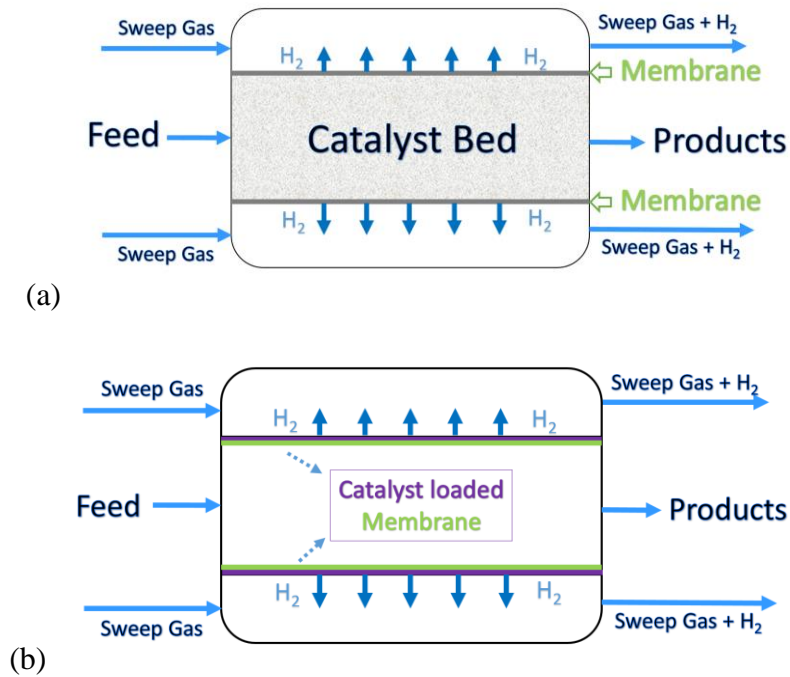


**Figure 2 (a) Schematic of an Inert Membrane Reactor (b) Catalytic Membrane Reactor in Hydrogen Production**

An extractor, as its name implies, selectively removes one or more components from the reactor. It integrates one of the most well-known features of the membrane. The purpose of selective removal is varied. For equilibrium-limited reactions, selective removal increases the conversion. For catalyst consideration, removal of particular reaction-rate inhibitor improves the catalytic activity<sup>4</sup>.

A contactor typically functions oppositely with the extractor. It provides an alternative way of supplying one of the reactants. It is widely utilized in multi-phase reactions where the feed rate is required to be controlled to avoid undesirable products while the reaction is restricted by mass transfer.

While catalytic membrane reactor is highly integrated, it requires the addition of entirely new equipment in existing industrial processes. The more practical adoption is membrane-assisted reactors.

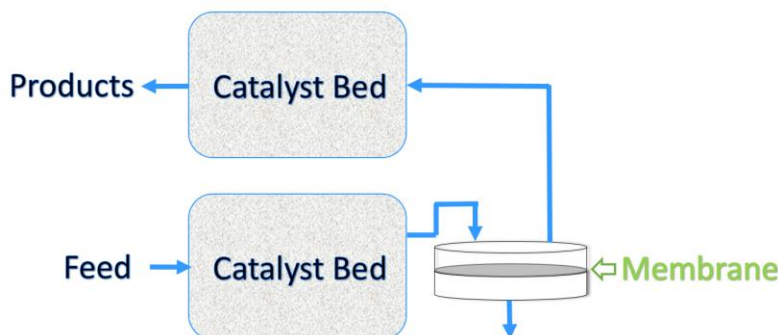


**Figure 3 Schematic of Membrane-assisted Reactor**

The concept is additional external membrane units to function as the separation units. In continuous reactor configurations, membrane units are placed between multiple packed-beds. In batch or semi-batch setups, the stream flow through the external membrane unit then circulates back to the batch reactor.

The material and morphology of the membranes in membrane reactors are very diversified. Common materials are metallic, ceramic, zeolite (inorganic) and polymeric (organic). In this study, polymeric materials are investigated<sup>4</sup>. Common appearances of the membranes are flat sheet, tubular and hollow fiber while their structure could be symmetric or asymmetric. The types of membranes will be discussed in the following context. In this study, major focus is on flat sheet asymmetric membranes prepared by phase inversion.

In conclusion, MR can be used either to increase the conversion (circumventing equilibrium limitations via Le Chatelier principle) or to increase the selectivity (through distributive feeding of a reactant through the membrane).

In this dissertation, we evaluated two membrane reactor systems in varied application of energy and chemical production. Chapter 2-4 introduced the hydrogenation of soybean oil and hydroprocessing of bio-oil using a 3-phase membrane contactor with a PEI membrane. Chapter 5-8 is focused on the dehydrogenation of alkanes in a membrane assisted packed-bed reactor using Matrimid/PBI blend membrane.

## 1.2 Transport Mechanism in Polymeric Membranes

As shown in the schematic below (Figure 4 and 5), there are different mechanisms in gas permeation. Most of current commercial gas separations are based on the dense polymer membrane shown above. It occurs by the solution diffusion mechanism<sup>5,6</sup>.

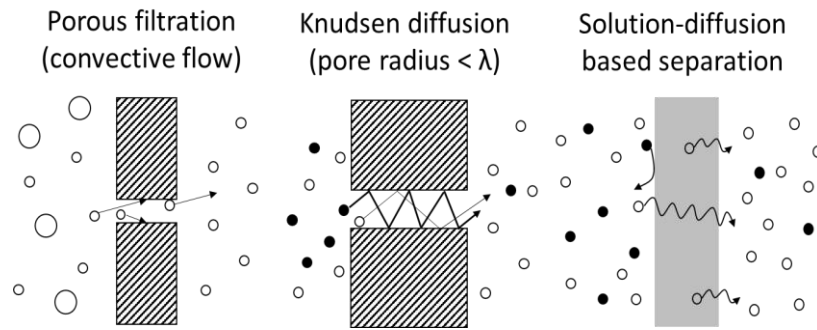


**Figure 4 Different Types of Mechanisms of Gas Permeation**

The driving forces of pressure, temperature, concentration and electrical potential cause the gradient in chemical potential, which can be described as,

$$J_i = -L_i \frac{d\mu_i}{dx} \quad (1)$$

where  $\frac{d\mu_i}{dx}$  is the chemical potential gradient of component  $i$  and  $L_i$  is a coefficient of proportionality linking the chemical potential driving force to flux.

In compressible gases, the molar volume changes with pressure, then the chemical potential gives

$$\mu_i = \mu_i^0 + RT \ln(\gamma_i n_i) + RT \ln \frac{p}{p_{i,sat}} \quad (2)$$



For the membrane phase, the chemical potential gives

$$\mu_i = \mu_i^0 + RT \ln(\gamma_i n_i) + v_i(p - p_{i_{sat}}) \quad (3)$$

Where  $n_i$  is the mole fraction of component  $i$ ,  $\gamma_i$  is the activity coefficient linking mole fraction with activity,  $p$  is the pressure, and  $v_i$  is the molar volumes of component  $i$ .  $\mu_i^0$  is the chemical potential at the reference pressure  $p_i^0$ , which is defined as the saturation vapor pressure of  $i$ ,  $p_{i_{sat}}$ .

R is gas constant. T is temperature.

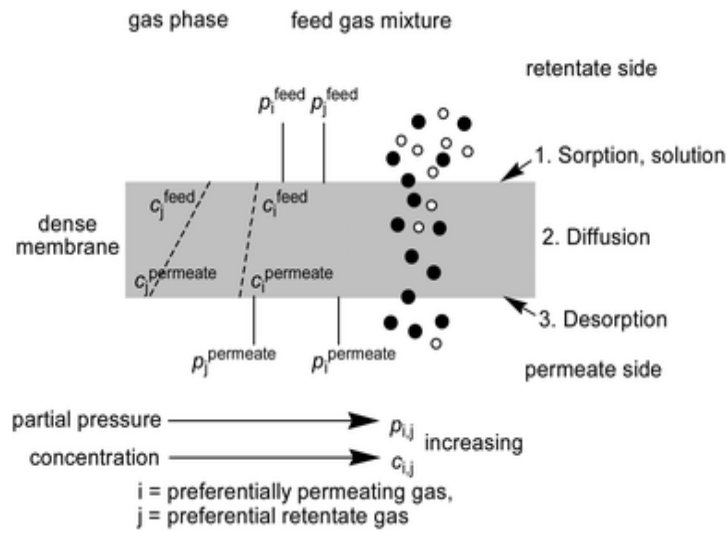


**Figure 5 Detailed Schematic of Solution Diffusion Mechanism Over a Dense Film<sup>7</sup>**

At the gas/membrane feed interface,

$$\mu_i^0 + RT \ln(\gamma_i n_i) + RT \ln \frac{p}{p_{i_{sat}}} = \mu_i^0 + RT \ln(\gamma_i n_i) + v_i(p - p_{i_{sat}}) \quad (4)$$

Then the concentration of component I at the feed interface of the membrane is simplified to

$$c_{i_{o(m)}} = m_i \rho_m \frac{\gamma_{i_0}^G p_{i_0}}{\gamma_{i_{o(m)}} p_{i_{sat}}} \quad (5)$$

Define gas phase sorption coefficient  $S_i^G$  as

$$S_i^G = \frac{\gamma_{i_0}^G m_i \rho_m}{\gamma_{i_{o(m)}} p_{i_{sat}}} \quad (6)$$

Then

$$c_{i_0(m)} = S_i^G \cdot p_{i_0} \quad (7)$$

Similarly, the concentration at the membrane/permeate interface is written as

$$c_{i_l(m)} = S_i^G \cdot p_{i_l} \quad (8)$$

Combined above two with Fick's first law, we have the governing equation expression

$$J_i = \frac{D_i S_i^G (p_{i_0} - p_{i_l})}{l} \quad (9)$$

where  $J_i$  is the mass flux and  $D_i$  is the diffusion coefficient. Or

$$j_i = \frac{D_i S_i (p_{i_0} - p_{i_l})}{l} \quad (10)$$

where  $j_i$  is the volume flux [ $cm^3(STP)$  of  $i$ ]/ $cm^2 \cdot s$ ,  $S_i$  is the sorption coefficient [ $cm^3(STP)$  of  $i/cm^3$  of polymer]·pressure.

The product of  $D_i S_i$  is called the permeability  $P_i$ , and is the ability of the membrane to permeate gas. The ability of a membrane to separate two gases,  $i$  and  $j$ , is the selectivity  $\alpha_{ij}$ , which is acquired from the ratio of their permeabilities,

$$\alpha_{ij} = \frac{P_i}{P_j} \quad (11)$$

The ratio of the diffusion coefficients  $D_i/D_j$  of two gas components is viewed as the mobility selectivity, reflecting the different sizes of the two molecules. The ratio of the sorption coefficients  $S_i/S_j$  reflects the relative condensabilities of the two gases, which is regarded as the sorption or solubility selectivity. In polymeric materials,  $D_i$  decreases with increasing molecular size while the magnitude of  $D_i/D_j$  depends significantly on whether the material is in glassy or rubbery state.  $S_i$  increases as molecular diameter increases. When the polymer is below glass transition temperature, diffusivity ( $D_i$ ) is usually dominant, permeability drops with increasing permeate size, and small molecules permeate preferentially<sup>8</sup>.

## Chapter 2 Background on Bio-oil Hydroprocessing in a Membrane

### Contactor

#### 2.1 Bio-oil Hydroprocessing

The heavy global dependence on fossil fuels causes many concerns, including potential future lack of resource availability due to fossil fuel depletion, environmental harm due to associated CO<sub>2</sub> emissions, and potential conflict due to limited geographic resource availability. Developing more environmental friendly alternative energy resource with equal or better quality is in demand.

Renewable energy has increased its proportion in the energy consumption in recent years (Figure 6). Among the renewable energies, biomass holds half of the share. Certainly, biomass derived products are very promising. Despite the complexity in composition and processing, biomass as a feed for bio-fuels is still the most reasonable source for the carbon-based fuels<sup>9</sup>.

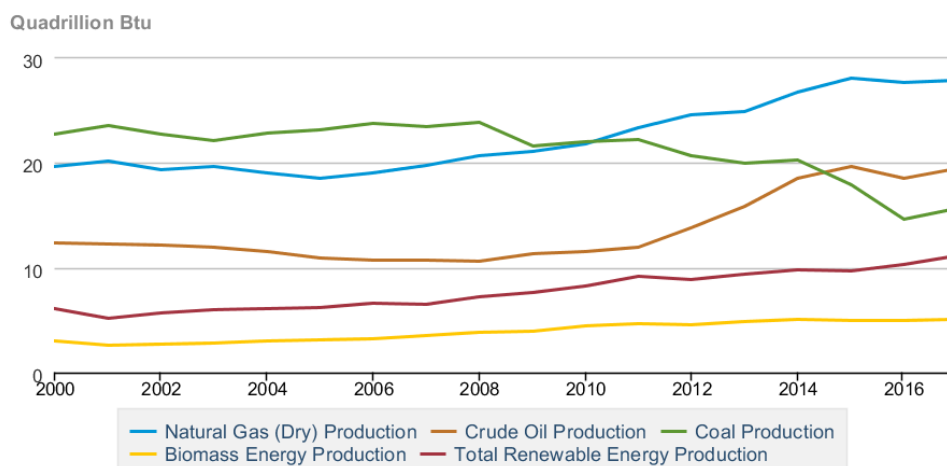
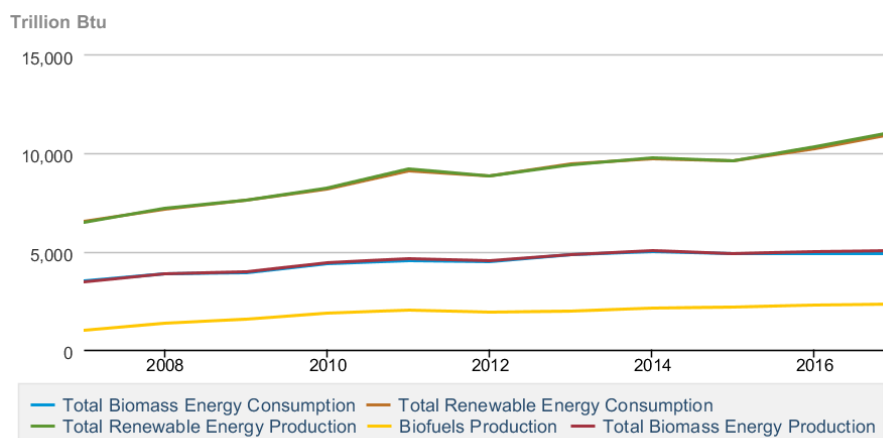


Figure 6 Primary Energy Production by Source since 2000<sup>10</sup>



**Figure 7 U.S. Renewable Energy Production and Consumption from 2007-2017<sup>11</sup>**

Different parts of the world have implemented the first generation bio-fuels, which includes bio-ethanol produced from sugar or starch and bio-diesel produced from vegetable oil or animal fat. However, the competition with food industry raises ethical questions since the limitation of food is still a serious issue in some parts of the world. From an economic consideration, the energy efficiency is rather lower than fossil fuels<sup>12</sup>. For these reasons, research has focused on fuels derived from non-edible biomass, such as agricultural waste and woods, referred as the second-generation bio-fuels. To achieve the production of transportation fuels from biomass, new biofuels technologies that are suitable for a variety of biomass feedstock must be developed which are cost-effective or comparable in price to fuels made through conventional petroleum processing<sup>13</sup>.

Several routes for biomass conversion exist, including syngas production (Fischer-Tropsch reaction) and bio-oil production from high pressure liquefaction, aka fast pyrolysis<sup>14,15</sup>. Fast pyrolysis is a thermal decomposition process in the absence of oxygen that occurs at moderate temperatures with a high heat transfer rate to the biomass particles and a short vapor residence time in the reaction zone<sup>16,17</sup>. In this way, the energy density is increased by a factor of 7-10.

Lignin-cellulosic bio-oil (fast pyrolysis oil) contains more than 300 compounds that are primarily derived from depolymerization and fragmentation of cellulose, hemicellulose and lignin<sup>15</sup>. As shown in Table 1, one of the crucial differences between bio-oil and crude oil is the oxygen element content and water content.

**Table 1 Comparison between bio-oil and crude oil<sup>17</sup>**

	Bio-oil	Crude Oil
Water (wt%)	15-30	0.1
pH	2.8-3.8	-
$\rho$ (kg/l)	1.05-1.25	0.86
$\mu_{50^{\circ}\text{C}}$ (cP)	40-100	180
HHV (MJ/kg)	16-19	44
C (wt%)	55-65	83-86
O (wt%)	28-40	<1
H (wt%)	5-7	11-14
S (wt%)	<0.05	<4
N (wt%)	<0.4	<1
Ash (wt%)	<0.2	0.1

Ketones, aldehydes, carboxylic acids and esters, aliphatic and aromatic alcohols, ethers have been detected in significant quantities. The presence of heteroatom oxygen is responsible for many deleterious properties such as high viscosity, thermal instability, corrosiveness (acidity), low HV and catalysts coking, which set much of the challenges in the direct utilization of fast pyrolysis as transportation fuels or compatibility to conventional fuels in refinery<sup>18,19</sup>.

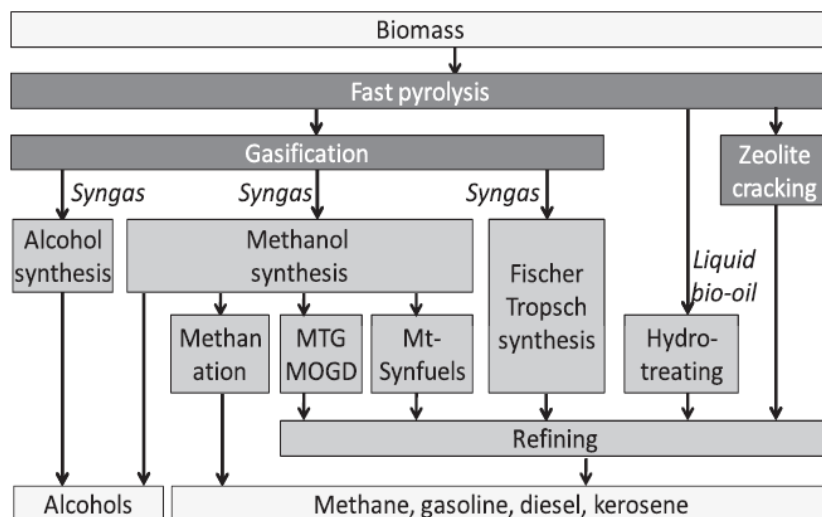


**Figure 8 Ways of upgrade bio-oil to biofuels and chemicals<sup>20</sup>**

As a result, an upgrading process for fast pyrolysis oil to reduce the oxygen content is crucial before further application, which usually is accomplished by two main routes: catalytic hydroprocessing and catalytic cracking. In spite of being regarded as a cheaper route, catalytic cracking still faces significant challenges such as high coking tendency (up to 40%) and low fuel quality<sup>17,18</sup>.

The other option is catalytic hydroprocessing<sup>21,22</sup>. Similar to refinery hydrotreating aiming to eliminate sulphur (hydrodesulphurization), nitrogen (hydrodenitrogenation) and metals (hydrodemetallation) from the stream, bio-oil hydrotreating is particularly concerned with removing oxygen (hydrodeoxygenation; HDO) from bio-oil. Oxygen can be removed as water, carbon dioxide and/or carbon monoxide through a combination of decarbonylation, decarboxylation, HDO. Jones et al.<sup>23</sup> reported that decarboxylation occurs at the expense of lowered carbon yield (high H/C). Thus, HDO by expelling water is a more preferred idea. In this process, the fast pyrolysis oil is treated with hydrogen in the presence of a heterogeneous catalyst with the aim to hydro(deoxy)genate to a product with improved properties<sup>21,24</sup>.

## 2.2 Membrane Contactors

In a liquid/gas reaction, in order to form contact between the two phases, either gas is dispersed in liquid, or liquid is dispersed in gas. The addition of another phase, a solid catalyst only complicates the situation. For example, in a conventional slurry reactor, the gas must be dissolved to liquid phase before reaching the active sites of the catalyst. If the solubility of gas in particular liquid is low, then the mass transfer resistance becomes significant. When the reaction becomes mass transfer limited, the tendency of side reaction increases, as well as the energy consumption. Membrane contactor is a type of membrane reactor that is typically utilized in multi-phase reactions, such as a liquid/gas reaction. The membranes function differently from those for general separation purposes. In a membrane contactor, instead of a separation unit, the membrane acts as a support to provide a contact area between the phases<sup>25</sup>.

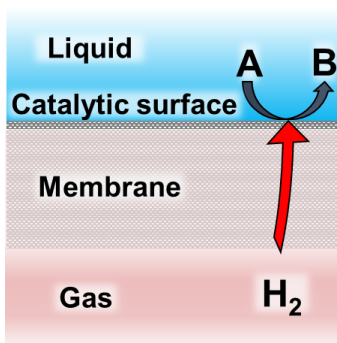


**Figure 9 Mechanism of the Gas Supply in a Membrane Contactor<sup>26</sup>.**

One of the advantages is overcoming the mass transfer limitation in multi-phase reactions. Instead of dissolving gas into liquid, the supply mechanism for gas is to permeate from one side of the membrane, through to the other, where catalyst is being supported on. In this fashion, the surface of the membrane serves as the contact area for liquid and gas phase. The driving force for

gas to reach the catalytic sites is the partial pressure difference between the two sides of the membrane. As a result, the mass transfer limitation is overcome.



## Chapter 3 Fabrication and Characterization of Asymmetric Polyetherimide Membranes

### 3.1 Introduction

#### 3.1.1 Polyetherimide

Polyimides have been in mass production since 1955. With their high heat-resistance, polyimides enjoy diverse applications in applications demanding rugged organic materials, e.g. high temperature fuel cells, displays, and various military roles.

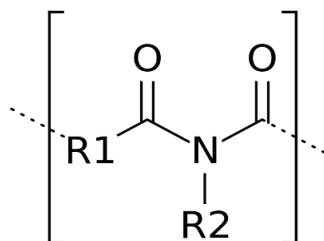


**Figure 10 General Structure of Polyimides**

Polyetherimide (PEI) is one of the widely used polyimides<sup>27,28</sup>. PEI is an amorphous, amber-to-transparent high performance engineering thermoplastic<sup>29</sup>. It is widely used in broad fields as resin because of the outstanding characteristics include high strength and rigidity at elevated temperatures, long term heat resistance, dimensional stability and good electrical properties<sup>27</sup>.

PEI has the molecular formula of  $(C_{37}H_{24}O_6N_2)_n$ , and its structure is shown in Figure 11.

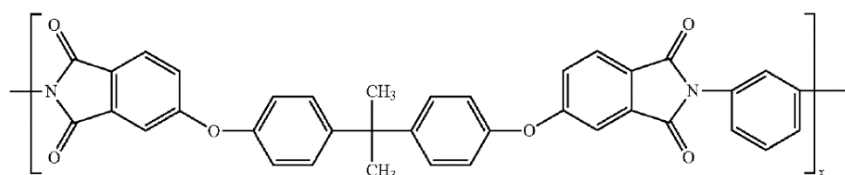


**Figure 11 Chemical Structure of Polyetherimide<sup>30</sup>**

### 3.1.2 Asymmetric Membranes and Phase Immersion

A membrane is a discrete, thin interface that moderates the permeation of chemical species in contact with it<sup>31</sup>. Polymer-based membranes are arguably the cheapest and easiest processed of the materials comparing to metallic, zeolites, etc. Polymers possess the greatest flexibility in their synthetic compositions and the available organic chemistries for component pre- and post-fabrication modification. Other advantages in most applications are a good ability to cope with large pressure drops and low cost.

Symmetric membranes has consistent structure over the cross-section of the membrane. It is either dense or porous. The permeation rate is determined by the thickness of the entire membrane. To facilitate permeation efficiency, an asymmetric membrane consisting a thin dense layer and a porous substructure is used<sup>32</sup>. The thin dense layer determines the permeation rate and separation characteristic, while the porous substructure provides mechanical stability. There are two types of asymmetric membranes, intrinsically skinned and composite. An intrinsically skinned asymmetric membrane uses same material for the dense skin and the porous support, and is usually fabricated to an entirety by phase inversion technique. A composite asymmetric membrane consists of different materials for the skin layer and the support with the separation layer deposited onto the substructure.

For intrinsically-skinned asymmetric polymeric membranes used in this study, the fabrication method adopted is the non-solvent induced phase separation (NIPS), which is one of the phase inversion methods. Following are the steps to prepare an asymmetric membrane using the NIPS method<sup>33</sup>.

1. One or more polymers are dissolved in appropriate solvents to form a homogeneous solution.
2. The solution is cast into a film shape of 100-500  $\mu\text{m}$  thickness.

3. Immersion in a non-solvent coagulation bath leads to precipitation.
4. The resultant membrane may undergo treatments such as annealing or drying.

## **3.2 Experimental**

### **3.2.1 Material**

P-Xylene, Dichloromethane, Acetic Acid, 1,1,2,2-Tetrachloroethane, Acetone, Polyetherimide (PEI) Powder

### **3.2.2 PEI Membrane Fabrication**

The intrinsically asymmetric PEI membrane is prepared by phase immersion method<sup>34</sup>. Dissolve 54 g of PEI powder into a mixture of 70 ml of p-Xylene, 140 ml of Dichloromethane, 23 ml of acetic acid and 10 ml of 1,1,2,2-tetrachloroethane. Fully stir the solution for 48 hours. Stop stirring 30 minutes before casting. Cast the membrane on an 11x8.5 inch glass plate with a Gardner casting knife. The wet gap thickness is 350  $\mu\text{m}$ . Fully immerse the nascent membrane into an acetone bath along with the glass plate after ~5 seconds of free convection evaporation in air. The membrane sheet will detach from the glass plate in several minutes. Take the membrane sheet out after 30 minutes and hang dry in air. Cut the membrane into circular stamps with the size of 13.8  $\text{cm}^2$ .

### **3.2.3 Membrane Characterization**

The transport properties of the membranes are measured by the constant-pressure-variable-volume flux measurement system<sup>35</sup>.

H<sub>2</sub> and N<sub>2</sub> permeance are measured at room temperature (23-32°C). The pressure difference between permeate and retentate side was 50 psig.

The permeance is acquired by the following equation

$$\frac{P}{\ell} = \frac{\Delta V}{\Delta p \times A_{\text{membrane}} \times \Delta t} \times 10^6 \quad (12)$$

where:  $\frac{P}{\ell} \equiv$  Permeance [GPU]

$\Delta V \equiv$  Ideal gas volume that permeates the membrane [ $\text{cm}^3$  (STP)]

$\Delta p \equiv$  Pressure difference across the membrane [cmHg]

$A_{\text{membrane}} \equiv$  Area of the membrane available for flux [ $\text{cm}^2$ ]

$\Delta t \equiv$  Time interval of flux [s]

The ideal  $\text{H}_2/\text{N}_2$  selectivity of the membrane is determined by the following equation:

$$\alpha_{\text{H}_2/\text{N}_2} = \frac{\left(\frac{P}{\ell}\right)_{\text{H}_2}}{\left(\frac{P}{\ell}\right)_{\text{N}_2}} \quad (13)$$

### 3.2.4 Catalyst Loading

Noble metal platinum or palladium are selected as catalyst for the hydrogenation reaction<sup>36</sup>.

Various approaches on catalyst loading have been investigated. Numbers of membranes are sputter coated with Pd by using a DESK II magnetron sputter coater (9 seconds at 45 milliamps).

Others are spin coated by using a Best Tools SC100 spin coater (Appendix A). All membranes are tested for their  $\text{H}_2$  and  $\text{N}_2$  fluxes again in the aforementioned flux measurement system.

Typically, the fluxes decrease by at least half. Changes in  $\text{H}_2/\text{N}_2$  selectivity show irregularity as the uncoated membrane might have defects. By sputter coating a layer of dense Pt metal over the defects, an increase in  $\text{H}_2/\text{N}_2$  selectivity should be observed.

### 3.3 Results and Discussion

The appearance of the membrane is shown on Figure 12. For an uncoated membrane, the surface of the membrane is smooth and reflective. The back side of the membrane is matte. Both sides are in the color of creamy white. After coated with Pd, the membrane is still smooth and reflective while the color turned to grey.

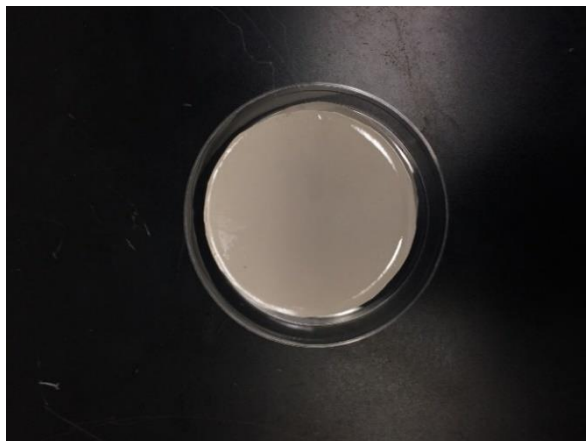


**Figure 12 PEI Membrane Sputter Coated with Pd**

The  $H_2$  permance of the casted membranes before catalyst deposition varies from 10-170 GPU. The ideal selectivity of  $H_2/N_2$  varies to as high as 192, which is the theoretical ideal selectivity of the PEI material. The rule of thumb for a “decent” membrane has a  $H_2$  permance of at least 80 GPU and ideal  $H_2/N_2$  selectivity of at least 50. Such membranes are determined to be suitable for further applications.

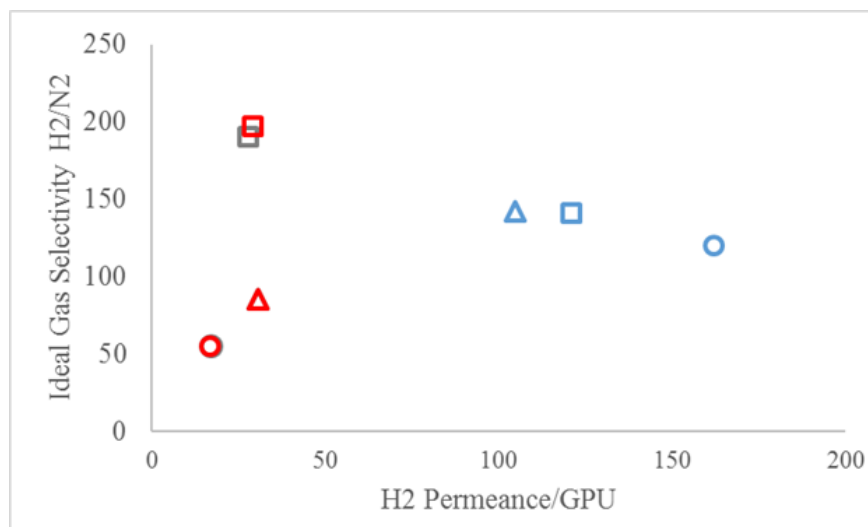


**Figure 13 Membranes used in Soybean Hydrogenation Runs. Each shape represents one particular membrane. Different colors represent different stages of the membrane. Blue: nascent; grey: sputter-coated with catalyst Pd; red: Reduced in H<sub>2</sub> after coated with catalyst.**

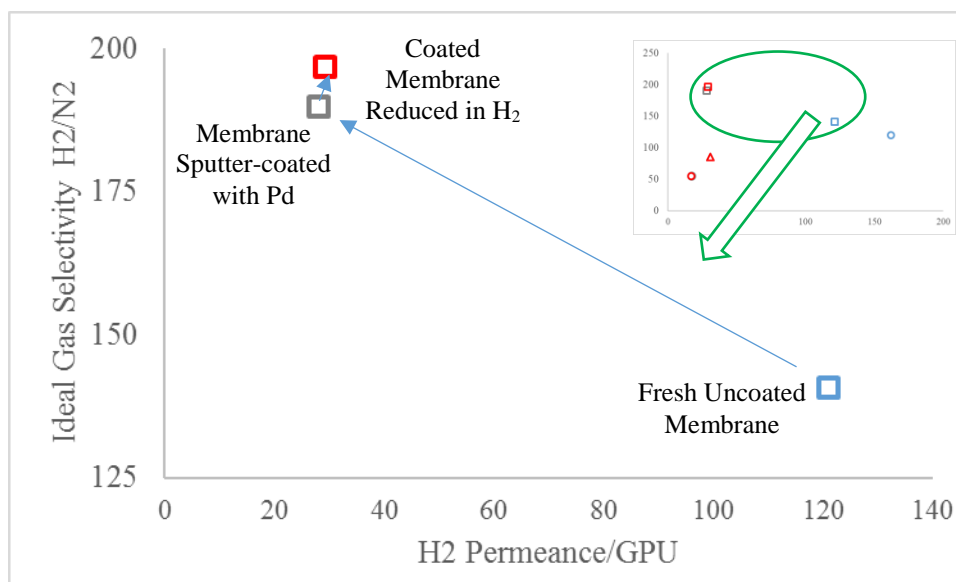


**Figure 14 Permeance and Selectivity of One Particular Membrane before Coated with Catalyst, after Sputter-coated with Pd and after Reduction with H<sub>2</sub>**

Figure 13 shows some of the membranes that fall into the above criteria. These membranes are utilized in the hydrogenation processes in the next chapter.

Taken one particular membrane from Figure 14, the casted and cut membrane stamp has a  $H_2$  permeance of 120 and ideal  $H_2/N_2$  selectivity of 141. After Pd catalyst deposition,  $H_2$  permeance dropped drastically to 28. Obviously, the dense metal layer slows down the permeation of  $H_2$  through the membrane. On the other hand, the  $H_2/N_2$  improved from 141 to 190. The reason behind this is clear. Due to human error, the dense layer of the casted membrane is likely to have defects which undermine the ideal selectivity. However, by sputter coating Pd metal on the surface of the membrane, such defects are filled which results in an increase in the ideal selectivity of  $H_2/N_2$ . After reduction, both permeance and selectivity slightly improved since the metal oxide is reduced to metal resulting in a more permeable metal layer.

**Table 2 Permeance of Gases and Selectivity**

	Nascent PEI Membrane	PEI Membrane Coated with Pd
$P_{H_2}$ (GPU)	120	28
$P_{N_2}$ (GPU)	0.85	0.15
$S_{H_2/N_2}$	141	190

GPU: Gas permeation unit.  $GPU = 10^{-6} cm^3(STP)cm^{-2}s^{-1}cmHg^{-1}$

## Chapter 4 Soybean Hydrogenation and Bio-oil Hydroprocessing

### using 3-Phase Membrane Contactor

#### 4.1 Soybean Hydrogenation

##### 4.1.1 Introduction

Comparing to Bio-oil, which consists of more than 300 components, vegetable oils have much simpler and clearly identified compositions. They are a mixture of triglycerides.

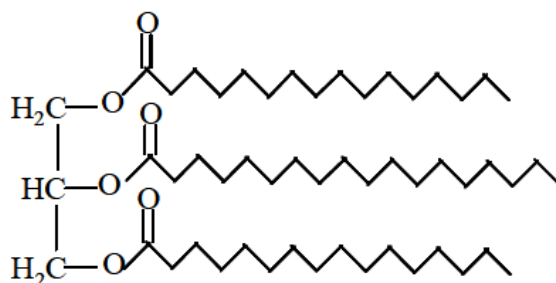


**Figure 15 Chemical Structure of a triglyceride, which consists of one glycerol backbone and three fatty acids**

Thus, before the investigation of bio-oil hydrogenation, soybean oil was studied in the 3-phase membrane contactor to validate the efficacy of the membrane reactor (contactor).

The hydrogenation of soybean oil is industrially utilized to improve oxidative stability in order to extend the shelf life of the product. After hydrogenation, the solid content is increased that makes the product more suitable for the production of margarines and shortenings. In addition, during the partial hydrogenation of soybean oil, the amount of  $\text{H}_2$  participating in the reaction determines the content of trans-fatty acids (TFA), which has become a concern for health. Therefore, minimizing the production of trans-fatty acids also serves as a goal of the hydrogenation process.



In conventional industrial processes, the reaction is carried out in 3-phase (catalyst-oil-hydrogen) slurry reactors. In this setup, the reaction becomes mass-transfer limited due to the low solubility of hydrogen in soybean oil. A typical industrial process requires a pressure of ~70 psi. The starvation of hydrogen at the catalyst surface leads to the formation of TFA.

The membrane contactor, however, completely changes the H<sub>2</sub> supplying mechanism to the active catalytic sites (Figure 9).

Iodine Value is the mass of iodine consumed by 100 grams of oil. It is used to determine the saturation level of the oil. More unsaturated double bonds in oil require more iodine compounds to react with, indicating a low saturation level. It is calculated by the following equation<sup>37</sup>

$$IV = (\%C16:1 \times 0.9502) + (\%C18:1 \times 0.8598) + (\%18:2 \times 1.7315) + (\%C18:3 \times 2.6152) \quad (14)$$

Typical IV of soybean oil is about 130-135.

## **4.1.2 Experimental**

### **4.1.2.1 Material**

Regular table soybean oil is obtained from Walmart. Ultra high purity H<sub>2</sub> and N<sub>2</sub> are obtained from Matheson Tri-gas.

### **4.1.2.2 Apparatus**

The equipment used in the reactor system includes autoclave with stirrer from Parr; 47 mm filter holder (membrane chamber) from Milipore; thermocouples and temperature controller from Omega; Pressure gauges from Omega, GJ series cavity pump from Micropump. All tubing and fittings are 316 stainless parts from Swagelok. All the tubing are wrapped with heating tape from BriskHeat Corp for insulation.

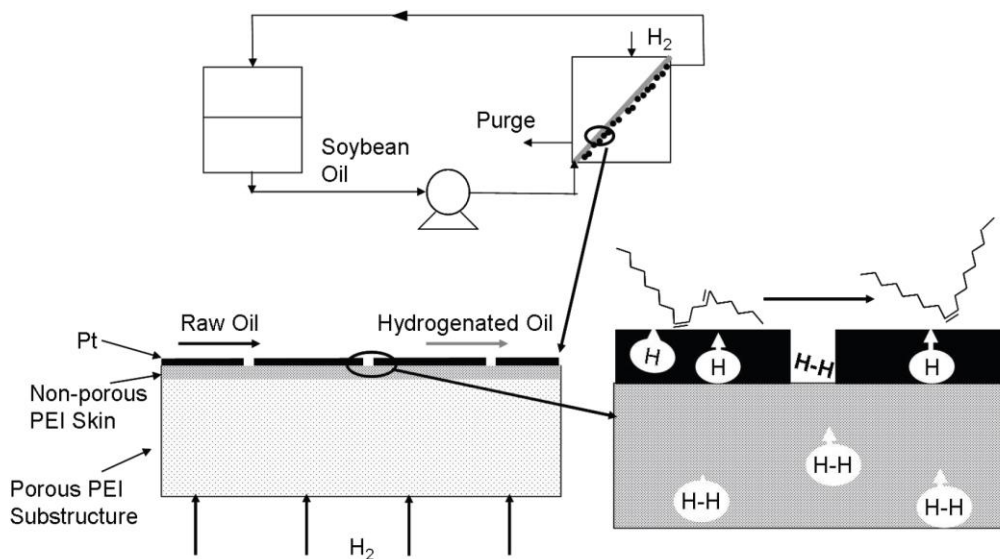


**Figure 16 Schematic of Soybean Oil Hydrogenation in a 3-Phase Membrane Contactor<sup>38</sup>**

Figure 16 demonstrates the setup of the reactor system. The oil will circulate in the system while the reaction takes place on the surface of the membrane on which the catalyst is deposited on. The sample port is below the Parr reactor using a 3-way valve. The sample is then analyzed by FID (Flame Ionization Detector) equipped Agilent 6890 Gas Chromatography.

#### 4.1.2.3 Reaction Procedure

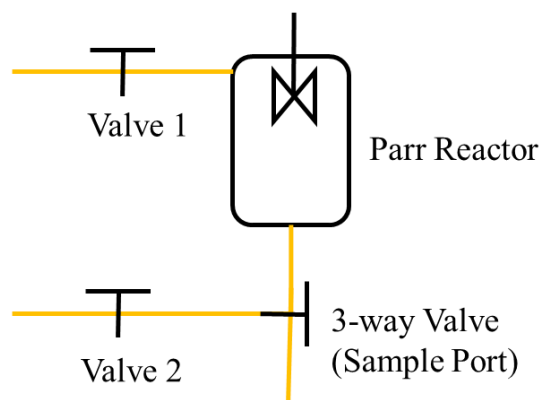


**Figure 17 Schematic of the Parr Reactor**

After the membrane (using the fabrication, characterization and catalyst deposit methods in Chapter 3) is deemed to be viable for the experiment, it is placed in the constant-pressure

variable-volume flux measurement system for catalyst reduction. The catalyst is reduced for an hour under 50 psig  $H_2$ . After reduction, the membrane is tested for  $H_2$  and  $N_2$  permeance in the same system. The membrane is then transferred to the membrane cell in the reactor system.

Purge the system with  $N_2$  to extrude the air out of the system.

The lid of the Parr Reactor is opened to fill with soybean oil. The lid then is closed. Turn on the heater and stirrer to heat the oil in the Parr reactor. After desired temperature ( $70^\circ C$ ) is reached, valve 2 in the above schematic is opened to allow the oil flow to the pump. Turn on pump to circulate the oil through the system. After the temperatures monitored at the membrane cell and the reactor become consistent, which indicates the oil is uniformly heated and the system circulates well, 50 psi  $H_2$  is introduced from the retentate side of the membrane.

Samples are taken at 0 hr (right after  $H_2$  is supplied), 12 hr, 24 hr and 48 hr by a glass vial.

### 4.1.3 Results and Discussion

In this part of the study, the emphasis is on the efficacy of the membrane contactor, especially on the functionality of the membrane as H<sub>2</sub> supplying path, catalyst support and phase barrier.

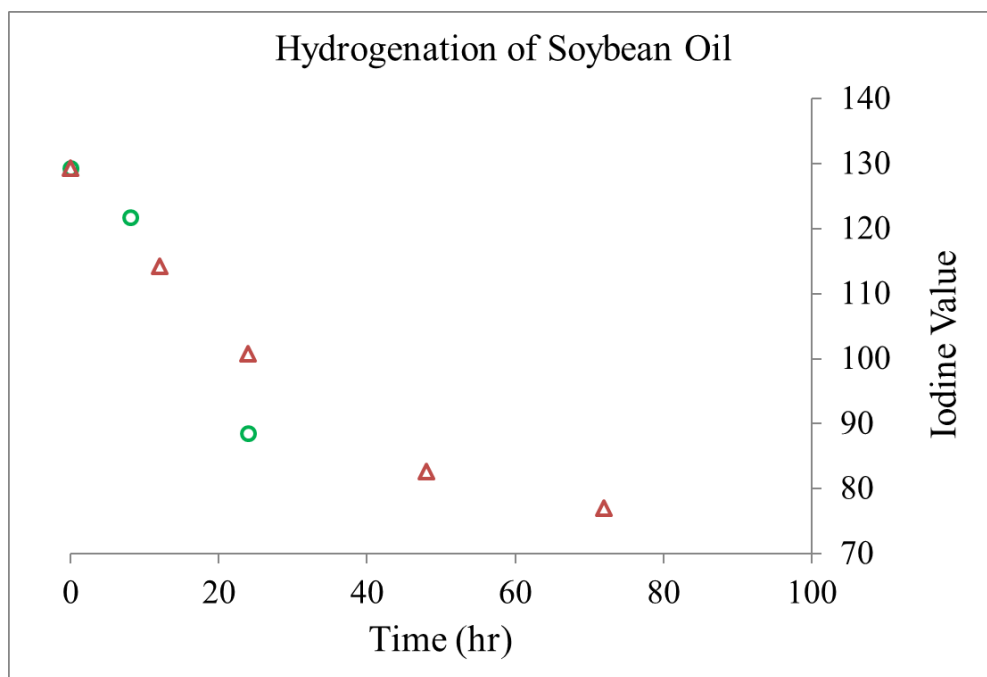


**Figure 18 Iodine Value of Soybean Oil after Dehydrogenation. Each shape represents each individual run.**

The latter one is confirmed as no oil was detected on the hydrogen feed side of the membrane.

Videlicet, the PEI membranes remained stable being covered by soybean oil at 70°C. To validate the membrane's performance on providing H<sub>2</sub> feed and support for Pd catalyst, the degree of hydrogenation is showed in Figure 18.

Generally, IV of the soybean oil declined in various runs against time. In both runs shown in Figure 18, Iodine Value starts at 131, the IV of soybean oil. Reaction rates varied between two runs; nevertheless, the oil is being partially hydrogenated in continuance. For one run, the hydrogenation went underway for 72 hours as the IV dropped to 74. This indicates that,  $H_2$  is constantly permeating through the membrane and arriving at the active catalytic sites on the surface of the membrane. In addition, the Pd catalyst remained active throughout the entire experiment.



**Figure 19 PEI Membrane after 72 hours of Reaction Run**

The above evidence proved the PEI membrane has accomplished its tasks in the contactor. Nonetheless, to completely evaluate the membrane and the reactor, other parameters are to be investigated. As mentioned in previous context, the selectivity of catalyst is crucial in soybean oil hydrogenation, since undesirable side product trans-fatty acids forms in  $H_2$  starvation. Thus,  $H_2$  feed rate control, catalyst selectivity and deactivation should be studied to minimize the formation of undesirable products. These kinetics study is reported somewhere else<sup>39</sup>. Moreover, the ability of the catalyst to adhere on the surface of the membrane is another challenge. As seen in Figure 19, a portion of the membrane surface became visible in spite of the deposited layer of Pd after 72 hours of reaction run, which indicates the coated Pd has detached from the membrane

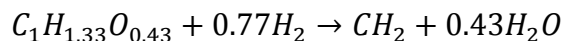
and has migrated to the bulk oil phase. This indefinitely will compromise the catalyst selectivity since  $H_2$  has to diffuse through the oil to reach the catalytic site. Polymer based adhesion agent (such as PVP) is a possible solution to this issue. It is not discussed here since for the practical purpose of this experiment, the validation of the effectiveness of the membrane, change in IV is the focused parameter, investigation of other parameters are hence omitted.

## 4.2 Preliminary Bio-oil Hydro-deoxygenation

### 4.2.1 Introduction

From the experimental results of soybean oil hydrogenation, the effectiveness of catalytic membrane contactor has been justified. It is proven that the membrane reactor demonstrated a more efficient method for 3-phase reactions (gas, liquid and heterogeneous catalyst) than traditional 3-phase reactors.

As mentioned in previous content, the oxygen content in bio-oil is very high at about ~35-38%. The high content of oxygen is resulted from the composition of biomass, which cannot be altered by the production (pyrolysis) process. It leads to poor stability of the product, and non-miscibility with hydrocarbons<sup>15</sup>. Hydroprocessing rejects the oxygen as the form of water by catalytic reaction with H<sub>2</sub>. That is why the process is also referred as hydro-deoxygenation. It can be depicted by the conceptual reaction below:



Typically, the process is carried out at high pressure (up to 20 Mpa) and elevated temperature (up to 400°C). The elevated hydrogen pressure aids in overcoming the mass transfer limitations in the liquid phase caused by poor hydrogen solubility in the liquid causing slow delivery of hydrogen to the catalyst surface. Hydrogen-starved catalysts also tend to coke and/or may promote unwanted products.

Although the reactant supplying mechanism is similar, comparing to soybean oil, bio-oil possess a more complicated composition. Thus, it brings more challenges in the hydroprocessing of the bio-oil. For instance, catalyst deactivation in the more hostile environment; efficacy of the membrane of multiple composition in two-way permeation (H<sub>2</sub> from permeate to reactor side; generated water from reactor side to permeate, which is essentially a pervaporation process).

In this chapter, we investigate the hydro-deoxygenation of bio-oil using a 3-phase membrane contactor with an intrinsically skinned asymmetric polyetherimide (PEI) membrane sputtered coated with palladium catalyst. Figure 20 is a schematic that depicts the configuration of the reaction system and the functionality of the membrane ( $H_2$  transport medium, phase contactor and catalyst support). Comparing to other applications, in this setup, partial pressure of  $H_2$  is significantly lowered (70 psig).

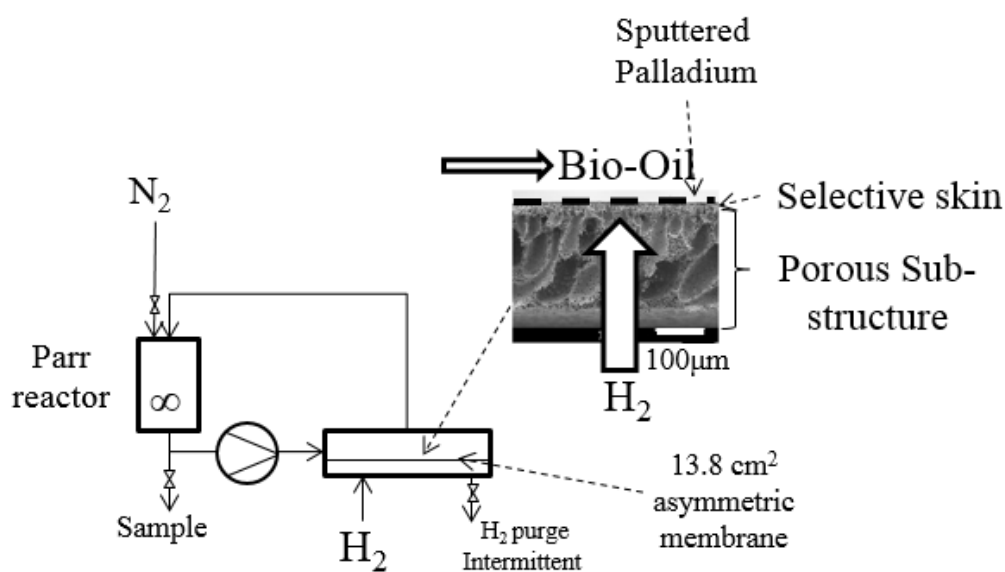


**Figure 20 Schematic of the Membrane Reactor**

## 4.2.2 Experimental

### 4.2.2.1 Materials

Asymmetric PEI membranes were fabricated, tested, and deposited with catalyst as introduced in Chapter 3. Bio-oil (fast pyrolysis oil) was acquired from the research group of Dr. Alan Zecker (Chemical and Biological Process Development, Pacific Northwest National Laboratory, Richland, WA).



#### **4.2.2.2 Analytical**

Karl-Fischer titration measures the water content of the bio-oil samples<sup>40</sup>. The coulometric titration system (Model 275KF, Model 260 Controller) is from Denver Instruments. The system is calibrated by commercially acquired standards (0.001 wt% water) before and after the titration.

#### **4.2.2.3 Apparatus**

The 3-phase membrane contactor reaction system is altered from the system that performed the soybean oil dehydrogenation described previously. The membrane cell is modified on the permeate side with a welded Swagelok hydrogen inlet and a hydrogen purge outlet connected with a liquid nitrogen condenser and a bubble flow meter.

#### **4.2.2.4 Reaction Procedure**

After the membrane (using the fabrication, characterization and catalyst deposit methods in Chapter 3) was deemed to be viable for the experiment, it was placed in the membrane cell for reduction. The catalyst is reduced for an hour under 50 psig H<sub>2</sub>. The rest of the procedure was described in previous context. Approximately 80 grams bio-oil is used each run. The reaction temperature was at 90°C. H<sub>2</sub> supply pressure was at 50 psig. Reactor side was applied with 70 psig N<sub>2</sub>. The sample was collected by a gas tight syringe and injected to a glass vial with a rubber septum to avoid water evaporation.

Each sample was diluted in 3ml of Methanol and 1ml of chloroform before analyzed by Karl-Fischer Titration.

## **4.2.3 Results and Discussion**

### **4.2.3.1 Hydro-deoxygenation of Bio-oil**

The membrane contactor evaluated the hydro-deoxygenation of bio-oil at relatively mild conditions (90°C and 50 psig H<sub>2</sub> pressure). Preliminary results are shown in Figure 21. The initial water content is about 22%. However, as the reaction run carried out, the water content unexpectedly declined despite the anticipation to increase. This indicates that the various forms of oxygen in the bio-oil has not been hydrogenated to water. The premature judgement for this phenomenon is the deactivation of the catalyst. However, although the water content decreased with time, the change of water content was not random. There was clearly a pattern of the decline. This suggested there might be other reactions underway at the surface of the membrane. As mentioned in previous content, bio-oil consists of more than 300 compounds. There are other aspects of upgrades such as the removal of high acidity as well as the high content of water. The outcome of the process should not be simply negated by the unsuccessful hydro-deoxygenation. Further analysis of the reaction samples are required for more comprehensive conclusion. For example, the in-situ activity and deactivation of catalyst on the surface of the membrane is studied by AFM<sup>41</sup>.

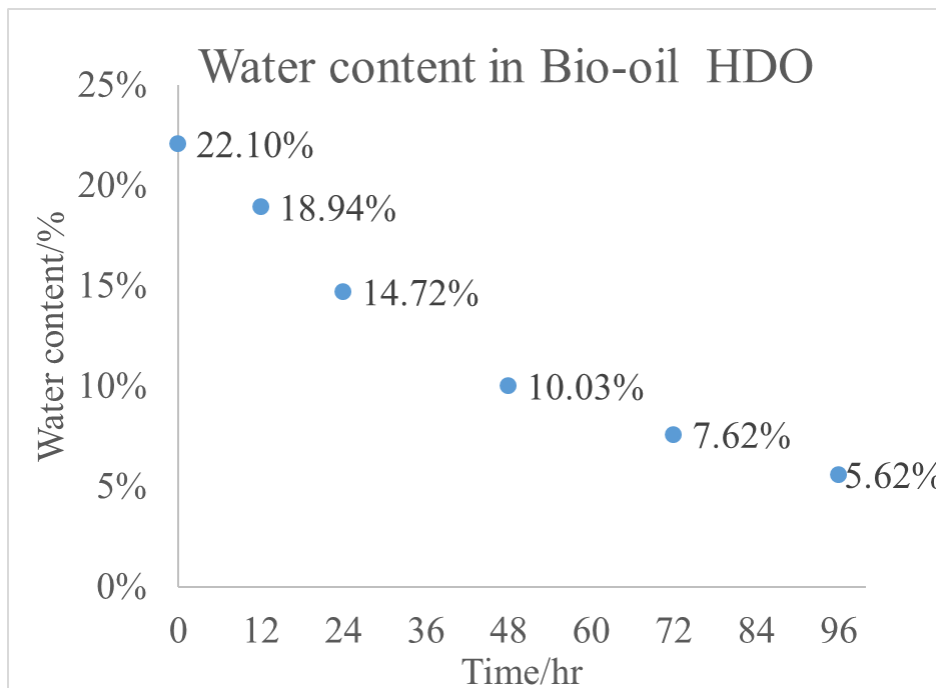


**Figure 21 Bio-oil HDO at 90°C**

#### **4.2.3.2 Effect on Water Removal**

In spite of the unideal results for the hydro-deoxygenation, the loss of water content could be the consequence of water permeation through the membrane. This hypothesis could be backed by the practical theory of pervaporation, as well as the water accumulation on permeate side shown on Figure 22. In this fashion, the transport through the membrane is induced by the vapor pressure difference between the reactor side and the vapor side<sup>42</sup>. A condenser then captures the vapor. Figure 22 demonstrates that as reaction time processes, water is constantly permeating through the membrane. Moreover, the mass of water accumulation at 72 hour is nearly ~50% of overall water content from the entire system (3.8g in condenser; 7.5 g in both oil and condenser). Unfortunately, the reaction scheme in the reactor is not identified; hence, the water removal performance by the membrane could not be accurately quantified. Nonetheless, the membrane still displayed admirable capacity at water removal from the bio-oil.

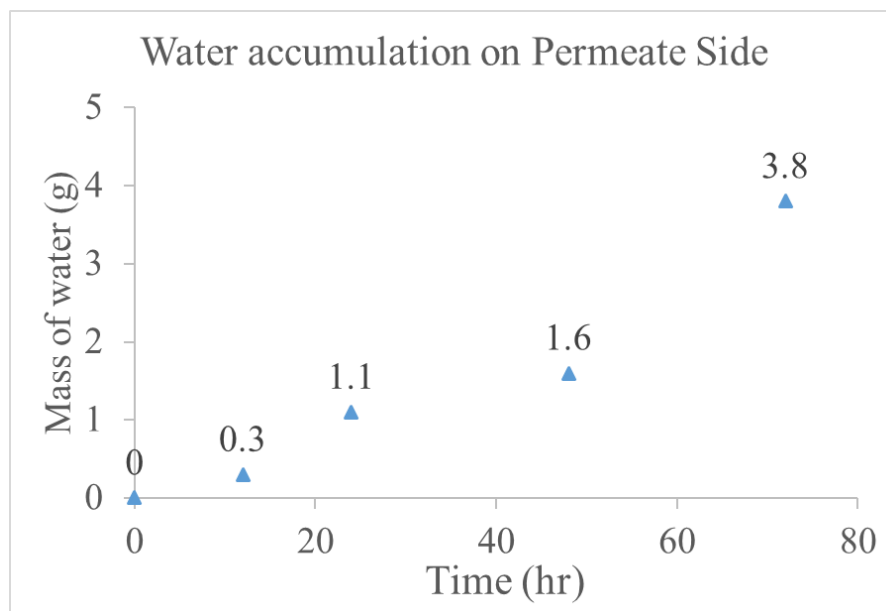


**Figure 22 Water Removal by pervaporation via the PEI membrane**

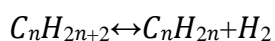
From Table 1, it is clear that the water content in bio-oil is significantly higher than crude oil, which inhibits its potential quality as alternative fuel. Thus, the removal of water by the membrane is not nuance in spite of the inadvertent discovery. Besides the expected role of a contactor, the membrane also serves as a separator. This also show the potential of the membrane contactor in the application of bio-oil upgrades.

# Chapter 5 Background on Alkane Dehydrogenation in a Membrane-assisted Reactor

## 5.1 Introduction

Dehydrogenation process is extensively utilized in various industries, i.e. petroleum, detergent and fine chemicals. In petrochemicals, dehydrogenation is involved in mass production of olefins and aromatics<sup>43</sup>. Due to its endothermic nature, an equilibrium-limited dehydrogenation reaction demand high temperature for high conversion. For instance, in the dehydrogenation of alkanes to alkenes, temperature of up to 1000 °C is required for complete conversion<sup>44</sup>. While it is economically consuming, other issues including compromised catalyst selectivity, coking and deactivation also appear for processes to operate at elevated temperatures.

According to Le Chatelier's Principle, removal of reactant/product in a chemical reaction shifts the equilibrium to a desired direction to break the thermodynamic barrier<sup>45</sup>. Typically, removal of product H<sub>2</sub> from the alkane/alkene mixture in the alkane dehydrogenation shifts the equilibrium forward; hence, a higher conversion of alkane can be realized.



This could be accomplished by various separation methods, including pressure swing adsorption, distillation and membrane separation. Unlike the former pair, that requires either an additive plus a pressure change or a phase change, membrane separation owns the advantages such as low energy consumption, continuous process, mild conditions and flexible scalability<sup>43,46</sup>.

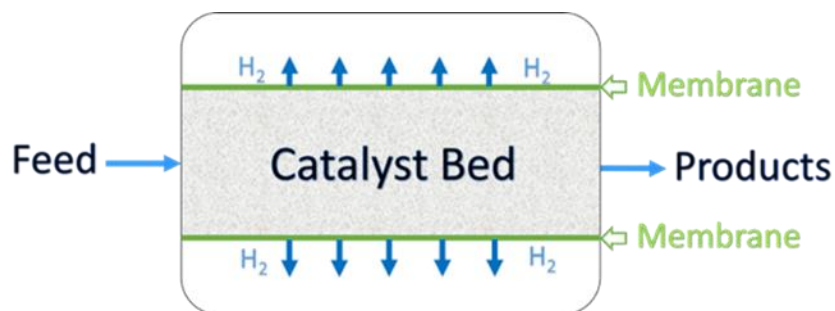


**Figure 23 Concept of Product Selectively Removed by Membrane Separation**

Polymers are often utilized as membrane material in gas separation membranes because of their excellent permeabilities and selectivities. In addition, they are inexpensive to fabricate and simple to scale up<sup>47</sup>. Nevertheless, polymeric materials are perceived as unstable under temperatures over  $\sim 150\text{ }^{\circ}\text{C}$ <sup>48</sup>. Improvements in thermal stability of polymeric material will make it a competitive contestant in  $\text{H}_2$  removal in alkane dehydrogenation. One method is to blend existing polymeric materials to acquire their favorable qualities when a single polymer does not meet the requirements in certain applications.

In the present study, Matrimid® 5218 and Polybenzimidazole are selected as thermally stable polymeric materials. Moreover, its potential of separating  $\text{H}_2$  from hydrocarbons is investigated. Dense films are fabricated using the blend materials to measure their transport properties under elevated temperatures and the presence of hydrocarbons. The model reaction studied was the dehydrogenation of methylcyclohexane (MCH) to toluene.

The dehydrogenation of MCH to toluene is of interest for a variety of reasons, including:

1. Industrial catalysts are available to promote the rate of this reaction such that reactor size is commercially viable;
2. The catalysts produce toluene at nearly 100% catalytic selectivity, minimizing the need to consider the impact of byproducts;

3. The reaction proceeds to completion, resulting in the production of three hydrogen molecules for each molecule of toluene produced;
4. As the most selective temperature range for catalyst selectivity, the equilibrium conversion is less than 60% (like the scenario described in Figure 25).
5. This system is of great industrial interest as a potential liquid fuel hydrogen carrier. As described in Figure 24, the MCH to toluene cycle provides for the ability to supply hydrogen produced in an environmentally sustainable way to the liquid-transportation fuel system. To achieve this vision, it will be necessary to develop a system that allows for rapid dehydrogenation of MCH and efficient separation of the hydrogen produced. The membrane reactors that are the subject of this study provide a potential to achieve these goals.

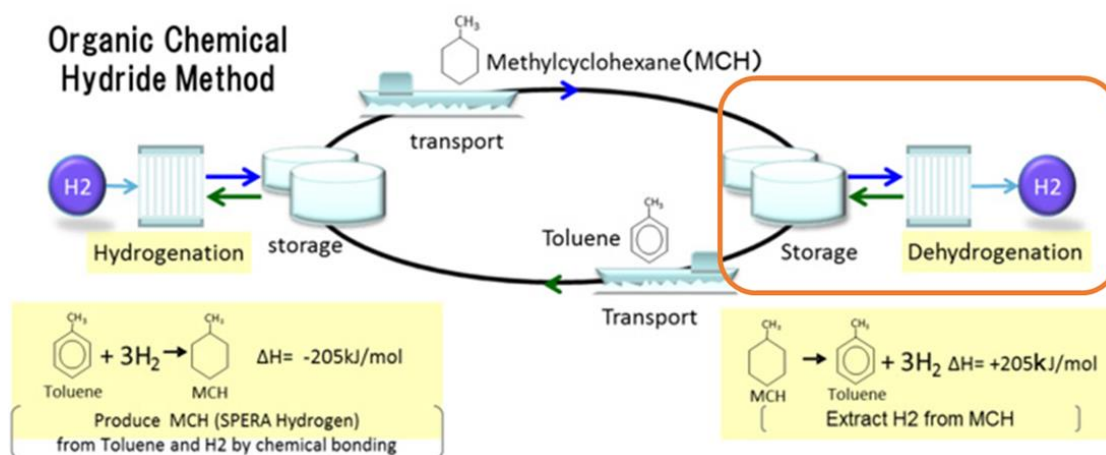


**Figure 24 The Methylcyclohexane, Toluene and H<sub>2</sub> Cycle in the Novel Hydrogen Storage Project by Using Methylcyclohexane as Hydrogen Carrier<sup>102</sup>**

## 5.2 Research Objective

Selective removal of hydrogen via polymeric membrane can break the thermodynamic barrier of dehydrogenation of methylcyclohexane. Current challenge of the reaction is the dilemma of achieving conversion and maintaining catalyst active. From the plot in Figure 25, higher conversion is achieved with the trade-off of catalyst performance (loss of activity and selectivity) at higher temperatures. The process is preferably operating in the left side of the plot to ensure catalyst activity and selectivity by sacrificing conversion. The objective of this research project is to operate the process in the left area (mild temperatures) where the catalyst is active and selective, while high conversion is reached by the removal of hydrogen using thermally stable polymeric membrane, which eventually results in a higher yield.

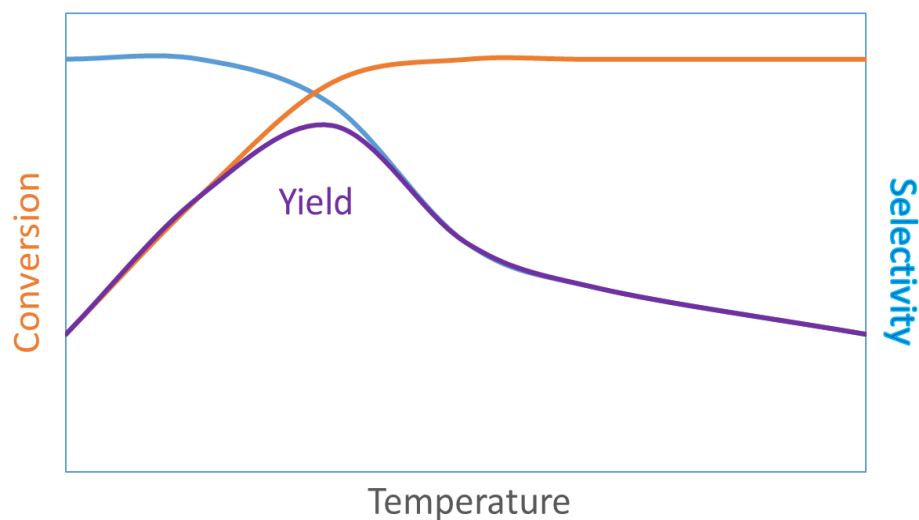


**Figure 25 Change of Yield, Selectivity and Conversion versus Temperature. Yield = Selectivity \* Conversion.**



# Chapter 6 Transport Properties and Thermal Stability of Matrimid/PBI Blend Materials

## 6.1 Introduction

### 6.1.1 Thermal Properties of Polymeric Materials

Glass transition temperature ( $T_g$ ) of polymer is defined as a temperature where polymer transitions from glassy state to rubbery state<sup>49</sup>.

In the glassy state, at temperatures below the  $T_g$ , the molecular movement of the polymer backbone is restricted. In the rubbery state, at temperatures above the  $T_g$ , coordinated movement of sections of the polymer backbone can occur. At glassy state, the polymer material has higher mechanical strength.

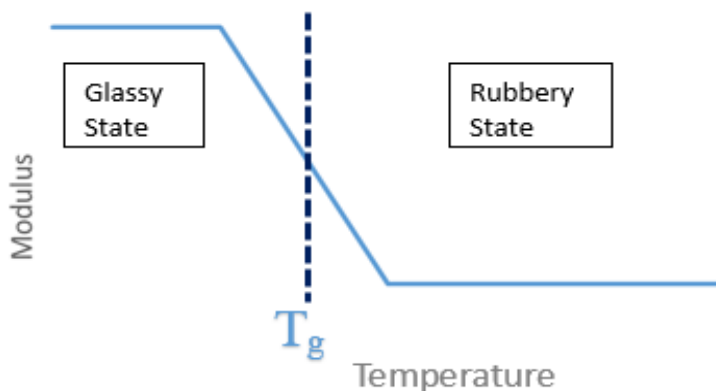


**Figure 26 Glass Transition Temperature**

A higher  $T_g$  is associated with stiff polymer backbones. Stiffer backbones will have less mobility at higher temperatures. For a polymeric membrane to be able to distinguish gases at higher temperatures, a more rigid backbone is required<sup>50</sup>. Usually polymeric materials with higher  $T_g$  is considered better for thermal stability as membrane materials.

Thermal Gravimetric Analysis (TGA) can also characterize thermal stability. TGA can capture the changes in chemical properties (such as decomposition, which is a sign for poor thermal stability) as a function of increasing temperature.

### 6.1.2 Effect of Temperature on Permeability of Polymeric Materials

Because permeability  $P_i = D_i S_i$ , it is affected by diffusivity and solubility. The thermal effects show opposite trends on sorption and diffusion. For gas sorption, solubility decreases with increase of temperature due to better condensability of the penetrant at lower temperatures. The solubility dependence with temperature is typically written in terms of the van't Hoff relationship<sup>51</sup>.

$$S = S_0 \cdot \exp\left(-\frac{\Delta H_s}{RT}\right) \quad (15)$$

where  $S_0$  is a constant and  $\Delta H_s$  is the partial molar enthalpy of sorption, where it can be written as

$$\Delta H_s = \Delta H_{condensation} + \Delta H_{mixing} \quad (16)$$

$\Delta H_{condensation}$  is the enthalpy associated with condensation of the gaseous penetrant to a condensed density;  $\Delta H_{mixing}$  is the enthalpy associated with creating a molecular scale gap in the polymer of sufficient size to accommodate the penetrating molecule. Combined are the two steps of the dissolution of a penetrant molecule into a polymer matrix. For low molecular weight, highly supercritical gases such as hydrogen and helium,  $\Delta H_{condensation}$  is very small thus  $\Delta H_s$  is governed by  $\Delta H_{mixing}$ . Interactions between polymers and these permeant gases tend to be weak, and  $\Delta H_{mixing}$  is positive, therefore, solubility increases with increasing temperature. For more condensable gases, like CO<sub>2</sub>, and many organic vapors,  $\Delta H_s$  may be negative due to the large contribution of  $\Delta H_{condensation}$ . Moreover, the solubility will decrease with increasing temperature<sup>51,52</sup>.

Temperature dependence on gas diffusion is expressed in terms of an Arrhenius type relationship, as movement of gas molecules through a membrane is considered a thermally activated process

$$D = D_0 \cdot \exp\left(\frac{E_D}{RT}\right) \quad (17)$$

where  $D_0$  is the constant pre-exponential factor and  $E_D$  is the activation energy of diffusion.

Diffusion is the most temperature sensitive transport parameter. Thus, gas diffusion coefficients typically increase appreciably with increasing temperature.

Combining the temperature dependence equations for the diffusion and sorption coefficients, the temperature effect on gas permeability is given as

$$P = P_0 \cdot \exp\left(\frac{E_P}{RT}\right) \quad (18)$$

where  $E_P$  is the activation energy of permeation and is an algebraic sum of  $E_D$  and  $\Delta H_s$ .

Therefore, in general, specifically in glassy polymers, permeability increases with increasing temperature (Figure 27).

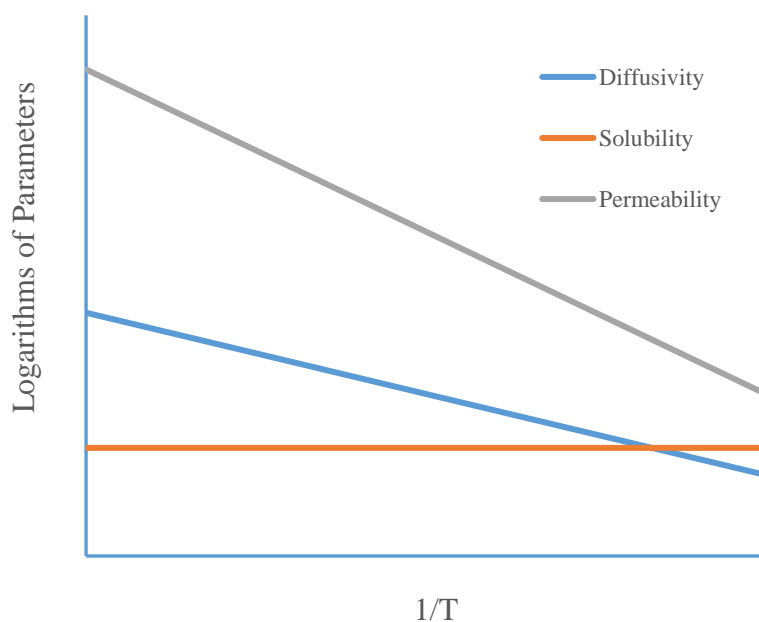


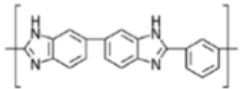
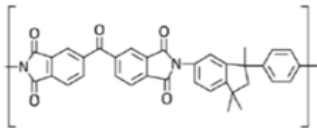
**Figure 27 Schematic of Permeability, Diffusion Coefficient, Sorption Coefficient against Temperature**

By acquiring consistent trend of changes in permeability as temperatures increase is another evidence for mechanical integrity of the material, which indicating desirable thermal stability.

### **6.1.3 Thermal Stability of Matrimid 5218, Polybenzimidazole (PBI) and Their Blend**

Matrimid 5218 (referred as Matrimid in the following context) and polybenzimidazole (PBI) are two selected polymers for membrane fabrication thanks to their thermal and chemical stability.

**Table 3 Chemical Structure of Matrimid and PBI**

Polymer	Repeat unit structure
PBI	
Matrimid	

Extensive studies on Matrimid have demonstrated its outstanding gas transport properties<sup>53-57</sup>.

The glass transition temperature of Matrimid is 323°C. PBI, although not as permeable as Matrimid, has a glass transition temperature of 435°C, indicates a better thermal stability<sup>58</sup>. The major deficiency of PBI is its difficulties to be fabricated into self-standing membranes because of brittleness after drying<sup>59</sup>. The good processibility of Matrimid can compensate for the poor processibility of PBI<sup>53</sup>. Both materials possess decent H<sub>2</sub>/N<sub>2</sub> selectivity. Following table shows the single gas permeability and selectivity of Matrimid and PBI.

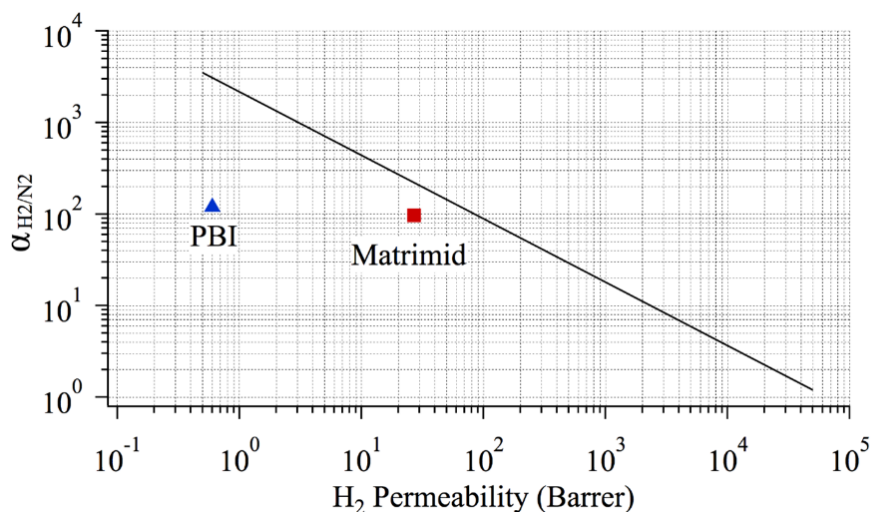


**Figure 28 Where PBI and Matrimid Stand in the Upper Bound Plot<sup>60</sup>**

**Table 4 Single Gas Permeabilities of Matrimid and Matrimid/PBI dense films at Room Temperature; Reference and Measured data.**

Films	Single Gas Permeability (Barrer)				Ideal Gas Selectivity	
	N <sub>2</sub>	H <sub>2</sub>	CH <sub>4</sub>	CO <sub>2</sub>	H <sub>2</sub> /N <sub>2</sub>	CO <sub>2</sub> /CH <sub>4</sub>
Matrimid <sup>61</sup>	0.22	14.0	0.16	4.9	62.5	31.8
50/50 Matrimid/PBI <sup>50</sup>	0.18	15.6	0.12	4.7	89	38
50/50 Matrimid/PBI	0.16	12.1	0.12	3.5	81	29
90/10 Matrimid/PBI	0.18	13.1	0.16	4.4	73	27

By blending the two polymers, the resultant properties neutralize between their properties as single polymers<sup>62,63</sup>. L. Schulte et al. has conducted a thorough study<sup>50</sup>. The study has proved that the blend material possess satisfactory transport properties. The addition of PBI slightly weakens the permeability of Matrimid as expected. The selectivities among some common gases, for example, H<sub>2</sub>/N<sub>2</sub> also maintains in the anticipated area. The blend material of Matrimid and PBI is also thermally stable and chemically resistant in several organic solvents at temperature up to 200 °C.

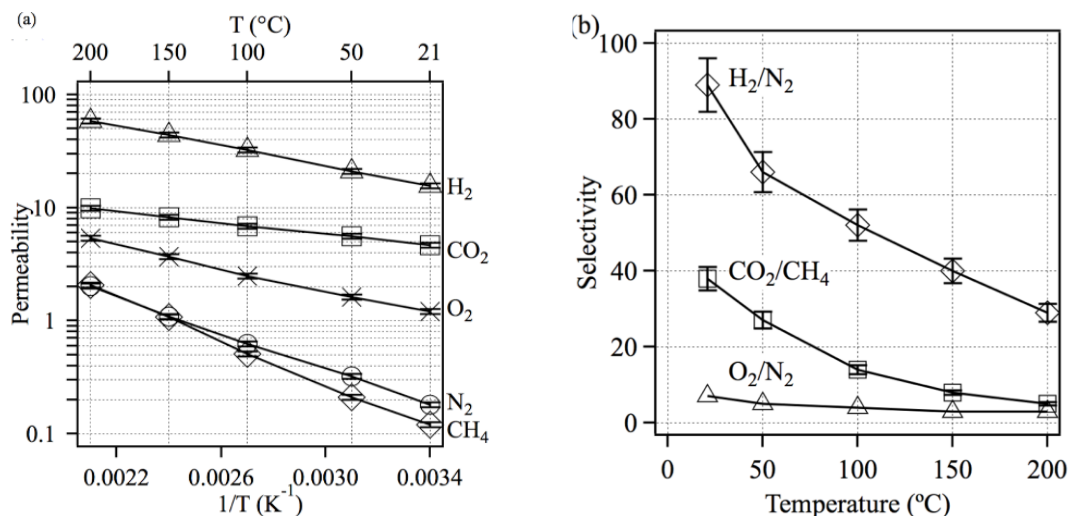


**Figure 29 a) Single Gas Permeabilities and b) Ideal selectivities for several industrially important separations of blended dense 50/50 PBI/Matrimid films<sup>50</sup>.**

Thus, the blend material of Matrimid and PBI has the potential to be utilized as membrane material in the dehydrogenation of alkanes. In this study, dense films with the consisting mass ratios 90% Matrimid 10% PBI (90/10) and 50% Matrimid 50% PBI (50/50) are fabricated. Single gas permeabilities of common gases and hydrocarbons of these films are measured. The selectivity of H<sub>2</sub> over hydrocarbons are calculated. The stability of these films with the presence of hydrocarbons up at elevated temperatures to 300 °C is monitored. By gathering the data and information above, the feasibility of utilizing this blend material in the alkane dehydrogenation, specifically the dehydrogenation of methylcyclohexane can be evaluated.

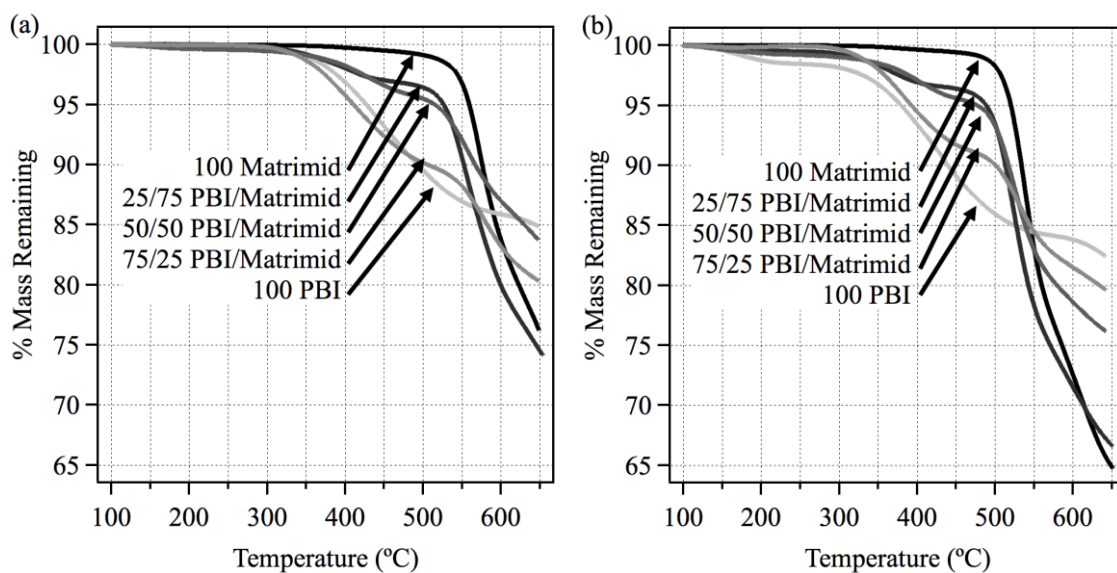


**Figure 30 Thermal Gravimetric Analysis of Matrimid Film, Matrimid/PBI Blend Films and PBI Film in a)  $N_2$ , b) Air up to 600 °C<sup>50</sup>. Despite the mass loss in the high temperature region, all films performed similarly and until 300 °C. The retention of mass in the 100 °C to 300 °C region indicates its optimal utilization in the dehydrogenation application.**



## 6.2 Experimental

### 6.2.1 Materials

Polymers PBI (100 mesh powder) was obtained from PBI Performance Products (Charlotte, NC, USA). Matrimid was obtained from Archway Sales (Kansas City, MO, USA).

Gas Ultra high purity  $H_2$  and  $N_2$  are obtained from Matheson Gas Products.

Hydrocarbons methylcyclohexane (minimum purity of 99%, extra pure) and Toluene (minimum purity of 99.8%) are purchased from Fisher Scientific.

Solvents ACS Reagent grade 1-Methyl-2-pyrrolidinone (NMP), Anhydrous Methanol and Hexanes are purchased from Fisher Scientific.

### 6.2.2 Apparatus

A constant-volume variable-pressure gas flux measurement system was built as a part of a membrane-assisted packed-bed reactor system for future experiments. The schematic of the system is shown below.

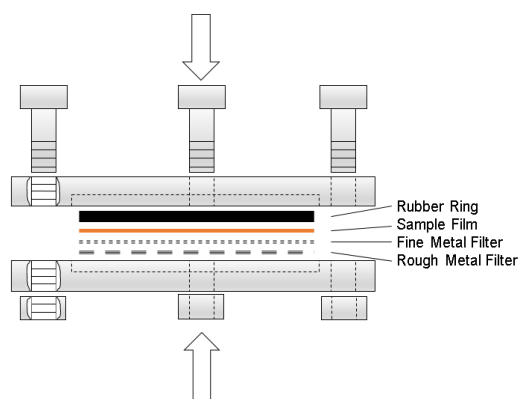


**Figure 31 Detailed Setup in the Membrane Cell<sup>61</sup>**

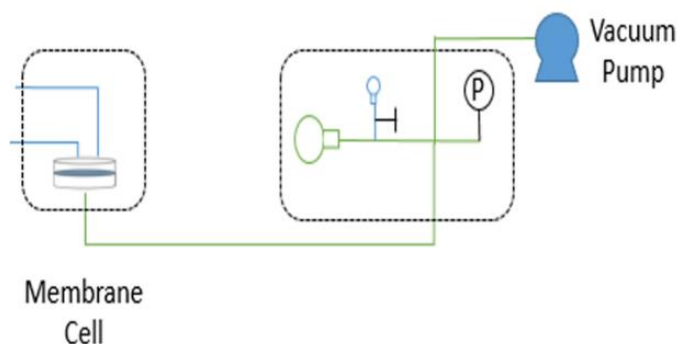


**Figure 32 Schematic of Constant-Volume Variable-Pressure Gas Flux Measurement System**

### 6.2.3 Fabrication of Dense Films

The fabrication method is improved from previous work conducted by Schulte et al<sup>50</sup>. The mass ratios of Matrimid/PBI of the blend films were respectively 90/10 and 50/50. The fabrication of 90/10 Matrimid/PBI films are demonstrated below. Dissolve 3.75g PBI in 85g of NMP and stir at 120 °C for 48 hours. Use 20µm filter paper to filter the undissolved PBI. Measure the mass of the remained solution, mass gain of the filter paper to determine the concentration of the filtered solution. Add 9.8g of Matrimid and stir at 60°C for another 48 hours. The concentration of the solution is ~15%wt. Stop stirring and lower the solution temperature to 35°C to allow degassing. Use casting knife to cast the above solution onto glass plate with a thickness of 450µm. Transfer the glass plate to a vacuum oven under 90°C with vacuum established. The film is dried for 32 hours before cooled to room temperature naturally. Then emerge the film into DI water bath. After it detaches from the glass plate, the film is solvent exchanged in three consecutive 30-minute methanol baths and three consecutive 30-minute hexanes to remove the excessive water and maintain the integrity of the film. Finally, transfer the film to a hexane-enriched environment

for 24 hours in order to slow the diffusion out of the film. Hang dry overnight. The thickness of the film was about 60 $\mu$ m. 50/50 films are prepared by the same method except for different mass ratios.

### 6.2.4 Permeability Measurement of the Dense Films

Single gas permeabilities for dense films of H<sub>2</sub>, N<sub>2</sub>, MCH and toluene are measured in the constant-volume variable-pressure system mentioned above. Ideal gas selectivity was obtained by the ratio of permeabilities of two gases.

$$\alpha_{A/B}^* = \frac{P_A}{P_B} \quad (19)$$

Tested area of the film is 7.9cm<sup>2</sup>. The permeabilities of H<sub>2</sub> and N<sub>2</sub> were measured from 25°C to 275°C. Permeabilities of MCH and Toluene were measured from 150°C to 275°C as they are in liquid forms in lower temperatures. The feed pressure is set at 15 psig. Permeate pressure is about 0.025 mmHg at the start of each measurement. Permeability is calculated by the equation below<sup>35</sup>

$$P = \frac{V_d l}{p_f A R T} \left[ \left( \frac{dp_{per}}{dt} \right)_{ss} - \left( \frac{dp_{per}}{dt} \right)_{vac} \right] \quad (20)$$

where,

$P$  is the permeability [*Barrer or cm<sup>3</sup>(STP)cm/cm<sup>2</sup> s cmHg*];  $V_d$  is the permeate side volume (*cm<sup>3</sup>*);  $l$  is the thickness of the film (*cm*);  $p_f$  is the absolute pressure of the feed side (*cmHg*);  $A$  is the film area available for gas transport (*cm<sup>2</sup>*);  $T$  is the absolute temperature (*K*);  $R$  is the gas constant at 0.278 *cmHg cm<sup>3</sup>/[cm<sup>3</sup> (STP) K]*;  $(dp_{per}/dt)_{ss}$  and  $(dp_{per}/dt)_{vac}$  are the steady-state rates of pressure rise (*cmHg/s*) in the permeate side at feed pressure and under vacuum, respectively.

## 6.3 Results and Discussion

### 6.3.1 Physical Appearance

The original appearance of the casted dense film is in the shape of a thin sheet (Figure 33). It has been cut to a round stamp with a size of  $13.8 \text{ cm}^2$  for measurement purpose, as it is the size of the membrane cell. The films are optically clear with a color of brown. The color becomes darker as the PBI content increases.



**Figure 33 Left: Sheet of Dense Film; Right: Dense Film Stamp**

Room temperature permeabilities of several single gases have been reported elsewhere<sup>50</sup>. In this work, the permeabilities of gases and the stability of the material at elevated temperatures are emphasized since the material is designed to be utilized in applications within the temperature range of  $150^{\circ}\text{C}$  to  $300^{\circ}\text{C}$ .

All the films are about  $60 \mu\text{m}$  thick.

### 6.3.2 Transport Properties of 50/50 Films

Figure 34 presents the permeabilities of N<sub>2</sub>, H<sub>2</sub>, CH<sub>4</sub> and CO<sub>2</sub> over the measured temperature range of 25°C to 275°C for 50/50 Matrimid/PBI films. The top figure presents the results as a function of temperature while the lower graph presents the data as an Arrhenius plot.

Examination of the raw data clearly indicates that the permeation rates of all gases measured increase with temperature. While there is very little permeation data available for the polymer blends studied here, some measurements have been made previously near room temperature.

The measurements made in this study are in good agreement with those reported previously<sup>64</sup>. Furthermore, the current data are well-fitted by the Arrhenius relationship (Equation 18) and presented as the solid lines in Figure 34. The ability to fit these data with a single line is an indication that the process occurring over the measured temperature range can be represented by a single activation energy for permeation, as would be expected for a homogeneous polymer blend operating in the glassy state.

The ideal selectivities of the 50/50 blend films are presented in Figure 36 and clearly decrease with increasing temperature. Selectivity is determined by diffusive selectivity and sorption selectivity. As temperature increases, the thermal motion of the polymer structure increases. As a result, it is more difficult for the material to discriminate between gases of similar sizes. This loss of discrimination is manifested in a reduction in the observed permeation selectivity.

Similar behavior has been observed in various thermal studies of the polymeric materials<sup>52,65,66</sup>.

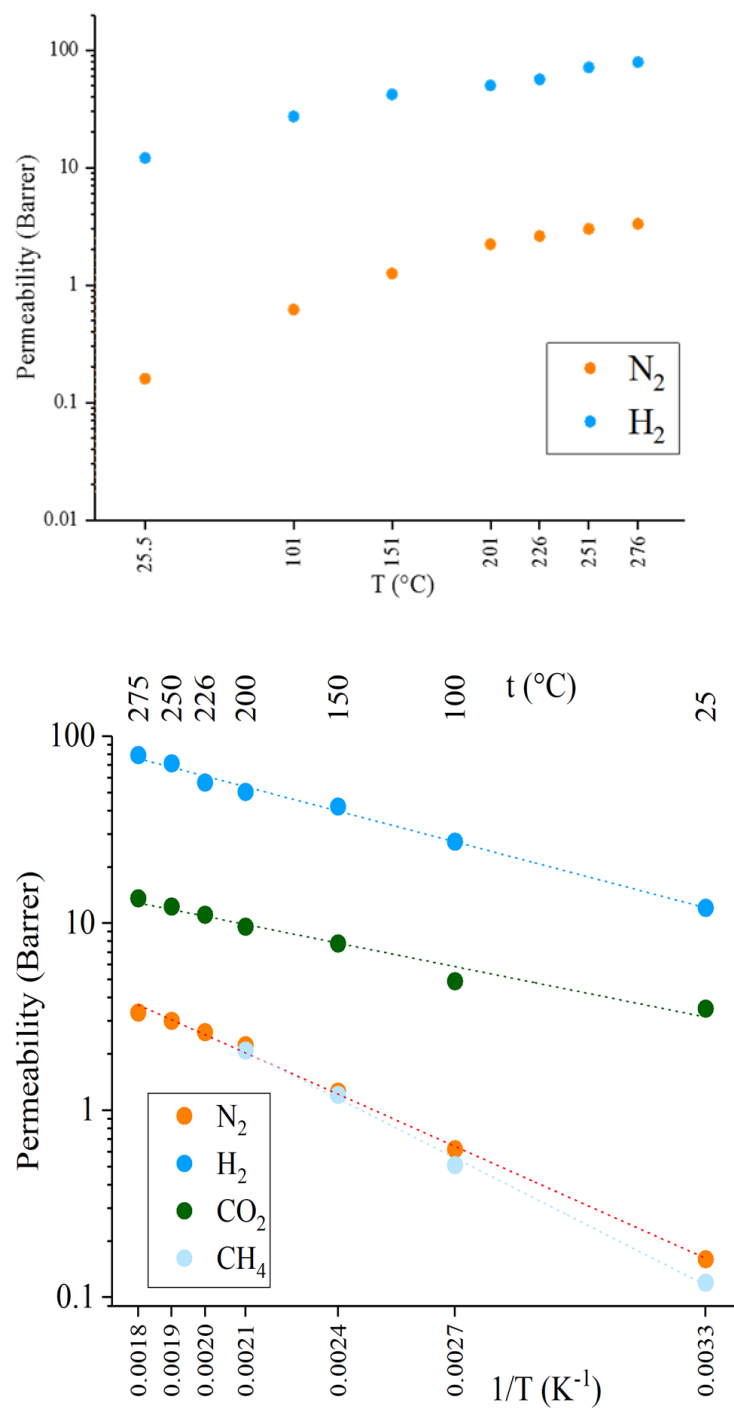


**Figure 34 Permeabilities of Single Gases of 50/50 Matrimid/PBI Material**

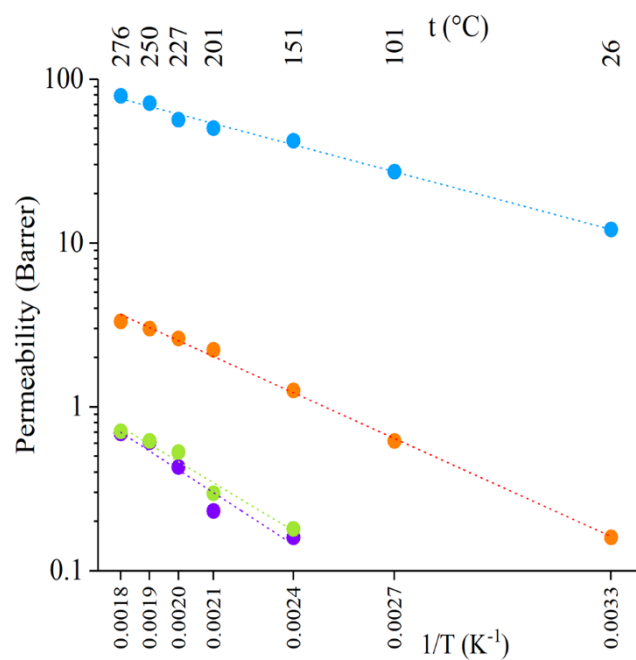


**Figure 35 Permeabilities of Dehydrogenation Components of 50/50 Matrimid/PBI Material**

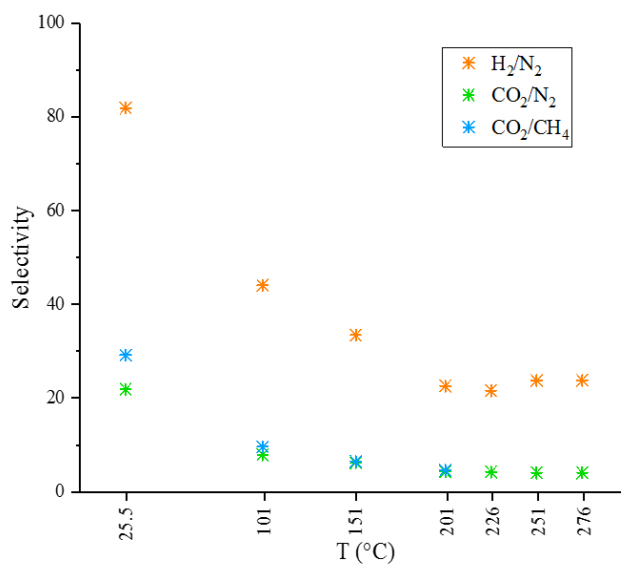


**Figure 36 Selectivities of Single Gases of 50/50 Matrimid/PBI Material**

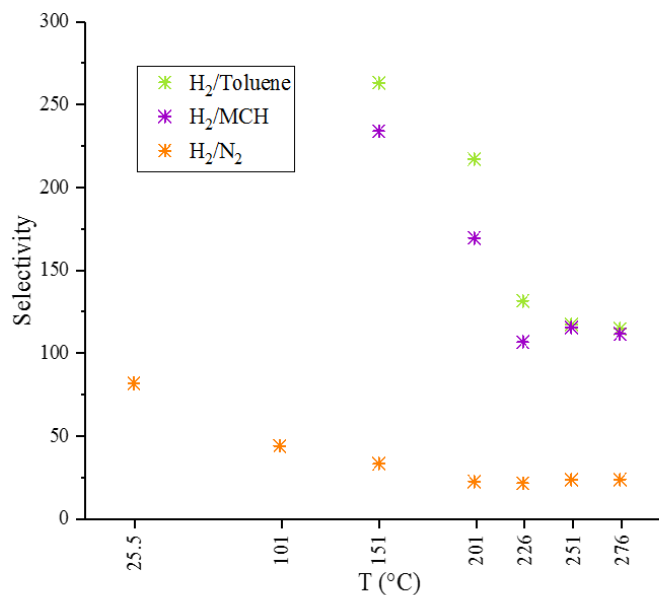


**Figure 37 Selectivities of Dehydrogenation Components of 50/50 Matrimid/PBI material**

The primary application of study in this project is in the dehydrogenation of alkanes, specifically the dehydrogenation of methylcyclohexane (MCH), the chosen model reaction. Thus, the ability of the material to permeate and separate hydrogen from MCH and toluene is a key function to evaluate. Figure 35 displays the permeabilities of H<sub>2</sub>, MCH and toluene from room temperatures to 275 °C (For hydrocarbons, from 150°C to 275°C) of the 50/50 Matrimid/PBI blend material. Data for the hydrocarbons is presented only over a temperature range where they exist in the gaseous state.

From Figure 35, for 50/50 Matrimid/PBI dense films, permeabilities of MCH and toluene increase rapidly as temperature increases. The linear relation between  $\ln P$  and  $1/T$  indicates the trend agrees with theory (Equation 18), which backs the stability of the film at these



temperatures. Because if the film undergoes structure failure or thermal disintegration as the temperature elevates, the change of permeability is very likely move off the linear trend.

The other key emphasis is the ability of the material to separate  $H_2$  from hydrocarbons at elevated temperatures. This ability is evaluated by the calculated selectivities of the blend. This blend material possess ideal hydrogen / hydrocarbon selectivities in excess of 200 at 151 C. As temperature increases, the selectivity of  $H_2$ /MCH and  $H_2$ /Toluene decrease, which is in consensus with theory as explained in previous context (Equations 15-18). Despite the loss, the selectivity of the material exceeds 100 at 275 C. This signifies that the material will provide a highly effective separation mechanism for the removal of hydrogen from the hydrogen/hydrocarbon stream.

The dense films permeabilities were also measured at temperatures higher than 275 °C. At 300 °C, fluxes of both  $H_2$  and  $N_2$  drastically soared to a degree where the figures on the pressure reader changed too fast that naked eye could not accurately record. From very rough estimate, the selectivity of  $H_2/N_2$  is close to one. Inspection of the film after removal from the test system indicated that indicates that a crack had developed across the sample leading to a whole that allowed non-selective transport of gases. Like the one shown in Figure 38, most of the films after testing in fact appear to be cracked. However, the exact time when the cracking took place was not confirmed. It is also possible that the film cracked at the time it was taken out of the membrane cell. Another possible explication is the failure of the system. The tubes inside the oven connecting the membrane cell and the measurement system consists one Swagelok® VCO fitting, where the Kalrez® O-ring is prone to flowing at temperatures over 250 °C.



**Figure 38 Picture of a Cracked Film after Test at above 275°C**

### **6.3.3 Transport Properties of 90/10 Films**

Comparing to 50/50 blends, the 90 wt% Matrimid/10 wt% PBI (hereafter referred to simply as 90/10) blends are lighter in color. While 50/50 films are more of a brown color, the color of 90/10 films is closer to yellow. Additionally, due to the higher presence of the more flexible Matramid material, these films were both easier to prepare and handle.

Figures 39-42 depict the transport properties of 90/10 Matrimid/PBI dense films. In the blend material, PBI has a higher  $T_g$  of 435 °C. From the Fox Equation, the less mass fraction of PBI results in lower  $T_g$  of the blend material. The permeabilities of 90/10 blend are remarkably similar to the 50/50 material. The permeability of each gas of 90/10 blend is slightly higher than it is of 50/50 blend. This is due to the higher proportion of Matrimid in 90/10 blend, since pure Matrimid has higher permeation coefficients for the gases of study than pure PBI. Nevertheless, the permeability difference between the two films are modest with the 90/10 material exceeding that of the 50/50 materials by less than 10% in most cases.

The Arrhenius plots (Figures 39 and 40) are linear indicating that the material exhibits only a single activation energy for permeation over the temperature range evaluated. Thus, there are no thermal transitions of the polymer material and it did not experience any impactful chemical

degradation over the temperature range studied. Furthermore, Figures 421 and 42 demonstrate the ability of this blend material to separate  $H_2$  from other gases, including hydrocarbons. Similar to the 50/50 films, as temperature increases, the selectivity of  $H_2$ /MCH and  $H_2$ /Toluene decrease but are maintained at approximately 100 in the 200-275 C range. This signifies that the material will provide a comparable performance with the 50/50 blend in the removal of hydrogen from the hydrogen/hydrocarbon stream.

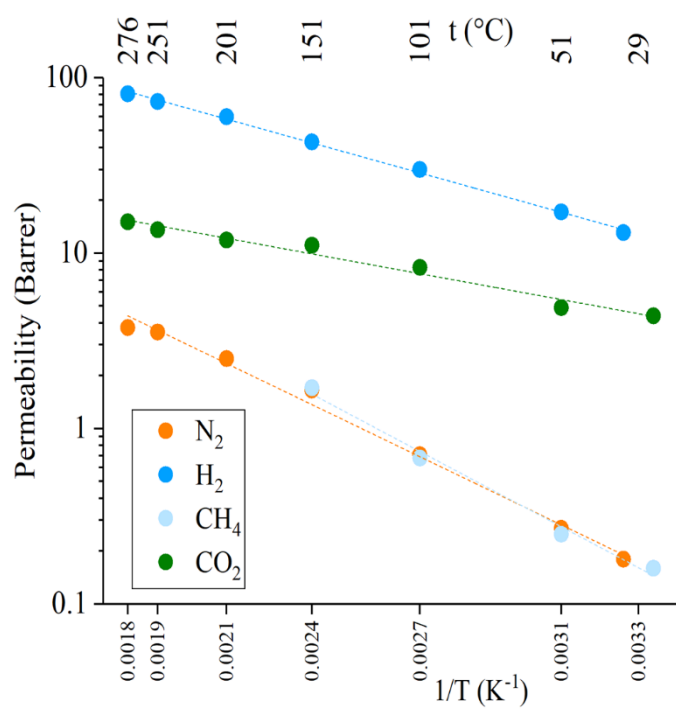
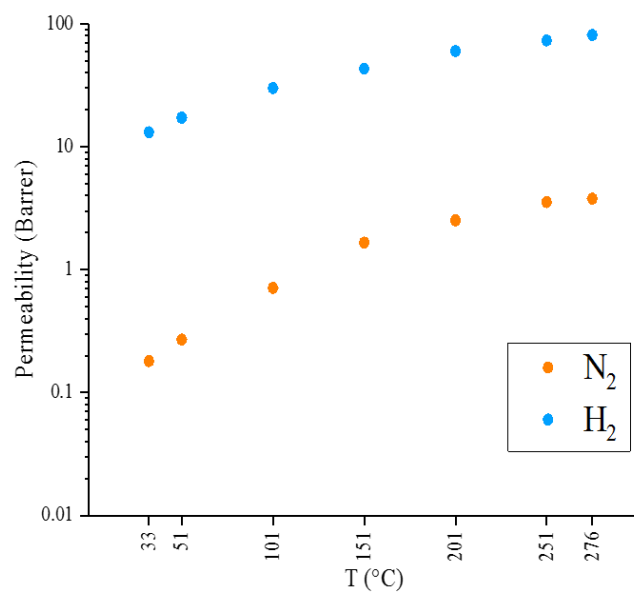


**Figure 39 Permeabilities of Single Gases of 90/10 Matrimid/PBI Material**

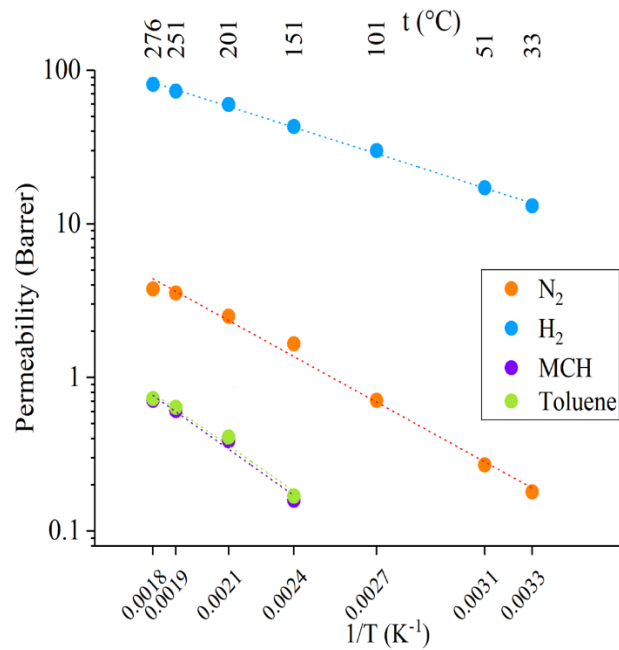


**Figure 40 Permeabilities of Dehydrogenation Components of 90/10 Matrimid/PBI Material**

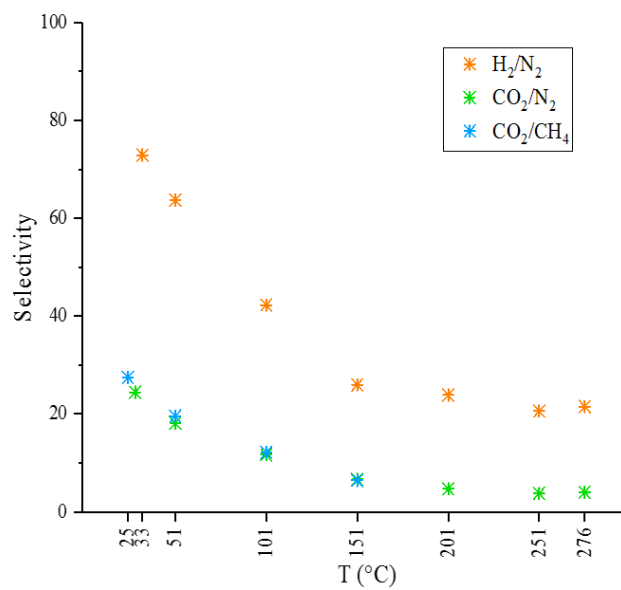


**Figure 41 Selectivities of Single Gases of 90/10 Matrimid/PBI Material**

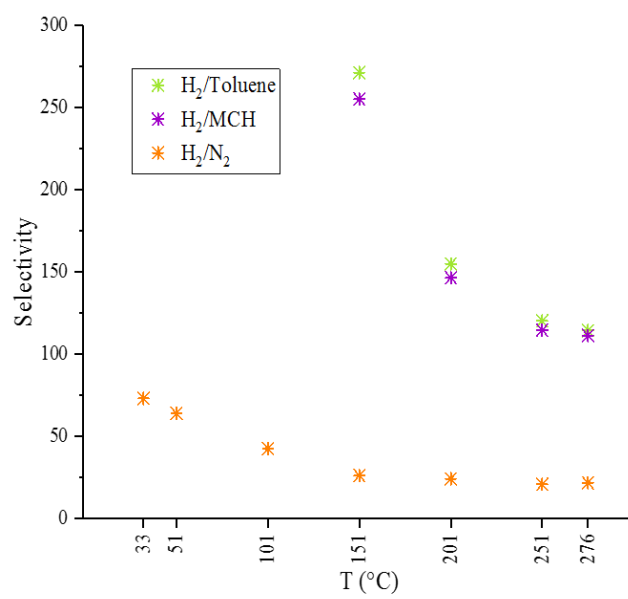


**Figure 42 Selectivities of Dehydrogenation Components of 90/10 Matrimid/PBI material**

## **Chapter 7 Dehydrogenation of Methylcyclohexane in Membrane-Assisted Packed-Bed Reactor: Finite Parameter Process Simulation**

### **7.1 Introduction**

#### **7.1.1 Alkane Dehydrogenation**

Dehydrogenation of hydrocarbons is a chemical reaction that involves the breaking of C-H bonds with the simultaneous formation of a hydrogen molecule and a molecule containing a double C=C bond<sup>44</sup>. Dehydrogenation processes are largely utilized in petroleum chemical productions. For example, the production of ethylene, styrene and ketones. These mass consumed chemicals represent a large and rapid growing market, whose production all involve dehydrogenation. One series of dehydrogenation that has a large market is the production of alkene (olefin) from alkane (paraffin), including the production of propylene and ethylene.

**Table 5 Annual Consumption of Typical Chemicals Produced from Dehydrogenation**

Chemical	Annual Consumption
Styrene	29.7 million tons (2015)
Formaldehyde	20 million tons (2013)
Ethylene	156 million tons (2014)
Propylene	90 million tons (2014)

One of the challenges of alkane dehydrogenation is its endothermic nature and thermodynamic barrier<sup>67</sup>. Figure 43 below shows the equilibrium conversion of alkane dehydrogenation at atmosphere pressure. It's obvious that dehydrogenation of these C<sub>2</sub> to C<sub>15</sub> hydrocarbons at least demands 600 °C to 900 °C to reach a conversion of 90% due to the thermodynamic barrier.

Elevated temperatures inevitably bring several obstacles, such as the difficulty for an active and selective catalyst to operate in such high and wide temperature range. At elevated temperatures, the tendency of coking and forming side product becomes larger, scilicet, the activity and selectivity of the catalyst is compromised.

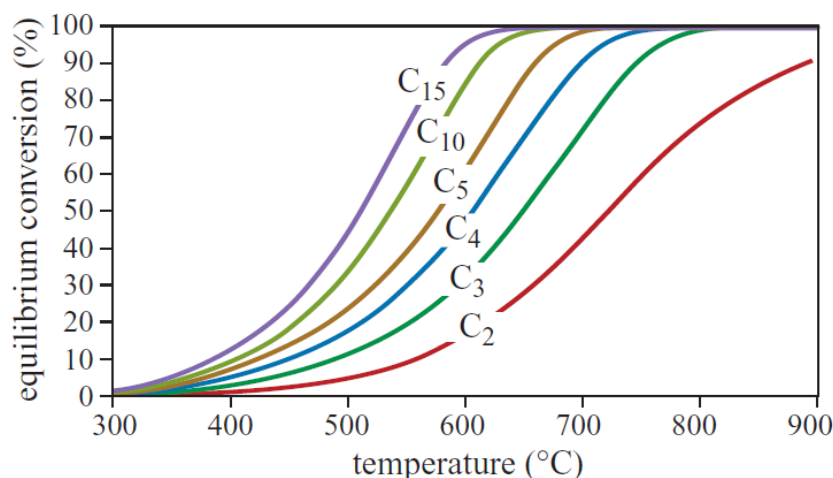


**Figure 43 Equilibrium Conversion of Alkane Dehydrogenation at Atmosphere Pressure<sup>44</sup>**

In addition, economically, harvesting a conversion as high as possible leads to better economic profits; conversely, this implies the process to be operated under higher temperatures, which increases the cost due to short cycling time of catalysts and stricter requirement of the equipment.

Researchers have exploited different catalysts and reactor setups for the alkane dehydrogenation. Following is a summarized figure for the dehydrogenation of isobutene using various setups.



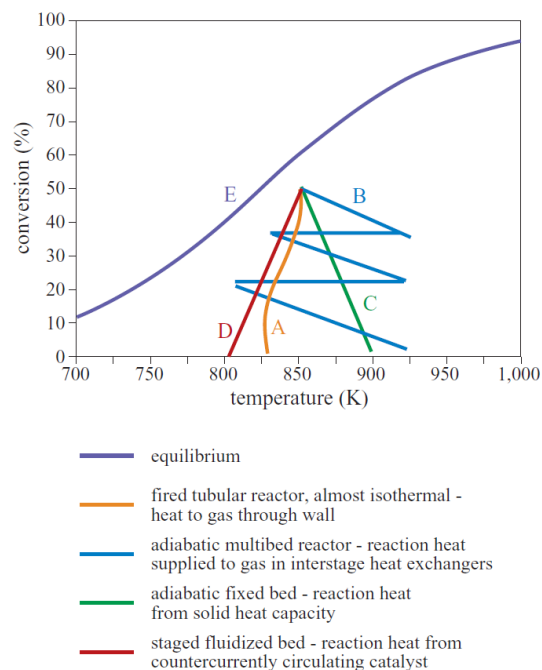


**Figure 44 Qualitative Profiles of Reactor Temperature-Conversion in Isobutene Dehydrogenation<sup>44</sup>.**

From the demonstration of this typical instance, different setup only helps with the distribution of heat and preserving the catalyst from deactivation. However, the thermodynamic nature of the reaction and the limitation of certain catalyst restrain the conversion at some particular point, where changing heating patterns does not affect the highest conversion it reaches eventually.

In chemistry, Le Châtelier's Principle, is used to predict the effect of a change of conditions in a chemical equilibrium. It is stated as

*When any system at equilibrium is subjected to change in concentration, temperature, volume, or pressure, then the system readjusts itself to (partially) counteract the effect of the applied change and a new equilibrium is established.*

Changing the concentration (partial pressure as in gaseous system) of a chemical will shift the equilibrium to the direction that would reduce that change in concentration. The chemical system will attempt to partially oppose the change affected to the original state of equilibrium. In turn,

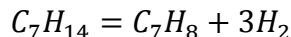
the rate of reaction, extent and yield of products will be altered corresponding to the impact on the system.

According to the theory above, selective removal of product hydrogen by membrane separation will break the equilibrium of alkane dehydrogenation, and push the equilibrium forward.

To predict the impact to equilibrium by utilizing a membrane, thermodynamics of the reaction are required to be studied. The model reaction is the dehydrogenation of methylcyclohexane.

### 7.1.2 Model Reaction

The dehydrogenation of methylcyclohexane (MCH) to toluene has been studied extensively<sup>68-71</sup>.



Methylcyclohexane (MCH) is considered a promising hydrogen precursor for H<sub>2</sub> fueled vehicles.

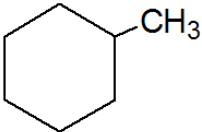
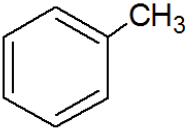
Hydrogen is a very clean fuel producing nothing other than water after combustion. However, hydrogen is not available naturally and must be produced by refining some hydrogen source.

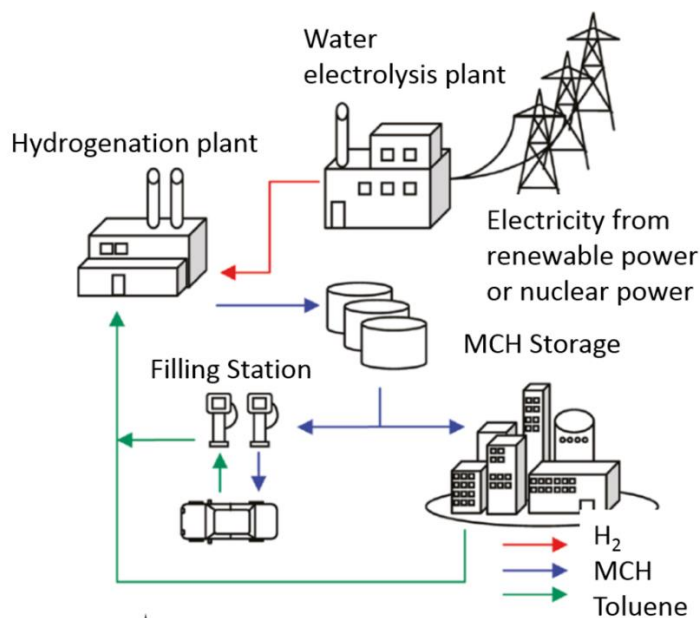
Also gaseous in nature and with extremely a low critical temperature (-253 °C), it has problems with transportation and storage, especially for on-board hydrogen utilization<sup>72</sup>. MCH is stable, relatively involatile, contains high hydrogen mass (6.2 wt%), and its product when dehydrogenated, toluene, is capable of undergoing easy hydrogenation to return back to MCH<sup>67,73</sup>.

The Methylcyclohexane-Toluene-Hydrogen system is frequently known as MTH system.

Vehicles are filled with MCH fuel instead of conventional fuel, such as gasoline. The dehydrogenation reactor installed within the vehicle itself produces hydrogen and toluene when charged with the reactant MCH. The core of the MTH system is the on-board catalytic dehydrogenation of MCH that requires an efficient dehydrogenation process.

**Table 6 Physical Properties of MCH and Toluene<sup>45</sup>**

	Methylcyclohexane	Toluene
Molecular Structure		
Molar Mass (g/mol)	98.19	92.14
Density at 20°C (g/cm <sup>3</sup> )	0.77	0.87
Boiling Point (°C)	101	110



Schematic diagram for the implementation of the MTH cycle in mobile and stationary application

**Figure 45 Schematic Diagram for the Implementation of the MTH Cycle in Mobile and Stationary Application<sup>74</sup>**

Operating the system at a considerably safe temperature with an acceptable conversion, high selectivity of catalyst is the objective of this application.

## 7.2 Thermodynamic Computation

To compare the effect of membrane, the thermodynamics of the dehydrogenation without product removal is studied by computation assuming equilibrium is instantaneously achieved with 100% catalyst selectivity. In alkane dehydrogenation, equilibrium at different temperature and pressure can be calculated with equilibrium constant  $K^{75}$ . In the dehydrogenation of methylcyclohexane (MCH) to toluene and hydrogen,

	$C_7H_{14} \rightarrow C_7H_8 + 3H_2$		
<i>Initial</i>	$n$	$0$	$0$
<i>Reacted</i>	$nx$	$nx$	$3nx$
<i>Equilibrium</i>	$n-nx$	$nx$	$3nx$

Where  $x$  is the conversion of MCH. At equilibrium,  $x = x_{eq}$ . Total moles in the system after equilibrium  $n_{total} = n-nx+nx+3nx = n+3nx$ .

The equilibrium constant at standard state  $K^\ominus$  defined by the equation below,

$$K^\ominus = \exp(-\Delta_r G_m^\ominus / RT) \quad (20)$$

Where  $\Delta_r G_m^\ominus$  is the standard molar reaction Gibbs free energy. It can be acquired by

$$\Delta_r G_m^\ominus = \Delta_r H_m^\ominus - T\Delta_r S_m^\ominus \quad (21)$$

Where  $\Delta_r H_m^\ominus$  and  $\Delta_r S_m^\ominus$  are standard molar reaction enthalpy and entropy respectively that can be obtained from chemical property handbooks. From another definition of  $K^\ominus$

$$K^\ominus = \frac{\left(\frac{p_{H_2}}{p^\ominus}\right)^3 \cdot \frac{p_{TOL}}{p^\ominus}}{\frac{p_{MCH}}{p^\ominus}} \quad (22)$$

$p_i = y_i p$  is the partial pressure of the component (TOL: Toluene) where  $y_i = n_i/n_{total}$  is the mole fraction of component  $i$ . System pressure  $p = \sum p_i$ . Thus, the equation can be rewritten as

$$K^\ominus = \frac{y_{TOL} \left(\frac{y_{H_2} \cdot p}{p^\ominus}\right)^3}{y_{MCH}} = \frac{n_{TOL} \cdot n_{H_2}^3}{n_{MCH}} \cdot \frac{1}{n_{total}^3} \cdot \frac{p^3}{p^{\ominus 3}} \quad (24)$$

Where at equilibrium,  $n_{TOL} = nx$ ;  $n_{H_2} = 3nx$ ;  $n_{MCH} = n-nx$ . Rearrange, it becomes

$$\frac{K^\ominus p^{\ominus 3}}{p^3} = \frac{27x^4}{(1-x)(1+3x)^3} \quad (25)$$

$x$  can be acquired from the equation above.

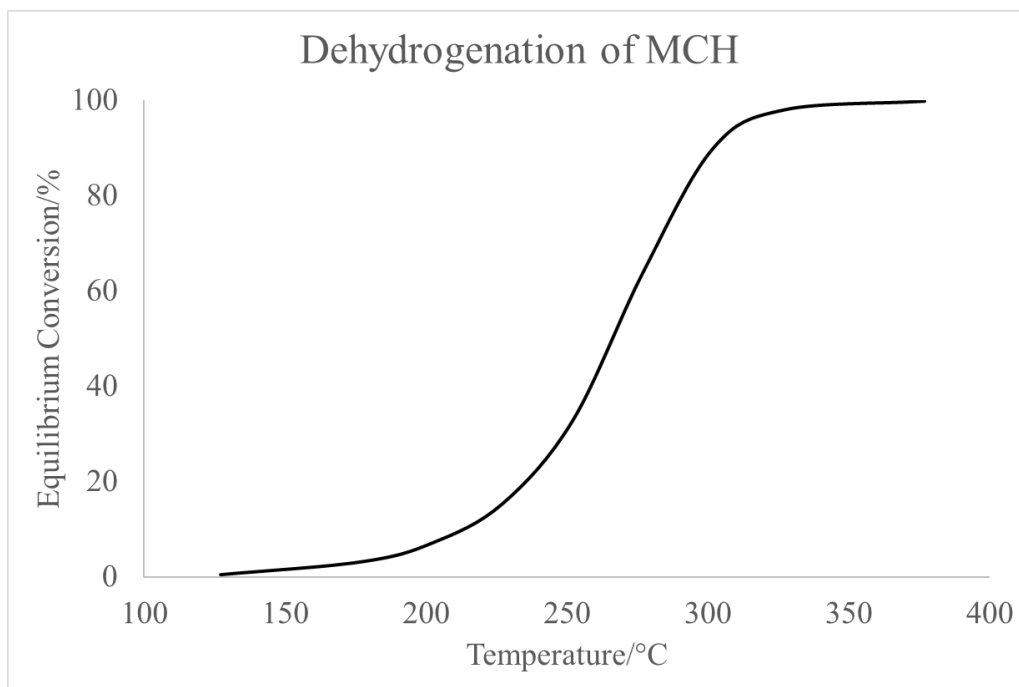


**Figure 46 Thermodynamics of Dehydrogenation of Methylcyclohexane**

## **7.2.1 Breaking the Thermodynamic Barrier**

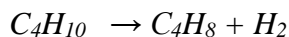
For alkane dehydrogenation, because of its endothermic nature, high temperature up to 650 °C is usually required for desired conversion<sup>76</sup>. This causes high capital and operating costs and other issues including catalyst coking. To achieve higher conversion at lower temperature and to reduce catalyst coking and operation cost, there are different approaches to shift the equilibrium.

### **7.2.2.1 Dilution**

To shift the equilibrium forward, the principle is to reach low partial pressure of alkane. This can be achieved by diluent addition or vacuum in industrial process. This also increases the requirement of the reactor system, thus increases the operational cost.

The impact of diluent addition can be computationed from equation 24 as well. Assuming equilibrium is instantaneously achieved with 100% catalyst selectivity.

The addition of diluent will change the total moles of the system, thus change the composition and partial pressure of each component. For example, in the dehydrogenation of butane where initial moles of butane is  $n$ , total moles after equilibrium is  $n_{total} = n + nx$ . In the circumstance of 1:1 Diluent to Butane dilution addition, total moles after equilibrium becomes  $n_{total} = 2n + nx$ . Taking dehydrogenation of butane for an example.



From computation, one can acquire the plot shown in Figure 47. It requires a temperature as high as 1000 K and 10X volume of diluent to reach conversion of 90%. The thermodynamic barrier is the main limitation to achieve high conversion<sup>77</sup>. Dilution also raised the tendency to form coke<sup>78</sup>.

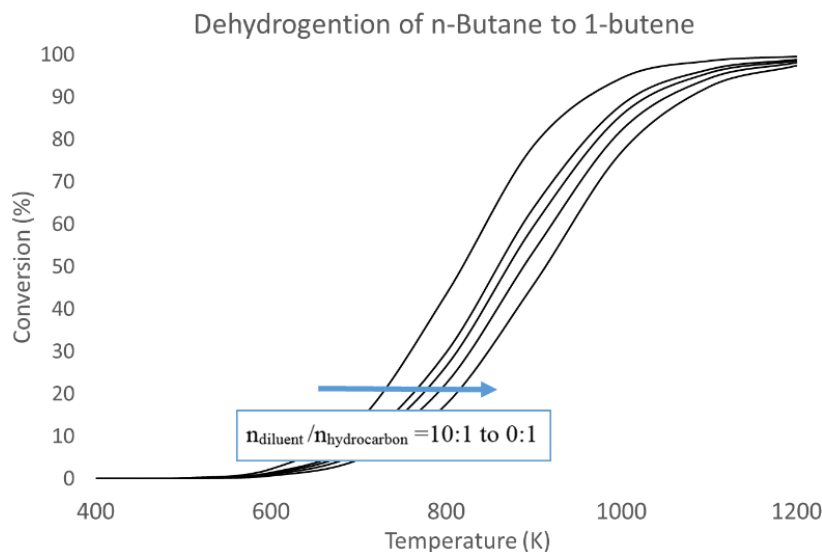


**Figure 47 Dehydrogenation of n-Butane with Hydrocarbon: Diluent Ratio 0:1 to 10:1 under Various Temperatures**

#### 7.2.2.2 Selective Removal of Product

Another solution is selective removal of product. According to Le Chatelier's Principle, in alkane dehydrogenation, removal of product hydrogen and/or alkene will shift the equilibrium forward.

Generally, gas separation can be achieved by pressure swing adsorption (PSA), distillation or membrane separation. .

PSA pressurizes and depressurizes gas around an adsorbent media to selectively adsorb certain components of a gas, allowing others to be selectively removed. PSA requires high pressure thus requires high energy consumption. In addition, low capacity and selectivity, high maintenance of adsorbent rises the challenges of PSA in gas separation.

First cooling it until it liquefies, then selectively distilling the components at their various boiling temperatures, can separate pure gases. A major disadvantage of cryogenic separation is the amount of energy required to provide the refrigeration necessary for the process. Thus, cryogenic distillation is typically only used for very high volumes because of its nonlinear cost-scale relationship, which makes the process more economical at larger scales.

Membrane separation is one of the options that can play an important role. Membranes owe their popularity largely to the following advantages<sup>46</sup>

- (generally) Low energy consumption;
- Possibility to carry out separation continuously;
- Mild process conditions;
- Easy scaling up;
- Absence of additives;
- Possibility to combine with other separation technologies,

which are beneficial for removal of product in alkane dehydrogenation.

Hydrogen selective membranes selectively separate hydrogen from the product stream. Thus, it changes the composition in the system that pushes the reaction to exceed the equilibrium barrier<sup>75</sup>.



### 7.2.3 Literature Review on Selective H<sub>2</sub> Removal in Methylcyclohexane

#### Dehydrogenation

Applying Vycor glass membrane reactor into the dehydrogenation of MCH were studied by Ferreira-Aparicio et. al.<sup>79</sup>. The MCH dehydrogenation reaction was carried out with a Pt/Al<sub>2</sub>O<sub>3</sub> catalyst. Only toluene and H<sub>2</sub> were obtained as reaction products at temperatures below 523 K<sup>79</sup>. The transport mechanism for light gases obeys the Knudsen-type diffusion model. The loss of hydrocarbons from the system through the membrane is a result of low H<sub>2</sub>/HC selectivity, which indicates a subpar separation efficiency.

Meng et al. applied inorganic membranes, for instance, silica membranes in the MCH dehydrogenation. A BTESE-derived organosilica membrane was fabricated (by sol-gel method) and applied to a catalytic membrane reactor for the dehydrogenation of MCH to toluene for H<sub>2</sub> production<sup>80,81</sup>. H<sub>2</sub> produced is immediately removed from the reactor by the multi-functioned membrane (hydrogen removal and catalyst support). Selectivity of H<sub>2</sub>/Toluene and H<sub>2</sub>/MCH are remarkably high as 16000<sup>82</sup>.

Oda et al. conducted similar researches. They integrated a hydrogen-selective amorphous silica membrane prepared with dimethoxydiphenylsilane and oxygen and employing counter-diffusion chemical vapor deposition with a PBR. Dehydrogenation of methylcyclohexane was examined with carrier gas and sweep gas under a reaction temperature ranging from 473 to 553 K and reaction pressure ranging from 0.1 to 0.25 MPa. An equilibrium shift was achieved under all conditions<sup>83</sup>.

Hirota and colleagues investigated carbon membranes. The carbon membranes were prepared by a vapor-phase synthesis using furfuryl alcohol (as carbon resource). The activated carbon membrane was used in a membrane reactor for dehydrogenation of methylcyclohexane and

showed potential for application in the dehydrogenation of chemical hydrides in membrane reactors. However, to achieve the proper pore size, the membrane required a post-synthesis activation using  $H_2$  at 973K<sup>84</sup>.

Various researchers studied metallic membranes. Palladium membrane earned special interest<sup>43,77,85-87</sup>. Ali et al.<sup>85,86</sup> conducted the dehydrogenation of methylcyclohexane from 320 to 400 °C at 15 bar and 0.5-2.6 l/hr of liquid hourly space velocities (LHSVs), using palladium silver alloy (Pd77Ag23) membrane supported on  $\alpha-Al_2O_3$  tube. As a result, high conversion over the equilibrium was achieved due to the removal of hydrogen by membrane.

Ferreira et al.<sup>88</sup> conducted the dehydrogenation of methylcyclohexane with a palladium membrane supported on a porous stainless-steel tube by electroless-plating technique, in which platinum supported alumina pellets as catalyst were packed. The conversion to toluene was 100% at 350 °C and 1.4 bar and kept stable at least for 96 h.

Itoh<sup>89,90</sup> also examined the performance of Pd alloy membrane, experiments were carried out at 250–300 °C and 2–4 bar. The conversion with the membrane reactor was higher than that without membrane separation and exceeded the equilibrium conversion, whereby confirming that the membrane reactor was useful to recover hydrogen from the equilibrium limited reaction. It was observed that the percentage of increase in conversion increased in the range of high reaction pressure.

While reaction performance was examined, membrane performance such as transport properties, stability and versatility at different temperatures were not specifically discussed. Possible explanation is that metal membrane, although with its good permeance of hydrogen, lacks stability<sup>91</sup>. And it is not feasible to operate at mild temperatures.

Here, we will examine the outcome of using polymeric blend material Matrimid/PBI to construct a proper type of membrane and its effect on breaking the thermodynamic barrier in the dehydrogenation of methylcyclohexane.

## 7.2.4 Ideal Impact of Selective H<sub>2</sub> Removal in Methylcyclohexane

### Dehydrogenation by Membrane

The impact of selective removal of hydrogen by membrane can be studied by constructing a membrane-assisted system as shown in Figure 48. Conversion against temperature with and without the membrane will be calculated.

Equations 20-25 can still be applied to the computation. In the case of adding the membrane separation unit,  $n_{H_2}$  after the first reactor becomes 0 since all hydrogen generated is removed by the membrane. In the computation, it is assumed that equilibrium is instantaneously achieved with 100% catalyst selectivity; hydrogen is completely removed by the membrane; and the membrane is solely selective to H<sub>2</sub> over hydrocarbons (methylcyclohexane and toluene).



**Figure 48 Schematic of Multi-Stage Membrane-Assisted PBRs**

From the computation of dehydrogenation of methylcyclohexane, by the addition of a membrane separation unit between 2 packed-bed reactors (PBR), as shown in Figure 49 (assuming complete hydrogen removal by membrane), conversion of methylcyclohexane increases by an significant margin compared to one conventional PBR. Comparing diluent addition with membrane separation, we can conclude that membrane separation is more efficient and economical.

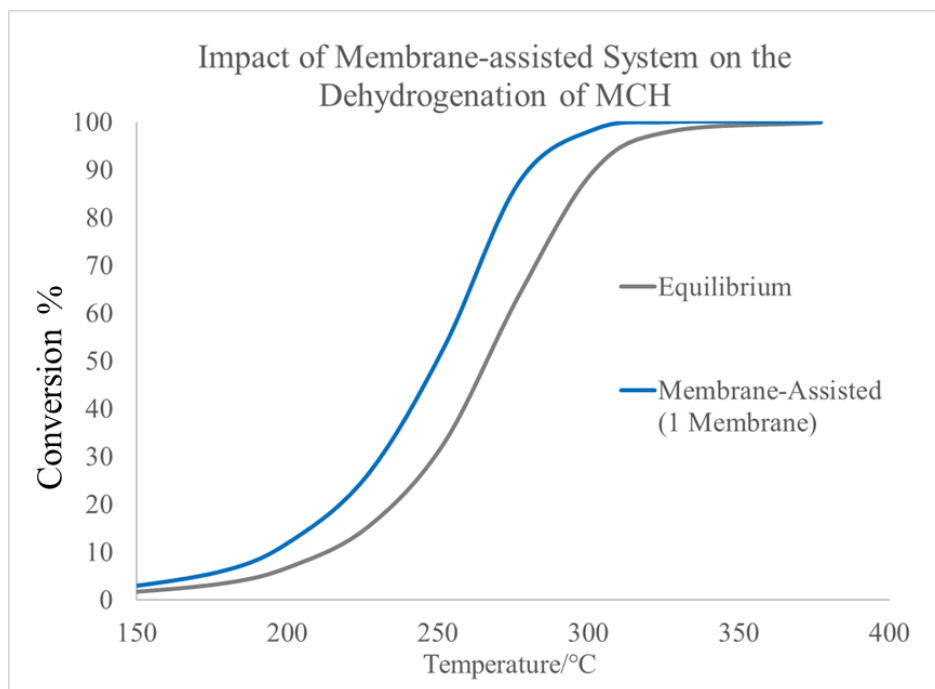


**Figure 49 Increase of Conversion Comparing Equilibrium and Membrane Assisted PBR**

More computations were conducted to evaluate the impact of multiple-stage membrane-assisted PBRs. As shown in Figure 50, theoretically, more membranes result in better increase of conversion in the ideal consumption where the membrane is solely selective to hydrogen over hydrocarbons and the membrane capacity is always sufficed.

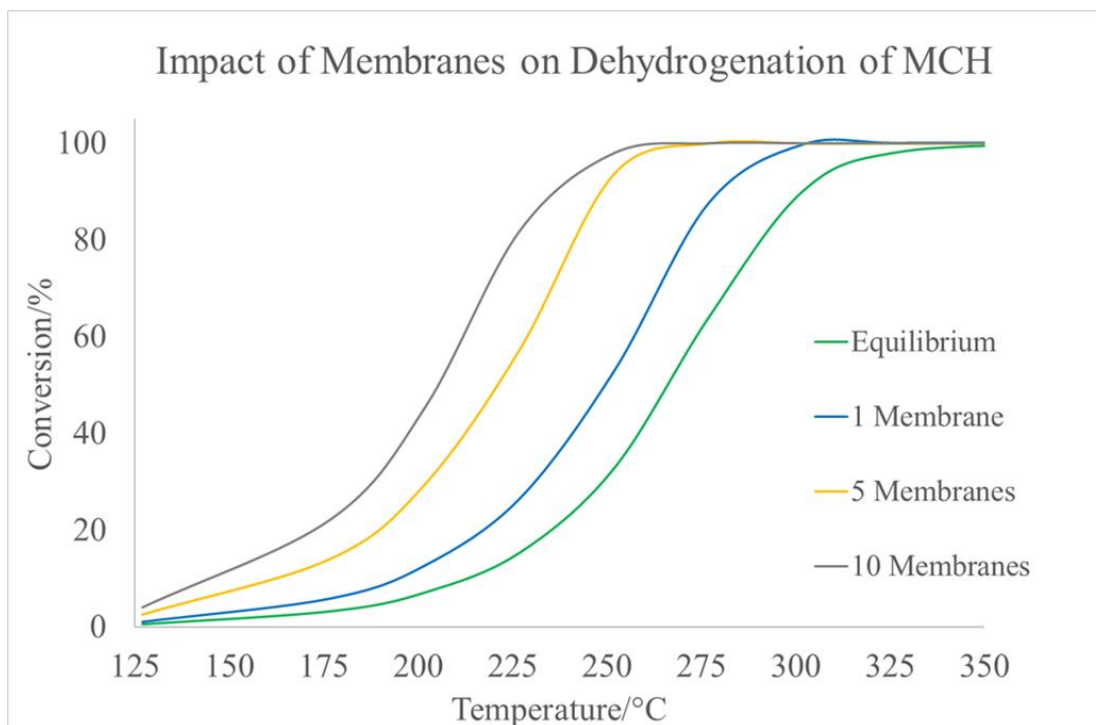


**Figure 50 Increase of Conversion in Multiple-stage Membrane-Assisted PBRs**

While it is unlikely to integrate multiple membrane separation units into multiple-stage PBRs for obvious practical reasons, the impact of adding one membrane separation unit between 2 PBRs is well worth studying, as the setup is practically viable to implement in existing industrial apparatus, and outcome is beneficial in various aspects.

## 7.3 Finite Parameter Process Simulation

### 7.3.1 Hypothesis

In order to evaluate the impact of a membrane-assisted packed-bed reactor in the dehydrogenation of methylcyclohexane in real-life scenarios, a model consisting finite parameters is developed. In this model, thermodynamics of dehydrogenation, catalyst performance and membrane performance have been taken into consideration. In addition, following assumptions are introduced:

- Equilibrium is reached instantaneously with suitable catalyst;
- There is no temperature or concentration gradients throughout the reactor system;
- Permeation properties of the membrane are independent of concentration.

A membrane-assisted packed-bed reactor model system is built to conduct the simulation. In this system, a membrane separation unit is added between two packed-bed reactors (Figure 51).

Ideally, the dehydrogenation will take place in the packed-beds. The reaction will reach a conversion in the basis of catalyst performance. Then, hydrogen generated from the first PBR permeates through the membrane and leaves the system. The remaining components in the system carry on to the next PBR where the dehydrogenation takes place again.

To conduct the simulation, these data are obtained:

- Catalyst performance on dehydrogenation of methylcyclohexane in a PBR without membrane;
- Membrane performance acquired from measured material permeation properties.

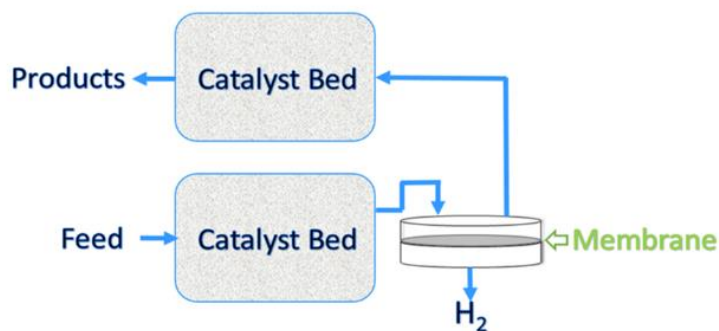


**Figure 51 Schematic of the Membrane-assisted Packed-bed Reactor System**

Thus, the main task in this computation is the integration of measured polymer transport properties into the experimental data of dehydrogenation of MCH.

## 7.3.2 Experimental

### 7.3.2.1 Materials

#### 7.3.2.1.1 Hydrocarbons and Gas

Extra pure methylcyclohexane (99%) and toluene are acquired from ACROS organics. Ultra High Purity  $H_2$  and  $N_2$  are acquired from Matheson Tri-gas.

#### 7.3.2.1.2 Catalyst

The catalyst used in this evaluation is a noble metal supported on a porous inorganic substrate. Platinum, 1% on gamma alumina powder and Platinum, 1% on 2.7-3.3 mm alumina pellets are purchase from Alfa Aesar. The catalyst morphology is a mixture of pellets and powder mentioned above. To avoid congestion in the reactor tube that builds up the pressure, pellets are grinded by mortar and pestle into 1/3 to half of their original size. Then, a mixture of 80 %wt grinded pellets and 20 %wt powder is packed into the reactor tube.

### 7.3.2.2 Apparatus

Reactor System

A reactor system is constructed as demonstrated in Figure 52. MCH feed is provided from a Hamilton 50ml gastight syringe specifically designed for syringe pump, which controls the feed rate. Two packed-beds are located inside a furnace, both leaded by coils for heating. Each packed-bed is a ¼-inch tube with a length of 10 cm. Sample ports are designated after each packed-bed. The membrane cell is not functioned in this part of the experiment. Exhaust is condensed and collected by a liquid Nitrogen cold-trap at the end of the system. Pressure are monitored by Omega pressure gauges with a full scale range of 0-30 psig. Thermocouples with extended-length probe and stainless steel sheath are used to monitor the temperature inside the furnace. Temperatures are read from Omega temperature controllers.

All tubes including the packed-bed are ¼-inch 316 stainless steel tubes from Swagelok. Fittings are also purchased from Swagelok. Syringe pump is an ATI Orion multi-rate infusion pump series M361. The syringe used for sample collection is a 1 ml gastight syringe from Hamilton Company. The sample is analyzed by Agilent Gas Chromatography/Mass Spectrum 5975C. The column used is DB-WAX.

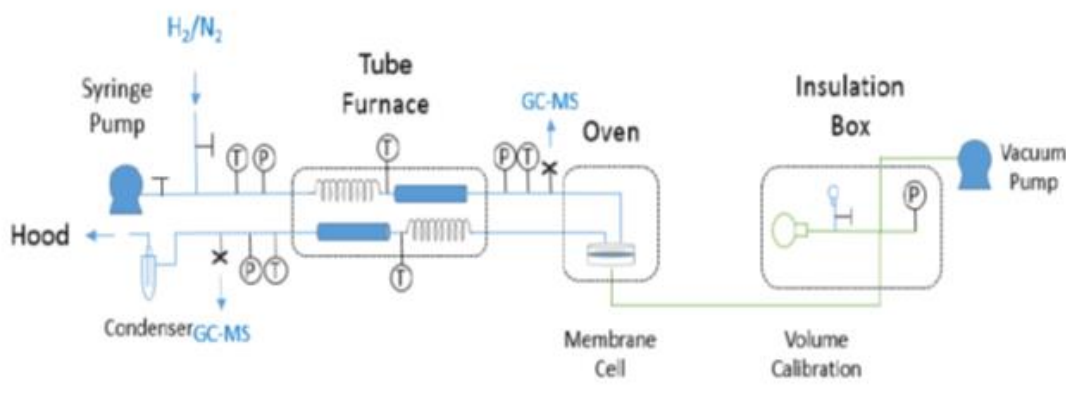


**Figure 52 Membrane-assisted Packed-bed Reactor System**



### 7.2.2.3 Catalyst

Methylcyclohexane is injected to the system with a syringe pump at a fixed flow rate. The reactant will be heated in the coil in the furnace. After the liquid reactant is gasified and heated to the desired temperature, the reaction will take place in the tube reactor filled with catalyst. The membrane cell is connected after the first reactor. In this part of the experiment, an Al foil with no permeation, instead of a real membrane, sits in the membrane cell.

Catalyst used is 1g of 1%wt Pt/ $\gamma$ -Al<sub>2</sub>O<sub>3</sub>, which is selected due to its high activity at elevated temperatures<sup>67</sup>. It is a mixture of powder (20% wt) and 2.7-3.3 mm sized pellets (80% wt) because by experiment, this type of morphology releases the maximum potential of the catalyst. The catalyst is evenly filled inside the reactor-tube (bed) with quartz-wool on both ends in case of catalyst escaping with reactant flow. Catalyst is reduced under 400°C for 3 hours with 100 ml/min H<sub>2</sub> flow. After that, MCH is injected to the system by syringe pump with the WHSV of the reaction at 3 h<sup>-1</sup>. The pressure of the system is at atmosphere. Samples are taken from the sample ports and analyzed by GC-MS.

**Table 7 Summary of Reaction Conditions**

Catalyst Type	1%wt Pt/ $\gamma$ -Al <sub>2</sub> O <sub>3</sub>
Catalyst Morphology	Powder: 0.2 g
	Pellets: 0.8 g
Mass of Catalyst Loaded	1 g
Temperature	200-400°C
Pressure	1 atm
Feed Rate	0.29 mol/h

## 7.2.3 Results and Discussion

### 7.2.3.1 Catalytic Performance

The composition of each sample collected is determined by Agilent Gas Chromatography/Mass Spectrum 5975C with a DB-WAX column. To quantify the concentration of MCH and toluene, a calibration curve is developed by making standard samples with known composition.

Conversion  $x$  here is defined as

$$x = \frac{n_{MCH\ reacted}}{n_{MCH\ feed}} = \frac{n_{MCH\ feed} - n_{MCH\ product}}{n_{MCH\ feed}} \quad (26)$$

where  $n_{MCH\ feed}$  is the molar flow rate of the feed,  $n_{MCH\ product}$  is the molar flow rate of MCH in product. The conversion of dehydrogenation from 177°C to 402°C is shown in Figure 53. The triangle data points are from Reference using similar catalyst<sup>92</sup>.

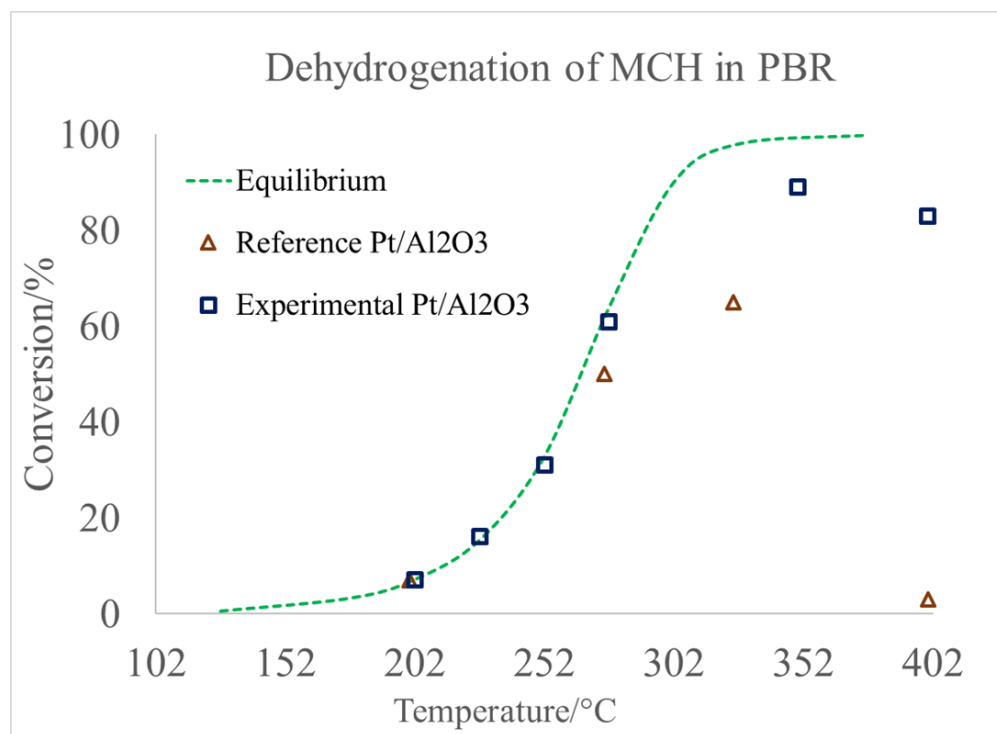


**Figure 53 Dehydrogenation of MCH in PBR**

The catalyst performance is satisfying as equilibrium is achieved until approximately 275°C. Comparing to reference data, catalyst used in the reaction endures slightly higher temperature. Nonetheless, its activity declined as the temperature climbs up. The catalyst no longer boosts the conversion to equilibrium. At 350°C and higher, side product Benzene appears in the GC spectrum indicating the compromise of selectivity as well. At 400°C, reference catalyst shows no activity. While the catalyst used in our experiment initially displays partial activity, it gradually weakens as the reaction runs for extended amount of time, which occurs around 3-4 hours. The loss of activity and selectivity of the catalyst is possibly due to coking, which tends to occur at elevated temperatures. The speculation is backed by the fact that the surface of catalyst has turned black, indicating its transformation to coke, after the reaction runs at 400 °C.

**Table 8 Side Product at 350/400 °C**

Reactor Temperature (°C)/Reaction Time(h)	Appearance of Benzene
350/0.5	No
350/1	No
350/3	Yes
400/0.5	No
400/1	No
400/3	Yes
400/4	Yes

In conclusion, the catalyst realizes its full potential between 200-300°C. It provides an idea of a rough temperature range for the next steps to be conducted. As a result, this catalyst is feasible for this reaction and for the membrane. The details will be discussed in the following context.

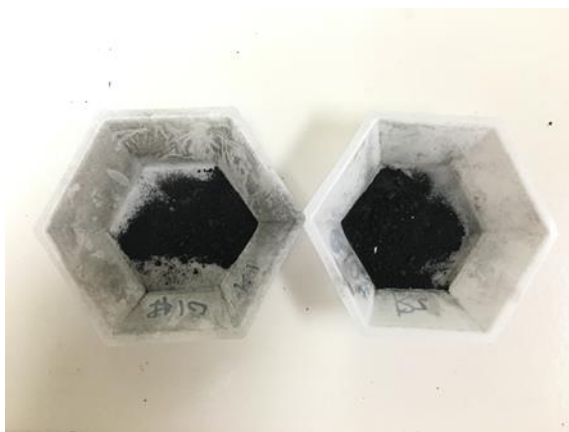


**Figure 54 Picture of catalyst coking after reaction run at 400 °C**

#### **7.2.3.2 Predicted Membrane Performance**

The transport properties including permeability and selectivity data of blend polymeric material Matrimid/PBI acquired from previous context can be used to deduce the performance of membranes fabricated from this blend material. The size of the membrane is determined by reactor configuration. The size of the membrane cell (13.8 cm<sup>2</sup>) in the reactor system becomes the size of membrane in the computation. The thickness of the dense separation layer is set at 0.25 μm, a common value for such sized polymeric membrane.

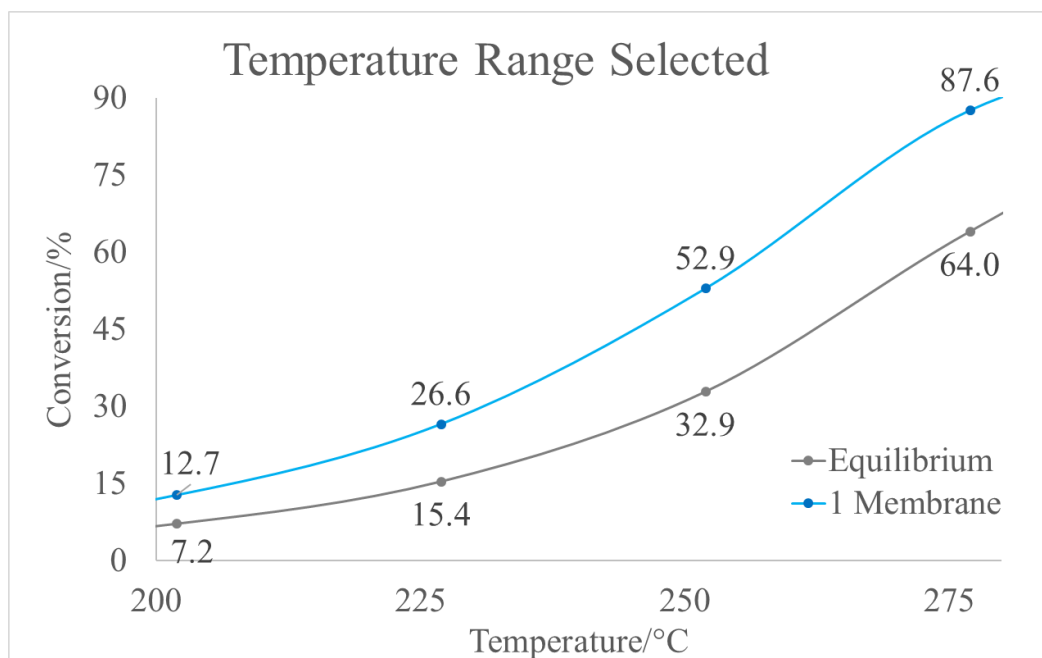
The reactor condition in the computation is assumed identical to the conditions in the catalytic performance evaluation step. In this fashion, the equilibrium conversion data is applied to the computation as it has proved the catalytic performance supported the reaction to achieve equilibrium. The selectivity of the catalyst is 100% where no side or intermediate product appear.

**Table 9 Membrane Configuration**

Membrane Type	Matrimid/PBI Blend Membrane
Membrane Size	13.8 cm <sup>2</sup>
Dense Layer Thickness	0.25 μm
Temperature	200-300°C
Pressure	1 atm

The reactor and separator system temperatures are set from 202-277 °C. This range selected because of the following reasons

- 1) The ideal increase of conversion in this range is maximized;
- 2) Catalyst performance in this range is consistent and stable indicating
  - No side product
  - Reaches equilibrium

**Figure 55 Temperature Range Selected**

The feed rate of MCH is varied from 0.29-0.39 mol/h, as they are fixed settings on the syringe pump.

The permeability data of MCH, toluene and H<sub>2</sub> of 90/10 and 50/50 blend materials is acquired from previous chapter. The thermal stability of the blend material in this temperature range is guaranteed by the investigation from previous chapter. The thickness of the separation layer here is set with a common thickness of 0.25 μm. In addition, the pressure on the reactor side (retentate side) is 1-2 bar. The vacuum on the permeate side is at 0.1 torr, an industrial level.

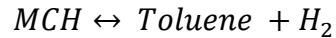
The permeation of the membrane is governed by the permeability of the material, the thickness of the separation layer and the pressure difference between the permeate side and retentate side of the membrane. From the conditions provided above, we can obtain the permeance of membranes under different temperatures and pressures. In the simulation process, MCH is heated and reacted in the first PBR, where the reaction reaches equilibrium. The equilibrium conversion is obtained from computation from previous chapter. Then, the mixture of MCH, generated toluene and H<sub>2</sub> enter the membrane separation unit, where a portion of the mixture leaves the system through the membrane according to the permeability and selectivity. The remaining MCH/toluene/H<sub>2</sub> mixture carry on to the second catalyst bed, where a new equilibrium conforms. The overall conversion obtained is compared to system with the same reactor conditions and WHSV but without a membrane separation unit.

Following is an example of the simulation computation of a Matrimid/PBI 90/10 blend membrane at 202 °C, 1 bar. The equilibrium conversion is  $x_1 = 7.17\%$ . The permeability is shown below.

**Table 10 Permeability of 90/10 Blend Material at 202 °C**

	MCH	Toluene	Hydrogen
Permeability (Barrer)	0.388	0.410	59.9

@ The first Packed-bed,



Initial (mol/h)	0.0294	0	0
Reacted/Generated (mol/h)	0.0021	0.0021	0.0063
Equilibrium (mol/h)	0.0273	0.0021	0.0063

@ The membrane separator,

Combining the size and thickness of the membrane and the pressure at the membrane cell, the unit is converted from GPU to mol/h using the table in Appendix H.

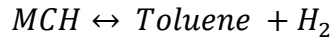
The following table displays the amount of each component leaving by permeating through the membrane (Permeate Side) and the amount of each component remaining in the system (Retentate Side).

In this case, all the H<sub>2</sub> generated by the first packed-bed is removed by the membrane. Only a trace amount of MCH and toluene left the system thanks to the decent selectivity of H<sub>2</sub>/hydrocarbon of the blend material.

**Table 11 Membrane Separation Performance at 202 °C, ΔP=1.0 bar**

	MCH	Toluene	Hydrogen
Permeate Side			
(mol/h)	0.000156	0.000165	0.0072
Retentate Side			
(mol/h)	0.0271	0.00194	0

@ The second Packed-bed,



Initial (mol/h)	0.0271	0.00194	0
Reacted/Generated (mol/h)	0.00164	0.00164	0.00493
Equilibrium (mol/h)	0.0254	0.00358	0.00493

The Reacted/Generated data is calculated by using equation (28)

$$K^{\ominus} = \frac{n_{TOL} \cdot n_{H_2}^3}{n_{MCH}} \cdot \frac{1}{n_{total}^3} \cdot \frac{p^3}{p^{\ominus 3}} \quad (28)$$

Thus, conversion of the second reactor is

$$x_2 = 6.06\%$$

Overall conversion is

$$x = 12.76\%$$

Compared to equilibrium conversion of no membrane unit utilized, the conversion increased by ~5%. Computation methods at other temperatures and feed rates are identical with the one introduced.

#### 7.2.3.2.1 Pressure at 1 bar

The following figures demonstrate the impact of utilizing a membrane-assisted packed-bed reactor in the dehydrogenation by simulation. In these figures, the green bar is equilibrium



conversion (PBR without membrane), the blue bar symbolizes the ideal situation where none hydrocarbon but all  $H_2$  is removed. For the scenarios with the system pressure at 1bar, the performance of membrane approximately agrees with the ideal situation at 202°C, which is a result of relatively high  $H_2$  permeance and  $H_2$ /hydrocarbon selectivity of the membranes regardless of their composition. At this temperature, the hydrogen removal capacity of both 50/50 and 90/10 membranes are not completely exploited. Thus, running the reaction at a higher WHSV (feed rate 0.389 mol/h) leads to a higher efficiency. However, starting from 227 °C, running the dehydrogenation at higher feed rate (0.389 mol/h) results in a subpar conversion comparing to running at 0.294 mol/h. The reason behind it is obvious, that at elevated temperature,  $H_2$  production from the 1<sup>st</sup> packed-bed increases, the hydrogen removal capacity of these membranes, although increases as well, are already fully exploited before all  $H_2$  generated is removed.

With more  $H_2$  carried on to the 2<sup>nd</sup> reactor, the driving force to push the thermodynamic barrier is not as powerful as the circumstance where there's less (0.294 mol/h feed rate) or no (ideal scenario)  $H_2$  presented. Thus, at 227°C and 252°C, only 50/50 membrane at slower feed rate (orange mark) completed the task to its full potential. In addition, 50/50 membranes are achieving better conversions than 90/10 membranes due to their superior transport properties.

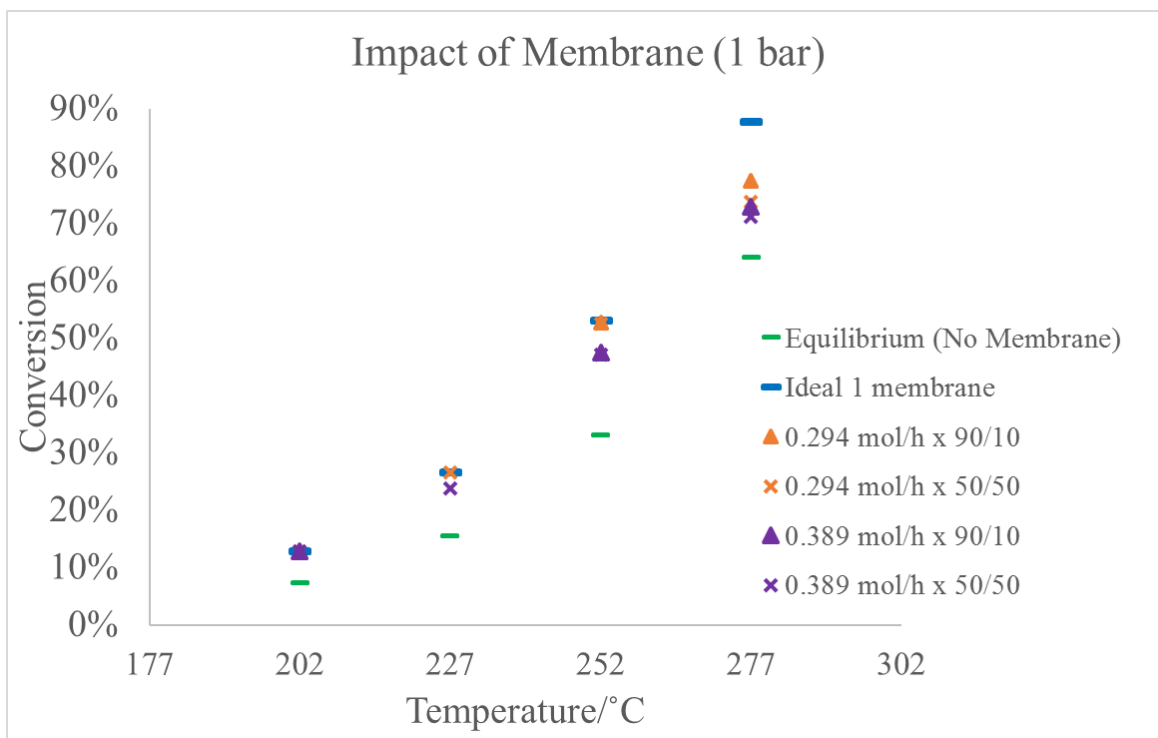


**Figure 56 Impact of Utilizing Membrane-assisted Packed-bed Reactor Comparing to Conventional PBR at 1 bar**

The results at 272 °C are similar to 227 °C. At this temperature, both 50/50 and 90/10 membranes perform at their highest capacity yet a portion of H<sub>2</sub> retains in the retentate side. Thus, the less H<sub>2</sub> presented at the membrane cell, the better increase of conversion it shows after the 2<sup>nd</sup> reactor, which is the lower feed rate scenario. Interestingly, at 252 °C, 50/50 membrane displays better removal capacity; yet at 272 °C, 90/10 membrane displays better removal capacity. The reason is explained in previous chapter.

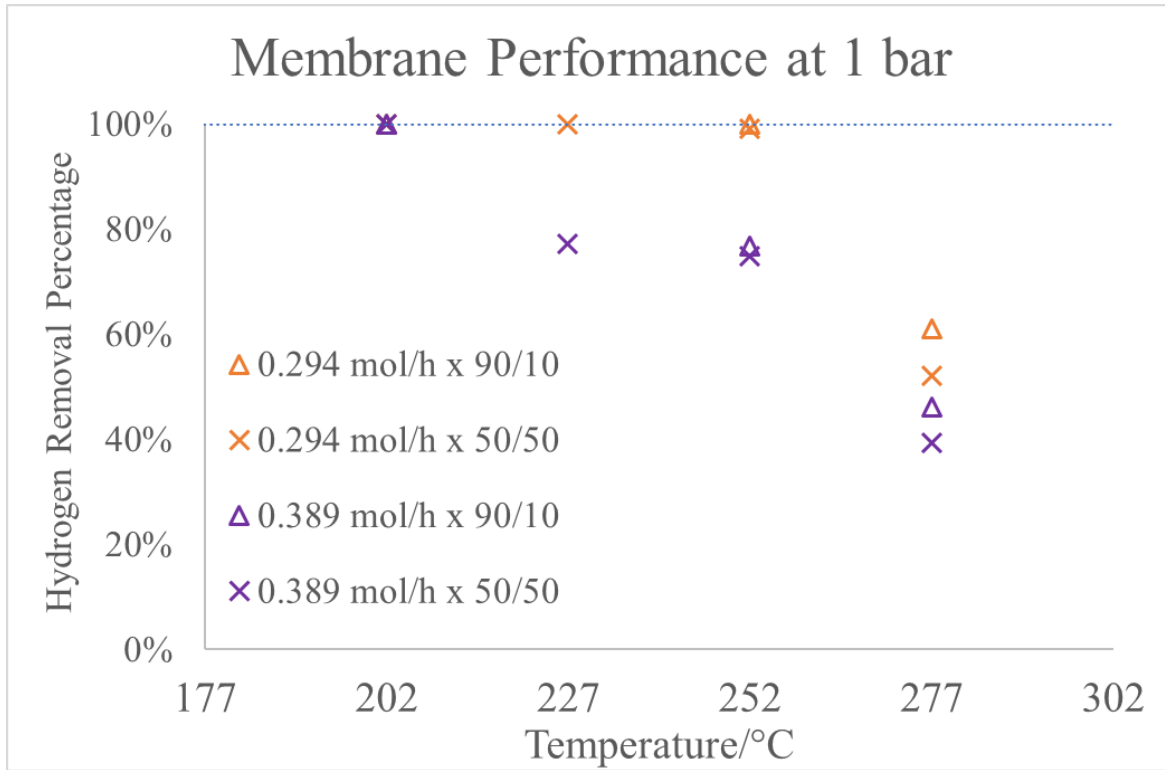


**Figure 57 H<sub>2</sub> Removal Performance at 1 bar**

Figure 57 illustrates the H<sub>2</sub> removal performance which is defined by

$$\theta = v_{HG}/v_{HR} \quad (29)$$

Where  $v_{HG}$  is the H<sub>2</sub> flow rate after the first packed-bed,  $v_{HR}$  is the H<sub>2</sub> permeation rate of the membrane. The ability of the membrane to remove H<sub>2</sub> directly affect the improvement of conversion of the system. At elevated temperatures,  $\theta$  has declined to approximate 50%, leading to the unsatisfying overall increase of conversion. There are several ways to facilitate the efficiency of the whole system. For instance, to slow down the H<sub>2</sub> flow rate at the membrane. This can be accomplished by slow down the MCH feed rate or increasing the reactor pressure (which reinforces the thermodynamic barrier). In addition, improving the performance of the membrane is another approach to enhance efficiency. This can be accomplished by enlarging the

membrane area, increasing driving force of permeation and emaciate the thickness of the separation layer.

The increase of conversion in each scenario is more intuitively demonstrated in Figure 58. By utilizing membrane-assisted packed-bed reactor at 1 bar, the conversion indefinitely increases regardless of certain membrane composition or selected MCH feed rate. The change of conversion is most drastic at the temperature of 252 °C. A maximum increase of 14% is achieved.

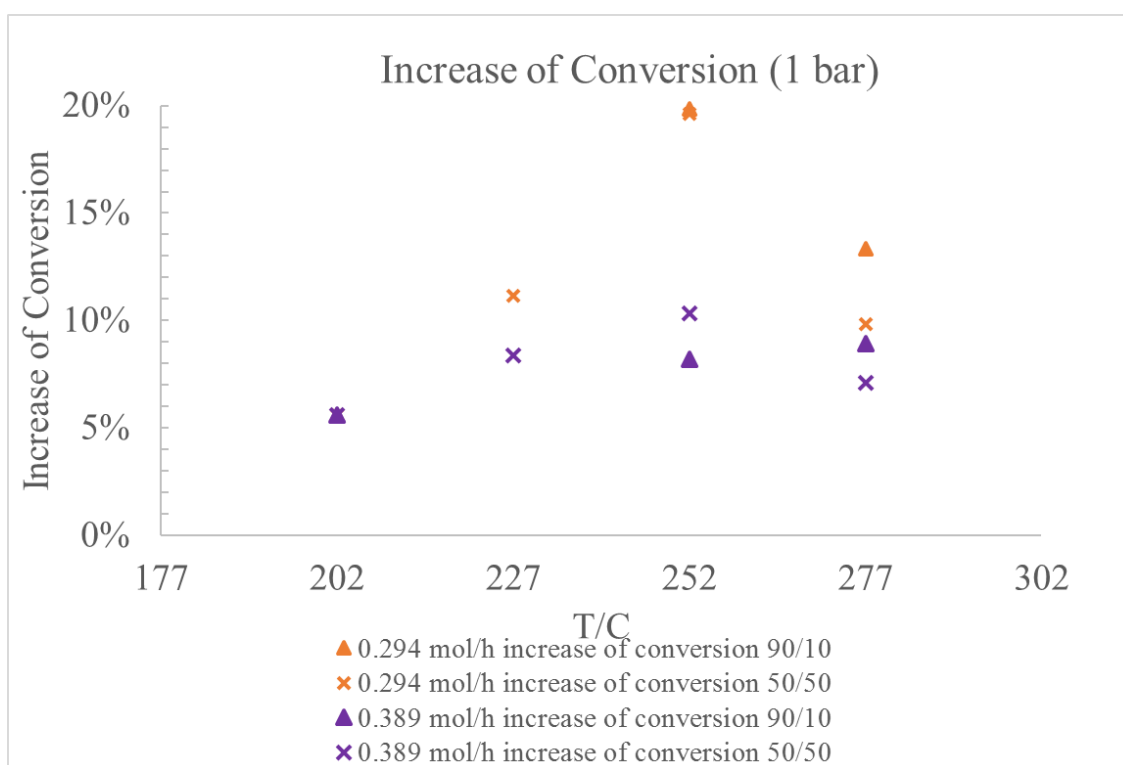
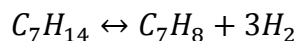


**Figure 58 Increase of Conversion in an Intuitive Illustration at 1 bar**

#### 7.2.3.2.2 Pressure at 2 bar

Pressure change has opposite effects on the membrane removal performance and dehydrogenation equilibrium conversion. For the dehydrogenation of MCH,



Increasing pressure induces equilibrium to shift backwards, representing a lower equilibrium conversion, which is not favorable to this application. Nevertheless, increasing pressure, on the other hand, increases pressure difference - the driving force of permeation - between permeate side and retentate side.

$$j_i = \frac{D_i S_i (p_{i0} - p_{iL})}{l} \quad (30)$$

As a result, as shown in Figure 59, thermodynamic barrier depresses the equilibrium curve to a lower position; while the hydrogen removal performance of the membrane enhances, indicating a better efficiency.

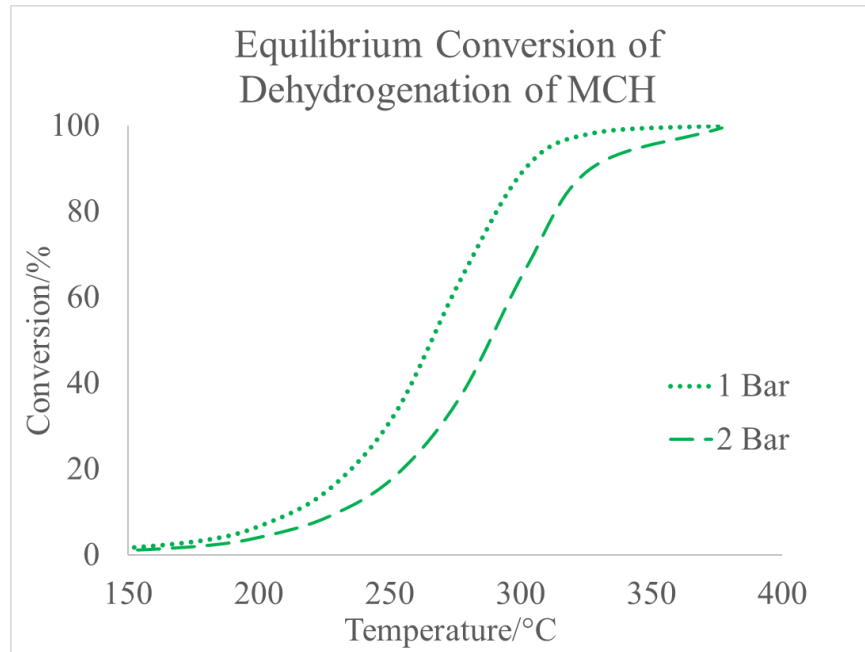


**Figure 59 Equilibrium Conversion of Dehydrogenation of MCH at 1 bar and 2 bar.**

Thus, similar investigation is conducted to predict the impact of utilizing membrane-assisted packed-bed reactor at 2 bar. Same membranes (90/10 Matrimid/PBI & 50/50 Matrimid/PBI) and feed rates (0.294 mol/h & 0.389 mol/h) are selected for computation.

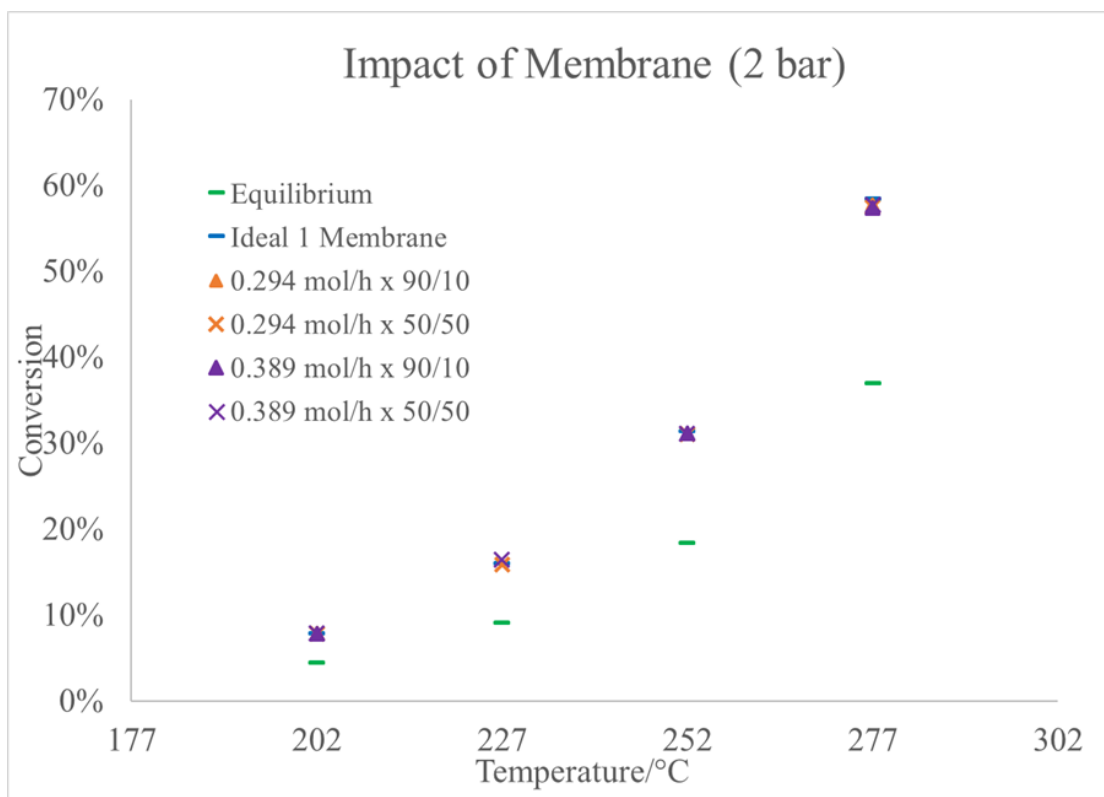


**Figure 60 Impact of Utilizing Membrane-assisted Packed-bed Reactor Comparing to Conventional PBR at 2 bar**

As illustrated in Figure 60, using the same membrane to operate at same feed rate displays distinct results from 1 bar to 2 bar. At 2 bar, from 202 °C to 277°C, every scenario eventually reaches the ideal conversion with the help of the membrane. This indicates that regardless of composition or feed rate, H<sub>2</sub> removal performance of the membrane always satisfies the demand at 2 bar.

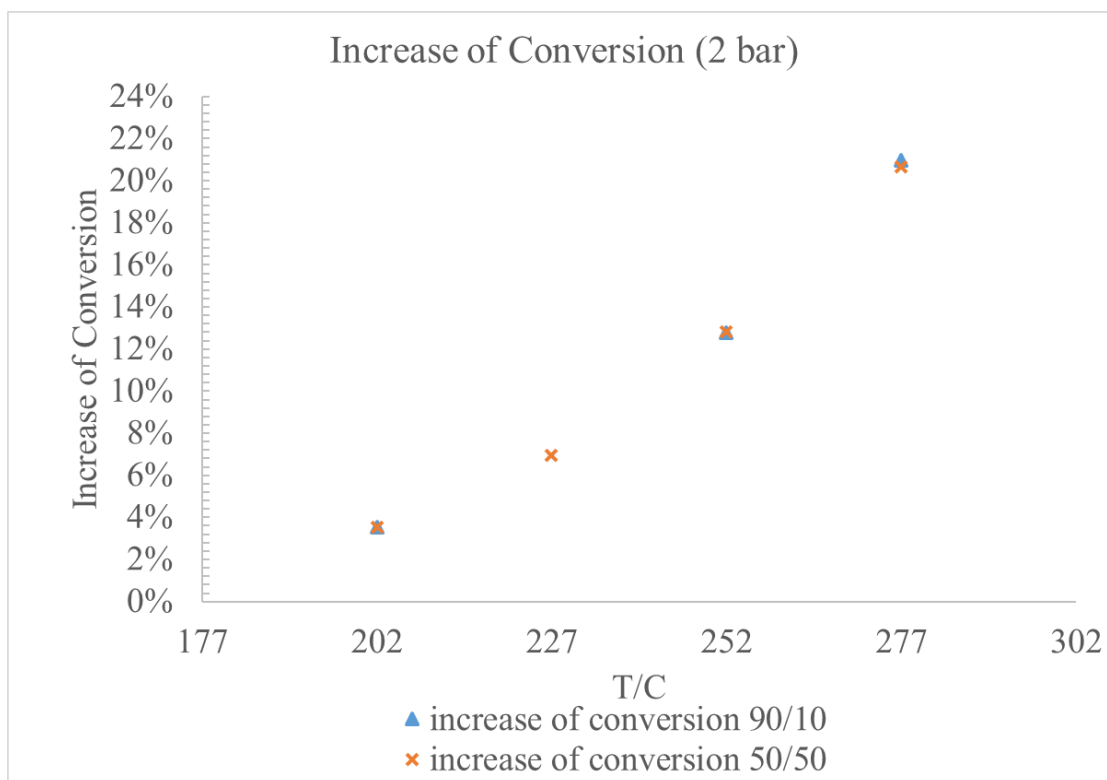


**Figure 61 Increase of Conversion in an Intuitive Illustration at 2 bar**

In conclusion, by combining the tested catalyst performance, measured transport properties of the material, and a hypothetical membrane configuration, it is shown that adding a single membrane separation unit between two packed-beds (membrane assisted packed-bed reactor), the thermodynamic barrier of the reaction can be broken through the selective removal of  $H_2$ . The overall conversion can be increased by up to 20%, beyond the equilibrium at either 1 or 2 bar system pressure.

Figure 62 compares the performance of the membrane at different pressure. At 1 bar, because of the higher equilibrium conversion at each temperature, a larger quantity of hydrogen is produced from the 1<sup>st</sup> packed-bed comparing to that produced at a system pressure of 2 bar. As temperature increased, the membranes evaluated are not sufficiently sized to remove 100% of the hydrogen. The residual hydrogen in the reaction mixture fed to the second catalytic bed limits the

additional conversion that can be achieved. Recall, that in all cases, the catalytic system goes to the equilibrium conversion possible. For these cases where some hydrogen is feed to bed two, the additional conversion possible is intermediate between that of the dashed blue line shown in Figure 62 (the equilibrium conversion with 0% of the hydrogen removed from the product of bed one), and the solid blue line (100% of the hydrogen removed from the product of bed one). The intermediate performance achieved by the various cases evaluated is represented by the blue symbols in Figure 62. In contrast, when the total system pressure is increased to 2 bar, although equilibrium conversion is lower at each temperature than at 1 bar, the membrane operated with a higher driving force and in all scenarios evaluated was fully capable of removing all the hydrogen from the first reactor.

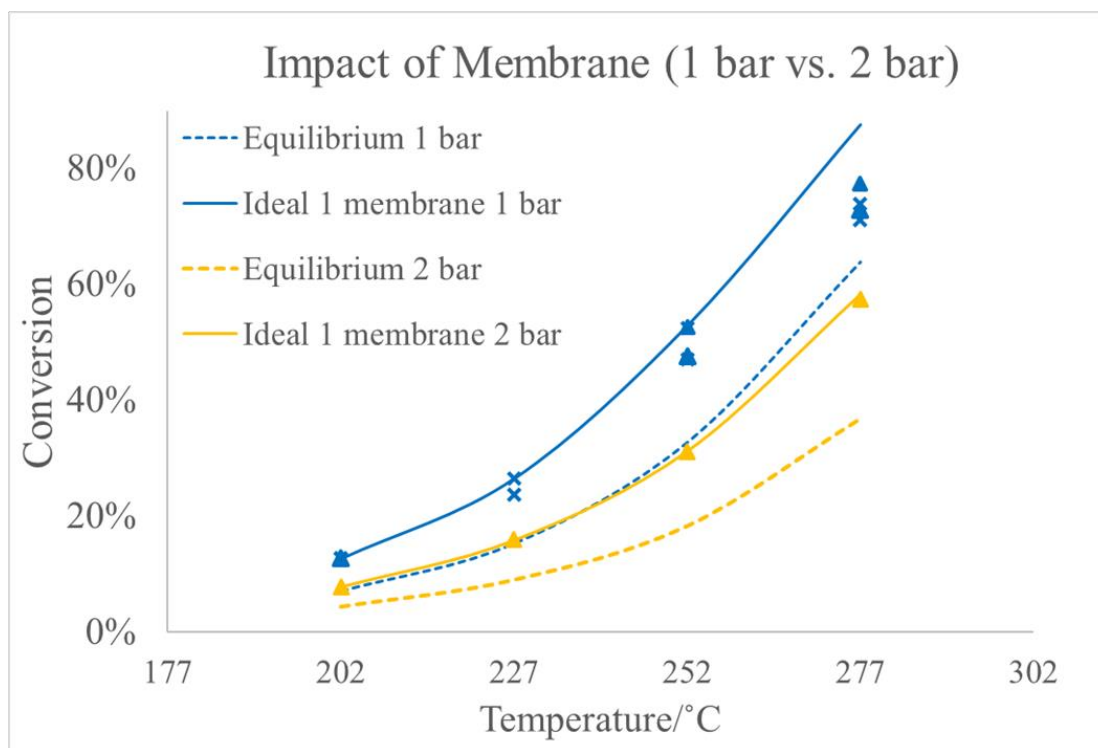


**Figure 62 Comparison on the Impact of System Pressure**

In the membrane-assisted packed-bed reactor system, operating at higher pressure in fact resulted in more efficient  $H_2$  removal by the membrane and superior performance of the system. For a



given conversion, operating at higher pressure also reduces the size of the membrane and size of the reactor, which will likely reduce the cost of operation. In contrast to the thermodynamic understanding, that the system is more efficient at lower pressure since greater equilibrium conversion is achieved by decreasing the system pressure, from an economical aspect, operating at an elevated pressure may be the more efficient choice. A thorough economic evaluation of the system will be required to fully answer this question, but the positive results of operating at elevated pressure are important to note.

## **Chapter 8 Dehydrogenation of Methylcyclohexane in Membrane-Assisted Packed-Bed Reactor: Experimental Validation**

### **8.1 Introduction**

From the last chapter, we can draw the conclusion that in theory, the idea of using a membrane-assisted packed-bed reactor to break the thermodynamic barrier and increase the conversion of the dehydrogenation of methylcyclohexane is feasible. The next step naturally falls on the experimental validation of the predicted results, where the methods and conclusion from Chapter 6 and Chapter 7 are combined.

In order to perform the experiment, a membrane using the proven thermally stable blend Matrimid/PBI material is the most significant part that need to be prepared. An intrinsically skinned asymmetric polymeric membrane is utilized in this work. The fabrication method is adopted from literature<sup>50</sup>. The membranes prepared by this phase inversion method is proven to be thermally stable up to 300 °C.

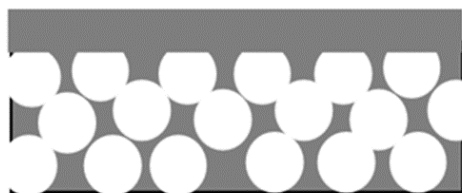


**Figure 63 A Schematic of Intrinsically Skinned Asymmetric Polymeric Membrane. It Consists of a Porous Substructure and a Thin Dense Separation Layer.**

Broadly, hydrogen selection membranes (based on the materials used) can be categorized into four types: polymer (organic), metallic, carbon, and ceramic<sup>93</sup>. Specifically, membranes for hydrogen separation should have the following characteristics:

1. High selectivity towards hydrogen.
2. High flux.
3. Low cost.
4. High mechanical and chemical stability<sup>94,95</sup>.

Permeance and  $H_2/HC$  selectivity are the crucial parameters to define if the membrane is suitable in separating hydrogen from methylcyclohexane and the other product toluene. From previous

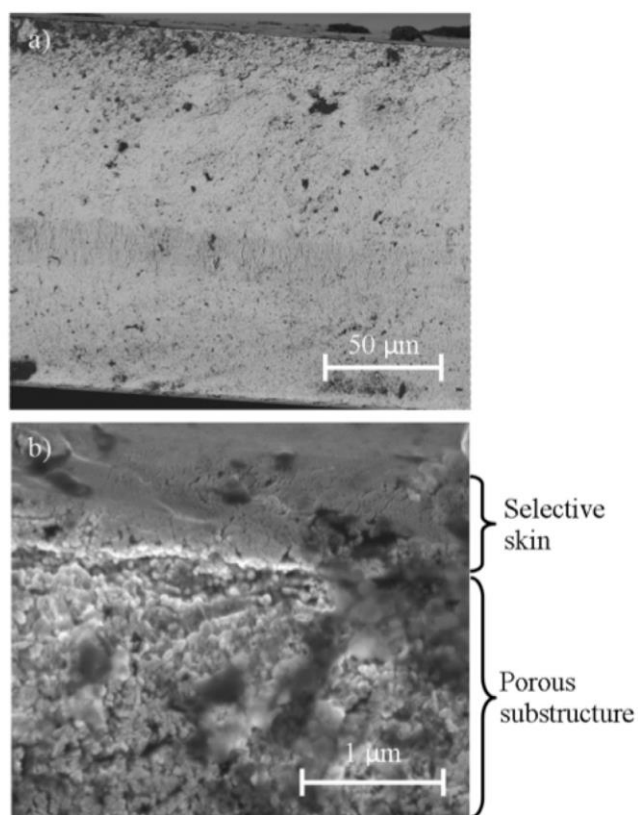


**Figure 64 SEM Images of Cross-section of 50/50 Matrimid/PBI Blend Membrane**

context, we have concluded that the blend material of Matrimid and PBI is provided with satisfactory selectivity of  $H_2/MCH$  and  $H_2/Toluene$ . Thus, the membrane fabricated by the blend material ought to possess the same property as the dense film. However, because of human error in the fabrication process, the structure of the membrane is not always perfect. For example, the failure to construct the asymmetric structure, the defects on the separation layer, etc. can cause the membrane to have minimal permeance, or large permeance with a  $H_2/HC$  selectivity close to one. From appearance, the surface of a defect-free membrane should be homogeneously constructed, without the presence of ditch and dent. Another simple and effective way to determine the quality of the membrane is to measure and calculate the selectivity of  $H_2/N_2$  under room temperature. A membrane with reasonable  $H_2$  permeance and  $H_2/N_2$  is considered good candidate to be utilized in the separation.

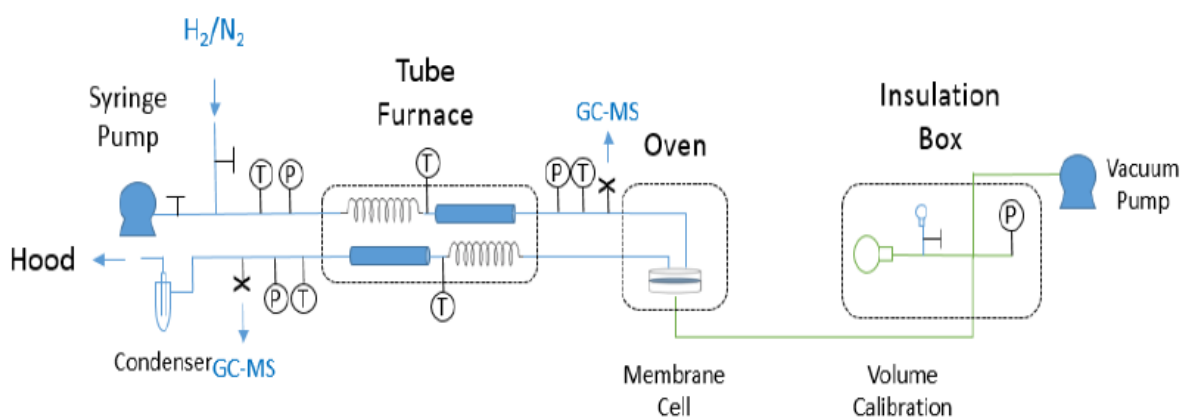


**Figure 65 Schematic of the Membrane-assisted Packed-bed Reactor**

The reactor system is the same one described in chapter 6. However, in the following context, an actual membrane is placed in the membrane cell for hydrogen removal as MCH is fed and reaction occurs.

## **8.2 Experimental**

### **8.2.1 Materials**

Catalyst, Hydrocarbons and Gas used in the experiments have been described in details in Chapter 7.

#### **8.2.1.1 Membrane Materials**

Matrimid 5218 and Polybenzimidazole are identical with the ones used in Chapter 6.

### **8.2.2 Apparatus**

The reactor system is adapted from the one introduced in Chapter 6. The temperature of the oven chamber where the membrane cell is located is monitored and controlled by Omega thermocouples and temperature controller.

### **8.2.3 Preparation of the Membrane**

Membranes were made with a PBI/Matrimid mass percent of 50/50. The following fabrication method is acquired from the work of Schulte et al. A solution with the following solvents: 23g of NMP, 23g of dimethylformamide (DMF), and 9g of toluene. 9.5g of PBI was added and the solution was stirred one day at 120°C. 9.5g of Matrimid is added to the solution. The solution was stirred for another 24 hours at 60°C. Then the solution temperature was lowered to 35°C without stirring. Membranes were cast 350µm thick on a glass plate using Gardner casting knife. The casted solution underwent a period of forced evaporation before being quenched in a bath of DI water for 24 hours. The membranes were solvent exchanged in three methanol followed by three hexane baths for 30 minutes each. Membranes were placed in a hexane-enriched environment for 24 hours. They were then hung to dry in air overnight<sup>50</sup>.

The membrane sheet is accordingly cut to a circular shape with the size of 13.8 cm<sup>2</sup>.

### 8.2.4 Characterization of Membrane

The permeation of the membrane is measure in a constant pressure-variable volume measurement system. All the measurement is in room temperature between 19-26 °C. The pressure difference between the permeate and retentate side is 50 psig. The permeance is acquired by the following equation

$$\frac{P}{\ell} = \frac{\Delta V}{\Delta p \times A_{\text{membrane}} \times \Delta t} \times 10^6 \quad (12)$$

Where:  $\frac{P}{\ell} \equiv$  Permeance [GPU]

$\Delta V \equiv$  Ideal gas volume that permeates the membrane [ $\text{cm}^3$  (STP)]

$\Delta p \equiv$  Pressure difference across the membrane [cmHg]

$A_{\text{membrane}} \equiv$  Area of the membrane available for flux [ $\text{cm}^2$ ]

$\Delta t \equiv$  Time interval of flux [s]

The ideal  $\text{H}_2/\text{N}_2$  selectivity of the membrane is determined by the following equation:

$$\alpha_{\text{H}_2/\text{N}_2} = \frac{\left(\frac{P}{\ell}\right)_{\text{H}_2}}{\left(\frac{P}{\ell}\right)_{\text{N}_2}} \quad (13)$$

### 8.2.5 Reaction and Separation Procedure

The selected membrane is placed in the membrane cell before the reaction starts. The following procedure is identical to the procedure in Chapter 7. The membrane chamber temperature is maintained at the same with the furnace temperature. This is very essential in industrial processes, as no external cooling or heating equipment is required. The process is evaluated from 175°C to 275°C at 1 bar. In the preliminary experiments, only flow rate at 0.294 mol/h is studied.

**Table 12 Summary of System****a) Reactor (Catalyst Bed) Conditions**

Catalyst Type	1%wt Pt/ $\gamma$ -Al <sub>2</sub> O <sub>3</sub>
Catalyst Morphology	Powder & Pellets
Mass of Catalyst Loaded	1 g each bed
Temperature	175-275°C
Pressure	1 bar
Feed Rate	0.29 mol/h

**b) Membrane Cell Conditions**

Membrane Type	50/50 Matrimid/PBI Blend Membrane
Membrane Size	13.8 cm <sup>2</sup>
Membrane Thickness	~120 $\mu$ m
Temperature	175-250°C
Pressure	1 bar

## 8.3 Results and Discussion

### 8.3.1 Transport Properties of the Membrane

H<sub>2</sub> and N<sub>2</sub> permeance of the membranes are measured. H<sub>2</sub>/N<sub>2</sub> selectivity is calculated from the permeation. Most of the membranes have a H<sub>2</sub> permeance of 40-120 GPU, N<sub>2</sub> permeance of 1-17 GPU at room temperature (25-28°C). H<sub>2</sub>/N<sub>2</sub> selectivity of membranes over 40 are utilized in the separation process in the reactor system.

As temperature increases from room temperature to around 275°C, it is expected that N<sub>2</sub> permeance will increase while H<sub>2</sub> permeation will decline due to the densification of the structure<sup>50</sup>.

### 8.3.2 Effect of the Membrane on the Dehydrogenation of Methylcyclohexane

The main effect in interest for the system is the change in conversion of the dehydrogenation of methylcyclohexane, as well as the selectivity of the conversion to the desired product toluene and hydrogen.

The conversion  $x_{overall}$ , is the overall conversion of the two packed-beds, which is defined as,

$$x_{overall} = \frac{n_{MCH \text{ overall reacted}}}{n_{MCH \text{ feed}}} = \frac{n_{MCH \text{ feed}} - n_{MCH \text{ final product}}}{n_{MCH \text{ feed}}} \quad (31)$$

where  $n_{MCH \text{ feed}}$  is the molar flow rate of the feed,  $n_{MCH \text{ final product}}$  is the molar flow rate of MCH in product after the 2<sup>nd</sup> catalyst bed.

$$Selectivity = \frac{n_{Tol}}{n_{MCH \text{ feed}}} \quad (32)$$

where  $n_{tol}$  is the molar amount of toluene produced.

The target here is apparent, to validate the results from the computational prediction, where overall conversion of dehydrogenation of methylcyclohexane is increased at high catalytic selectivity.



Following are the considerably successful preliminary results from many reaction runs. Catalytic selectivity from 177°C to 252° all remained at 100% as no side product is observed from the GC spectrum. This result agrees with the experiments without the presence of the membrane from Chapter 7. In addition, reaction at each temperature either achieve or surpass equilibrium conversion, indicating the membrane does not affect catalytic activity.

The focus is the increase of conversion. From Table 14, at 177 °C and 227 °C, the thermodynamic barrier is partially broken. The overall conversion was increased by a big margin from the equilibrium conversion. From the explicit surmount of equilibrium conversion at these temperatures, one can conclude that the removal of hydrogen by the membrane is effective.

**Table 13 MCH Dehydrogenations with Membrane Assistance**

Temperature (°C)	Equilibrium Conversion (%)	Overall	Overall	Side Product
		Conversion	Conversion	
		Simulated (%)	Experimental (%)	
177	3.3	5.9	5.6	None
227	15.4	26.6	23.9	None
252	32.9	47.3	30.5	None
*202	7.2	12.8	No data	None

\*The sample collected at 202 °C was not viable for analysis.

The effectiveness of hydrogen removal by the membrane is demonstrated indirectly from the comparison of the increases of conversion between the simulation and experimental validation in Figure 66. At 177 °C and 227 °C, both simulation and experimental data are available. The overall conversion from simulation and experiments are almost consistent, both being in the vicinity of the ideal scenario. From Chapter 7, at both temperature, the removal performance of

50/50 membrane at 0.294 mol/h is fully exploited. The experimental data being congenial to the predicted result reveals in the experiment, the membrane removed the majority of hydrogen produced from the first reactor tube.

The membrane remained its physical integrity and displayed no degradation after the process.

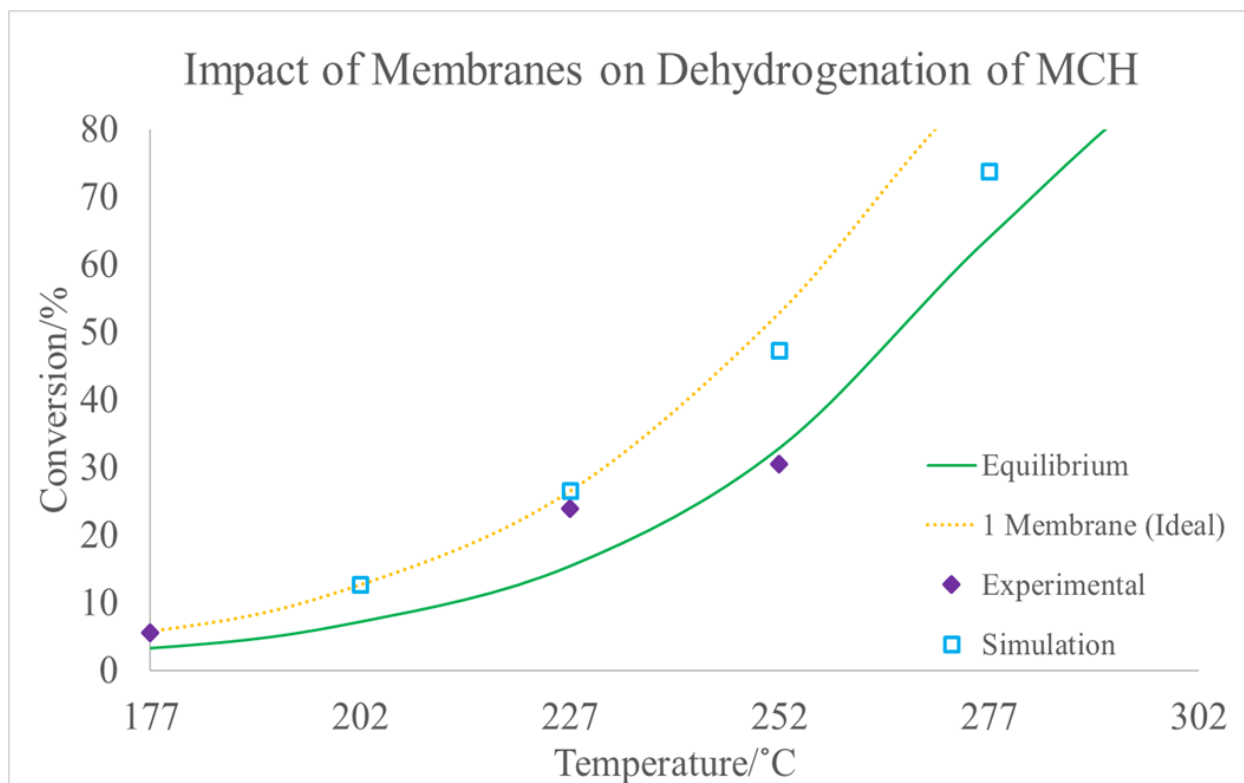


**Figure 66 Effect of the Membrane in the Dehydrogenation of Methylcyclohexane by Selective Removal of Hydrogen**

### 8.3.2.1 Mechanical Stability of the Membrane at Elevated Temperature

The exception was at 252 °C. Instead of an increase, the overall conversion of the reaction decreased by ~1.5 percent from the equilibrium conversion. Namely, the performance of the membrane is compromised. The possible reason is that the porous substructure of the membrane collapsed<sup>96,97</sup>. The densification of the substructure results in the drop of H<sub>2</sub> permeance. Thus, a

less amount of  $H_2$  is removed from the membrane; the thermodynamic limit hence is not surpassed under this situation.

Further investigation is required for more evidence for the failure of the membrane. However, there are various ways to reduce the effect. For instance, the substructure can be tightened by using a crosslinking agent<sup>98,99</sup>. In this way, the substructure becomes more rigid under elevated temperatures. Another approach is, instead of intrinsically skinned asymmetric, to utilize a composite membrane. In a composite membrane, the skin layer and the porous substructure are made from different materials. The skin layer is still be prepared using the polymeric blend material for high separation performance. Yet the skin layer is deposited on a substructure that is prepared from a more thermally resistant material, such as ceramic<sup>100,101</sup>.

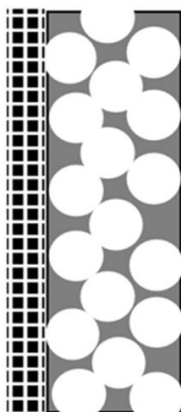


**Figure 67 Schematic of a Composite Membrane**

To better determine the effect of the membrane, more parameters are to be obtained. For example, the permeation rate of  $H_2$  and hydrocarbons at varied temperatures, mass balance of the entire system, and characterization of membrane after exposed to elevated temperatures and hydrocarbons.

To make the system more effective and efficient, catalyst performance also needs to be evaluated. At this stage, we can only conclude that the membrane was effective in the removal of hydrogen in the dehydrogenation of methylcyclohexane. In addition, the experimental data agrees with the computational data, proving both the experimental results and the simulation results are reliable.

## **Chapter 9 Conclusion and Future Work**

### **9.1 Conclusion**

Two types of membrane reactor systems, membrane contactor and membrane-assisted packed-bed reactor using robust PEI and Matrimid/PBI blend polymeric membranes have been investigated for various applications. Asymmetric PEI membranes, Matrimid/PBI blend dense films and asymmetric Matrimid/PBI blend membranes have been fabricated using different methods. The physical and transport properties of asymmetric PEI membranes, Matrimid/PBI blend dense films and asymmetric Matrimid/PBI blend membranes have been examined for proper utilization. Catalytic PEI membranes have been utilized in the hydrogenation of soybean oil and hydro-oxygenation of bio-oil in a 3-phase membrane contactor. The feasibility of using thermally stable Matrimid/PBI blend membrane in dehydrogenation of methylcyclohexane has been studied.

#### **9.1.1 Hydrogenation in 3-Phase Membrane Contactor**

Intrinsically skinned asymmetric PEI membranes have been fabricated using the phase inversion method. The membranes have demonstrated predominant  $H_2$  permeance and excellent  $H_2$  selectivity. Pd catalyst is successfully deposited onto the surface of the membrane by sputter coating. And the activity of catalyst is validated.

A 3-Phase membrane contactor has been utilized for the hydrogenation of soybean oil. By using a robust PEI membrane as the phase contactor,  $H_2$  supplier and catalyst support, soybean oil is partially hydrogenated. The saturation level increased as the Iodine Number dropped from 131 to 80 after the hydrogenation process.

The 3-phase membrane contactor is also adapted as the reactor system for the hydroprocessing of bio-oil to remove oxygen as the form of water (fast pyrolysis product of 2<sup>nd</sup> generation biomass).

The activity of the catalyst is challenged by the complicated composition and the dense viscosity of bio-oil. Nevertheless, the membrane successfully removed water, another undesired component from bio-oil by pervaporation.

These results indicate that the membrane contactor is a favorable choice for 3-phase heterogeneous catalytic reactions. Particularly with the reactions that are restricted by the mass transfer of gas approaching the catalyst. With the utilization of robust PEI membranes, the 3-phase contactor can be applied to various hydrogenations to acquire desirable products at relative mild conditions.

### **9.1.2 Alkane Dehydrogenation**

Thermal stability and transport properties of blend polymeric material PBI and Matrimid are investigated by examining dense film made from the blend material at varied mass ratio (50:50 and 90:10). The material demonstrated consistent performance from room temperature to 275°C. At elevated temperature, the permeability of common gases such H<sub>2</sub> and N<sub>2</sub> conformed with theory, indicating favorable thermal stability. In addition, the material remained stable with the presence of hydrocarbons methylcyclohexane and toluene, displayed decent selectivity of H<sub>2</sub>/Hydrocarbon, reveals the feasibility of using the material to fabricate thermally stable membrane for separation.

The viability of utilizing Matrimid/PBI blend membrane in dehydrogenation of methylcyclohexane to increase conversion and selectivity is then studied by using finite parameter process simulation. A membrane-assisted packed-bed reactor is built for preliminary catalyst (Pt/ $\gamma$ -Al<sub>2</sub>O<sub>3</sub>) performance examination without the assistance of the membrane. The temperature range of 200°C to 300°C at atmosphere is selected for the computational prediction due to the stabilizing activity and selectivity of the Pt catalyst. By combining tested catalyst

performance, measured transport properties of the material and hypothetical membrane configuration, it is proven that adding one membrane separation unit between two packed-beds (membrane assisted packed-bed reactor), the thermodynamic barrier of the reaction can be broken by the removal of  $H_2$ . The overall conversion can be increased by up to 20%, beyond the equilibrium.

Finally, integrally skinned asymmetric Matrimid/PBI blend membrane has been prepared by phase inversion for the experimental validation. The membranes demonstrates favorable  $H_2$  permeance and  $H_2/N_2$  selectivity. Viable membranes are utilized as a separation unit in the membrane-assisted packed-bed reactor. The dehydrogenation of methylcyclohexane is carried out in the reactor at ambient pressure from 175°C to 275°C. The membrane chamber is maintained at the same temperature with the packed-beds. The equilibrium conversions at 175°C, 200°C and 225°C are all partially exceeded in the dehydrogenation. This indicated the successful removal of  $H_2$  by the blend membrane, as well as the good thermal stability of the membrane at these temperatures with the presence of hydrocarbons. However, the equilibrium conversion at 250°C is not exceeded possibly due to the mechanical failure of the membrane substructure at certain temperature.

The positive preliminary results of the model dehydrogenation reaction indicates the potential of utilizing the membrane-assisted reactor system in practical industrial processes. First, the Matrimid/PBI blend material is capable of separating  $H_2$  from the hydrocarbons at elevated temperatures while maintaining stable. The intrinsically skinned asymmetric membrane has displayed great capacity in  $H_2$  separation in MCH dehydrogenation to break the thermodynamic barrier. The simple addition of membrane separation unit can be adapted to existing equipment. For particular reactions, like the dehydrogenation of MCH, the thermally stable Matrimid/PBI membrane can operate at the reaction temperature, which means it requires no extra heating or

cooling device. Therefore, it is a highly efficient system. The membrane-assisted reactor model can be utilized in various thermodynamically prohibited dehydrogenation reactions to improve conversion and catalytic selectivity.



## 9.2 Future Work

This study focused on the development of a system for the selective dehydrogenation of methylcyclohexane to form toluene in a membrane-assisted reactor. A catalyst capable of the selective dehydrogenation of MCH was identified. Yet, at temperatures above 300 °C, the catalytic selectivity was reduced to lost. Unfortunately, operation at 300 °C and 1 bar system pressure resulted in a conversion of only about 60%. Thus, the need for selective product removal to allow for higher conversion at the low operating temperature. This study found that at system temperatures in the 175-275 °C range, the incorporation of a hydrogen selective membrane allowed for the overall conversion to exceed that of the conventional system. Nevertheless, further improvements of the system will be required. I recommend the following modification be made to the laboratory system to allow for a more complete collection of data to support future design.

For the 3-phase membrane contactor in the MCH dehydrogenation study, potential future study includes:

1. Design and incorporation of sensors that will allow for the measurement of stream composition and flow for the individual process streams entering and leaving the membrane unit (one feed stream, and two product streams). In this way, the actual operating efficiency of the membrane can be measured. This will provide membrane fluxes and selectivities measured under operating conditions that can be used to more precisely predict the performance of industrial-scale systems.
2. Operation of the integrated system at a stable condition (perhaps 227° C and 1 bar) for an extended period to gain insight into the stability of the membrane in this integrated system. To date, due to the complexity of completing the experimental measurements, the

longest any membrane has been held at temperature within the integrated system was approximately two days. While no change in performance was observed during this testing, the period of study is short and is not likely to capture any slow chemical or mechanical changes occurring within the membrane or any deleterious effect of hydrogen removal might have on catalyst performance. To gain an appreciation for the potential challenges presented, the integrated system should be operated at elevated temperature for an extended period. At a minimum, the system should be operated for 14 days. Longer operation would be preferred. While it is impractical to operate these systems in the laboratory for the periods that they would be expected to operate in the field, these multi-week evaluations could provide insight into the stability of the integrated system. Following these tests, it is recommended to complete surface analysis on the catalyst in the beds prior to and following the membrane unit. Any differences in the level of carbon deposition might be related to the removal of hydrogen achieved by the membrane.

3. Exploit the potential of the Matrimid/PBI blend membrane materials at even higher temperature (up to 400°C). Thermal evaluation of the bulk polymeric materials indicates that they are chemically stable (i.e., demonstrate no weight loss during heating in either nitrogen or air) until approximately 400 °C. Unfortunately, in this study, the membrane performance was negatively impacted by heating to only 250°C. Post-mortem evaluation indicates that the membrane material was not chemically changed by this thermal exposure. Further, the polymer blends themselves were showed no instabilities up to 300°C. Thus, it appears that the highly microporous substructure of the polymeric membrane collapsed as the temperature was increased and the mechanical modulus was reduced. To overcome these limitations and exploit the polymer blends at higher temperatures, it is recommended that future studies include the development of polymer-

ceramic composite membranes. In this composite membrane form, the responsibilities for selective separation are formally split from those of ensuring mechanical stability and minimal transport resistance in the substrate layer. Indeed, the Matramid/PBI blend would be used as a thin, defect-free polymer film supported on a highly permeable nanoporous ceramic support. The larger mechanical modulus of the ceramic support will allow the system to be operated at temperatures beyond those studied in the current work.

4. In-depth investigation of breaking the equilibrium limit of alkane dehydrogenation at system pressures beyond 1 bar. The relationship between operating pressure and membrane/reactor efficiency observation from Figure 61 shows that operating at elevated pressure might become economically beneficial at the industrial level despite the decrease in equilibrium conversion. This draws an interesting topic about the balance between the theoretical consideration of thermodynamic and the practical considerations of efficient and effective operation in industrial process. Further experimental studies and a detailed economic evaluation should be completed to ascertain the potential advantages and disadvantages of operation of the combined membrane reactor system at elevated pressure. One interesting application for such a higher pressure (and conversely lower volume) system would be the on-board dehydrogenation of MCH with subsequent separation of toluene and hydrogen. The hydrogen would be used to fuel an on-vehicle fuel cell while the toluene would be stored in a second “product” tank. Once the MCH was depleted, the vehicle would be taken to a service station. There, the toluene would be off-loaded for re-hydrogenation at a large-scale, efficient system. Finally, before leaving the service station, the vehicle would refueled with MCH. This cycle would be repeated to provide energy for a hydrogen-powered vehicle fleet. While there are multiple technical challenges to overcome before such a system would be commercially viable,

the ability to completely and efficiently dehydrogenate the MCH and separate the produced hydrogen in a small on-vehicle system is a key technical milestone that would promote overall system success. Thus, work that focuses on optimizing the membrane dehydrogenation system at elevated pressure would be highly impactful.

## References

1. Koros, W.; Ma, Y.; Shimidzu, T. Terminology for membranes and membrane processes (IUPAC Recommendations 1996). *Pure and Applied Chemistry* 1996, 68, 1479-1489.
2. Gallucci, F.; Basile, A.; Hai, F. I. Introduction—a review of membrane reactors. *Membranes for Membrane Reactors: Preparation, optimization and selection* 2011, 1-61.
3. Drioli, E.; Fontananova, E.; Bonchio, M.; Carraro, M.; Gardan, M.; Scorrano, G. Catalytic Membranes and Membrane Reactors: An Integrated Approach to Catalytic Process with a High Efficiency and a Low Environmental Impact. *Chinese Journal of Catalysis* 2008, 29, 1152-1158.
4. Vital, J.; Sousa, J. M. Polymeric membranes for membrane reactors. In *Handbook of Membrane Reactors*; Basile, A., Ed.; Woodhead Publishing: 2013; Vol. 1, pp 3-41.
5. George, S. C.; Thomas, S. Transport phenomena through polymeric systems. *Progress in Polymer Science* 2001, 26, 985-1017.
6. Wijmans, J. G.; Baker, R. W. The solution-diffusion model: a review. *J. Membr. Sci.* 1995, 107, 1-21.
7. Tanh Jeazet, H. B.; Staudt, C.; Janiak, C. Metal-organic frameworks in mixed-matrix membranes for gas separation. *Dalton Trans.* 2012, 41, 14003-14027.
8. Stannett, V. The transport of gases in synthetic polymeric membranes — an historic perspective. *J. Membr. Sci.* 1978, 3, 97-115.
9. Department of Energy 2016 Billion-Ton Report: Advancing Domestic Resources for a Thriving Bioeconomy, Volume 1: Economic Availability of Feedstocks. Oak Ridge National Laboratory, Oak Ridge, TN. 2016.
10. [www.eia.gov](http://www.eia.gov) Primary energy production by source. 2018.
11. [www.eia.gov](http://www.eia.gov) Renewable Energy Production and Consumption. 2018.
12. Wenzel, H. Breaking the biomass bottleneck of the fossil free society. *Breaking the biomass bottleneck of the fossil free society. CONCITO, 2010* 2010.
13. Hicks, J. C. Advances in C-O Bond Transformations in Lignin-Derived Compounds for Biofuels Production. *J. Phys. Chem. Lett.* 2011, 2, 2280-2287.
14. Elliott, D. C. Historical Developments in Hydroprocessing Bio-oils. *Energy Fuels* 2007, 21, 1792-1815.

15. Mortensen, P. M.; Grunwaldt, J. D.; Jensen, P. A.; Knudsen, K. G.; Jensen, A. D. A review of catalytic upgrading of bio-oil to engine fuels. *Applied Catalysis A: General* 2011, *407*, 1-19.
16. Bridgwater, A. V.; Peacocke, G. V. C. Fast pyrolysis processes for biomass. *Renewable and Sustainable Energy Reviews* 2000, *4*, 1-73.
17. Czernik, S.; Bridgwater, A. V. Overview of Applications of Biomass Fast Pyrolysis Oil. *Energy Fuels* 2004, *18*, 590-598.
18. Zhang, Q.; Chang, J.; Wang, T.; Xu, Y. Review of biomass pyrolysis oil properties and upgrading research. *Energy Conversion and Management* 2007, *48*, 87-92.
19. de Miguel Mercader, F.; Groeneveld, M. J.; Kersten, S. R. A.; Way, N. W. J.; Schaverien, C. J.; Hogendoorn, J. A. Production of advanced biofuels: Co-processing of upgraded pyrolysis oil in standard refinery units. *Applied Catalysis B: Environmental* 2010, *96*, 57-66.
20. Bridgwater, A. V. Review of fast pyrolysis of biomass and product upgrading. *Biomass and Bioenergy* 2012, *38*, 68-94.
21. Elliott, D. C. Transportation fuels from biomass via fast pyrolysis and hydroprocessing. *Wiley Interdisciplinary Reviews: Energy and Environment* 2013, *2*, 525-533.
22. Elliott, D. C.; Hart, T. R.; Neuenschwander, G. G.; Rotness, L. J.; Zacher, A. H. Catalytic hydroprocessing of biomass fast pyrolysis bio-oil to produce hydrocarbon products. *Environmental Progress & Sustainable Energy* 2009, *28*, 441-449.
23. Department of Energy Production of gasoline and diesel from biomass via fast pyrolysis, hydrotreating and hydrocracking a design case. Pacific Northwest National Laboratory, Richland, WA.
24. Ardiyanti, A. R.; Khromova, S. A.; Venderbosch, R. H.; Yakovlev, V. A.; Melián-Cabrera, I. V.; Heeres, H. J. Catalytic hydrotreatment of fast pyrolysis oil using bimetallic Ni–Cu catalysts on various supports. *Applied Catalysis A: General* 2012, *449*, 121-130.
25. Dittmeyer, R.; Svajda, K.; Reif, M. A Review of Catalytic Membrane Layers for Gas/Liquid Reactions. *Topics in Catalysis* 2004, *29*, 3-27.
26. Stanford, J. P. Development and characterization of noble metal integrated polymeric membrane reactors for three-phase hydrogenation reactions, Kansas State University, 2016.
27. Johnson, R. O.; Burlhis, H. S. Polyetherimide: A new high-performance thermoplastic resin. *Journal of Polymer Science: Polymer Symposia* 1983, *70*, 129-143.
28. Seifert, B.; Mihanetzis, G.; Groth, T.; Albrecht, W.; Richau, K.; Missirlis, Y.; Paul, D.; Von Sengbusch, G. Polyetherimide: A New Membrane-Forming Polymer for Biomedical Applications. *Artif. Organs* 2002, *26*, 189-199.

29. Brandrup, J.; Immergut, E. H.; Grulke, E. A. *Polymer handbook*; New York : Wiley: New York, 1999; .
30. Biron, M. *Thermoplastics and Thermoplastic Composites* (2nd Edition). 2013.
31. Baker, R. W. *Membrane Technology and Applications*; Wiley: 2004; .
32. Pinnau, I.; Freeman, B. D. Formation and Modification of Polymeric Membranes: Overview. In *Membrane Formation and Modification* American Chemical Society: 1999; Vol. 744, pp 1-22.
33. Strathmann, H.; Giorno, L.; Piacentini, E.; Drioli, E. 1.4 Basic Aspects in Polymeric Membrane Preparation. *Comprehensive Membrane Science and Engineering* 2017, 65.
34. Peinemann, K. US Patenta 4673418, 1987.
35. Czichos, H.; Saito, T.; Smith, L. *Springer handbook of materials measurement methods*; Springer Berlin: 2006; Vol. 978.
36. Singh, D.; Rezac, M. E.; Pfromm, P. H. Partial hydrogenation of soybean oil using metal-decorated integral-asymmetric polymer membranes: Effects of morphology and membrane properties. *J. Membr. Sci.* 2010, 348, 99-108.
37. Pétursson Sigthór Clarification and expansion of formulas in AOCS recommended practice Cd 1c - 85 for the calculation of Iodine value from FA composition. *J Amer Oil Chem Soc* 2002, 79, 737-738.
38. Singh, D.; Rezac, M. E.; Pfromm, P. H. Partial Hydrogenation of Soybean Oil with Minimal Trans Fat Production Using a Pt-Decorated Polymeric Membrane Reactor. *J. Am. Oil Chem. Soc.* 2009, 86, 93-101.
39. Singh, D.; Pfromm, P. H.; Rezac, M. E. Overcoming mass-transfer limitations in partial hydrogenation of soybean oil using metal-decorated polymeric membranes. *AIChE J.* 2011, 57, 2450-2457.
40. Oasmaa, A.; Meier, D. Norms and standards for fast pyrolysis liquids: 1. Round robin test. *Journal of Analytical and Applied Pyrolysis* 2005, 73, 323-334.
41. Young, M. J.; Pfromm, P. H.; Rezac, M. E.; Law, B. M. Analysis of Atomic Force Microscopy Phase Data To Dynamically Detect Adsorbed Hydrogen under Ambient Conditions. *Langmuir* 2014, 30, 11906-11912.
42. Baker, R. W. *Membrane technology and applications*; 2004; .

43. Itoh, N. Membrane reactors for the dehydrogenation of alkanes to alkenes. In *Membrane Reactors for Energy Applications and Basic Chemical Production*; Basile, A., Paola, L. D., Hai, F. I., and Piemonte, V., Eds.; Woodhead Publishing: 2015; pp 491-518.
44. Beccari, M.; Romano, U. Vol. II, Refining and petrochemicals. In *Encyclopaedia of hydrocarbons* 2006; .
45. Perry, R. H.; Green, D. W. *Perry's Chemical Engineers' Handbook*. McGraw-Hill,: New York :, 2008; .
46. Mulder, M. Membrane Processes. In *Basic Principles of Membrane Technology*; Mulder, M., Ed.; Springer Netherlands: Dordrecht, 1996; pp 280-415.
47. Koros, W. J.; Mahajan, R. Pushing the limits on possibilities for large scale gas separation: which strategies? *J. Membr. Sci.* 2000, 175, 181-196.
48. Yampolskii, Y. Polymeric Gas Separation Membranes. *Macromolecules* 2012, 45, 3298-3311.
49. Brandrup, J.; Immergut, E. H.; Grulke, E. A. *Polymer Handbook, 4th Edition*; Wiley: 1999; .
50. Schulte, L. Blending high performance polymers for improved stability in integrally skinned asymmetric gas separation membranes, Kansas State University, 2015.
51. Ghosal, K.; Freeman, B. D. Gas separation using polymer membranes: an overview. *Polym. Adv. Technol.* 1994, 5, 673-697.
52. Costello, L. M.; Koros, W. J. Temperature dependence of gas sorption and transport properties in polymers: measurement and applications. *Ind Eng Chem Res* 1992, 31, 2708-2714.
53. Chung, T.; Guo, W. F.; Liu, Y. Enhanced Matrimid membranes for pervaporation by homogenous blends with polybenzimidazole (PBI). *J. Membr. Sci.* 2006, 271, 221-231.
54. Peter, J.; Peinemann, K. -. Multilayer composite membranes for gas separation based on crosslinked PTMSP gutter layer and partially crosslinked Matrimid® 5218 selective layer. *Journal of Membrane Science* 2009, 340, 62-72.
55. Sanders, D. F.; Smith, Z. P.; Guo, R.; Robeson, L. M.; McGrath, J. E.; Paul, D. R.; Freeman, B. D. Energy-efficient polymeric gas separation membranes for a sustainable future: A review. *Polymer* 2013, 54, 4729-4761.
56. Shishatskiy, S.; Nistor, C.; Popa, M.; Nunes, S. P.; Peinemann, K. Comparison of asymmetric and thin-film composite membranes having Matrimid 5218 selective layer. *Desalination* 2006, 199, 193-194.



57. David, O. C.; Gorri, D.; Urtiaga, A.; Ortiz, I. Mixed gas separation study for the hydrogen recovery from H<sub>2</sub>/CO/N<sub>2</sub>/CO<sub>2</sub> post combustion mixtures using a Matrimid membrane. *Journal of Membrane Science* 2011, 378, 359-368.
58. Zhang, H.; Li, X.; Zhao, C.; Fu, T.; Shi, Y.; Na, H. Composite membranes based on highly sulfonated PEEK and PBI: Morphology characteristics and performance. *Journal of Membrane Science* 2008, 308, 66-74.
59. Chung, T. -. A critical review of polybenzimidazoles: Historical development and future R&D. *J Macromol Sci Rev Macromol Chem Phys* 1997, 37, 277-301.
60. Robeson, L. M. The upper bound revisited. *J. Membr. Sci.* 2008, 320, 390-400.
61. Qiu, S. Preparation and characterization of Matrimid/P84 blend films, Kansas State University, 2015.
62. Chung, T.; Xu, Z. Asymmetric hollow fiber membranes prepared from miscible polybenzimidazole and polyetherimide blends. *Journal of Membrane Science* 1998, 147, 35-47.
63. Kung, G.; Jiang, L. Y.; Wang, Y.; Chung, T. Asymmetric hollow fibers by polyimide and polybenzimidazole blends for toluene/iso-octane separation. *J. Membr. Sci.* 2010, 360, 303-314.
64. Hosseini, S. S.; Teoh, M. M.; Chung, T. S. Hydrogen separation and purification in membranes of miscible polymer blends with interpenetration networks. *Polymer* 2008, 49, 1594-1603.
65. Costello, L. M.; Walker, D. R. B.; Koros, W. J. Analysis of a thermally stable polypyrrolone for high temperature membrane-based gas separations. *J. Membr. Sci.* 1994, 90, 117-130.
66. Costello, L. M.; Koros, W. J. Thermally stable polyimide isomers for membrane-based gas separations at elevated temperatures. *Journal of Polymer Science Part B: Polymer Physics* 1995, 33, 135-146.
67. Usman, M. R. The Catalytic Dehydrogenation of Methylcyclohexane over Monometallic Catalysts for On-board Hydrogen Storage, Production, and Utilization. *Energy Sources, Part A: Recovery, Utilization, and Environmental Effects* 2011, 33, 2231-2238.
68. Sinfelt, J. H.; Hurwitz, H.; Shulman, R. A. Kinetics of Methylcyclohexane Dehydrogenation over Pt/Al<sub>2</sub>O<sub>3</sub>. *J. Phys. Chem.* 1960, 64, 1559-1562.
69. Sinfelt, J. The turnover frequency of methylcyclohexane dehydrogenation to toluene on a Pt reforming catalyst. *J. Mol. Catal. A-Chem.* 2000, 163, 123-128.

70. Wang, Y.; Shah, N.; Huffman, G. P. Pure Hydrogen Production by Partial Dehydrogenation of Cyclohexane and Methylcyclohexane over Nanotube-Supported Pt and Pd Catalysts. *Energy Fuels* 2004, 18, 1429-1433.
71. Wolf, E. E.; Petersen, E. E. Kinetics of deactivation of a reforming catalyst during methylcyclohexane dehydrogenation in a diffusion reactor. *Journal of Catalysis* 1977, 46, 190-203.
72. Tarasov, B. P.; Lototskii, M. V.; Yartysâ€™™, V. A. Problem of hydrogen storage and prospective uses of hydrides for hydrogen accumulation. *Russian Journal of General Chemistry* 2007, 77, 694-711.
73. Yolcular, S.; Olgun, Ö Hydrogen Storage in the Form of Methylcyclohexane. *Energy Sources, Part A: Recovery, Utilization, and Environmental Effects* 2007, 30, 149-156.
74. Alhumaidan, F.; Cresswell, D.; Garforth, A. Hydrogen Storage in Liquid Organic Hydride: Producing Hydrogen Catalytically from Methylcyclohexane. *Energy Fuels* 2011, 25, 4217-4234.
75. Schildhauer, T.; Newson, E.; Müller, S. The Equilibrium Constant for the Methylcyclohexane–Toluene System. *Journal of Catalysis* 2001, 198, 355-358.
76. Usman, M. R.; Cresswell, D. L.; Garforth, A. A. Dehydrogenation of methylcyclohexane: parametric sensitivity of the power law kinetics. *ISRN Chemical Engineering* 2013, 2013.
77. Ali, J. K.; Rippin, D. W. T.; Baiker, A. Improving Methylcyclohexane Dehydrogenation with ex-Situ Hydrogen Separation in a Reactor-Interstaged Membrane System. *Ind Eng Chem Res* 1995, 34, 2940-2948.
78. Rezac, M. E.; Koros, W. J.; Miller, S. J. Membrane-assisted dehydrogenation of n-butane influence of membrane properties on system performance. *J. Membr. Sci.* 1994, 93, 193-201.
79. Ferreira-Aparicio, P.; Rodriguez-Ramos, I.; Guerrero-Ruiz, A. On the Performance of Porous Vycor Membranes for Conversion Enhancement in the Dehydrogenation of Methylcyclohexane to Toluene. *Journal of Catalysis* 2002, 212, 182-192.
80. Meng, L.; Yu, X.; Niimi, T.; Nagasawa, H.; Kanezashi, M.; Yoshioka, T.; Tsuru, T. Methylcyclohexane dehydrogenation for hydrogen production via a bimodal catalytic membrane reactor. *AIChE J.* 2015, 61, 1628-1638.
81. Meng, L.; Tsuru, T. Hydrogen production from energy carriers by silica-based catalytic membrane reactors. *Catalysis Today* 2016, 268, 3-11.
82. Niimi, T.; Nagasawa, H.; Kanezashi, M.; Yoshioka, T.; Ito, K.; Tsuru, T. Preparation of BTESE-derived organosilica membranes for catalytic membrane reactors of methylcyclohexane dehydrogenation. *J. Membr. Sci.* 2014, 455, 375-383.

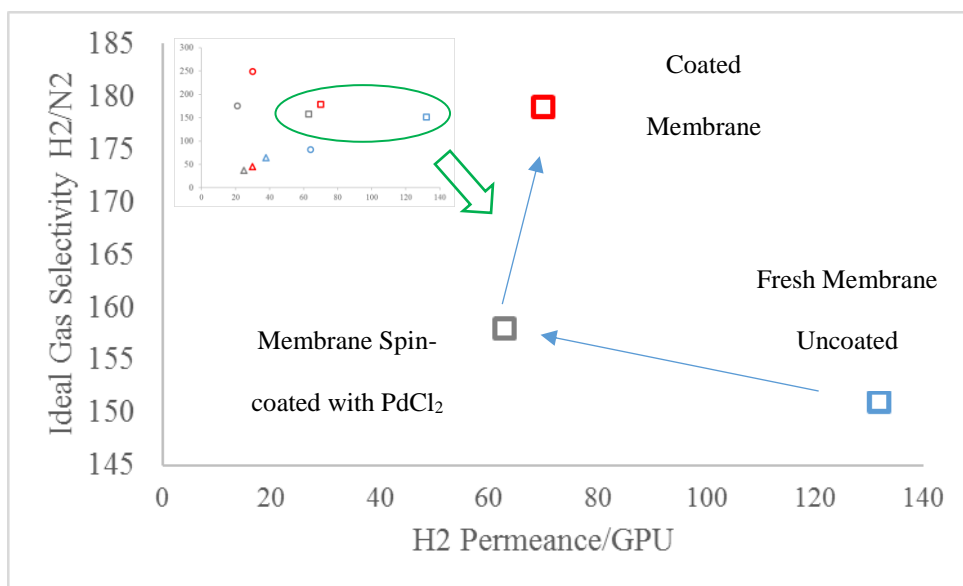
83. Oda, K.; Akamatsu, K.; Sugawara, T.; Kikuchi, R.; Segawa, A.; Nakao, S. Dehydrogenation of Methylcyclohexane To Produce High-Purity Hydrogen Using Membrane Reactors with Amorphous Silica Membranes. *Ind Eng Chem Res* 2010, *49*, 11287-11293.
84. Hirota, Y.; Ishikado, A.; Uchida, Y.; Egashira, Y.; Nishiyama, N. Pore size control of microporous carbon membranes by post-synthesis activation and their use in a membrane reactor for dehydrogenation of methylcyclohexane. *J. Membr. Sci.* 2013, *440*, 134-139.
85. Ali, J. K.; Newson, E. J.; Rippin, D. W. T. Exceeding equilibrium conversion with a catalytic membrane reactor for the dehydrogenation of methylcyclohexane. *Chemical Engineering Science* 1994, *49*, 2129-2134.
86. Ali, J. K.; Baiker, A. Dehydrogenation of methylcyclohexane to toluene in a pilot-scale membrane reactor. *Applied Catalysis A: General* 1997, *155*, 41-57.
87. Ali, J. K.; Rippin, D. W. T. Comparing Mono- and Bimetallic Noble-Metal Catalysts in a Catalytic Membrane Reactor for Methylcyclohexane Dehydrogenation. *Ind Eng Chem Res* 1995, *34*, 722-729.
88. Ferreira-Aparicio, P.; Rodriguez-Ramos, I.; Guerrero-Ruiz, A. Pure hydrogen production from methylcyclohexane using a new high performance membrane reactor. *Chem. Commun.* 2002, 2082-2083.
89. Itoh, N. Maximum conversion of dehydrogenation in palladium membrane reactors. *J. Chem. Eng. Japan* 1991, *24*, 664-666.
90. Lai, J.; Tung, K.; Lee, D.; Wang, D.; Itoh, N.; Watanabe, S.; Kawasoe, K.; Sato, T.; Tsuji, T. The Fourth Conference of Aseanian Membrane Society: Part 2 A membrane reactor for hydrogen storage and transport system using cyclohexane–methylcyclohexane mixtures. *Desalination* 2008, *234*, 261-269.
91. Namboodhiri, T. Hydrogen embrittlement of metallic materials. *Transactions of the Indian Institute of Metals* 1984, *37*, 764-793.
92. Hatim, M. D. I.; Fazara, M. A. U.; Syarhabil, A. M.; Riduwan, F. Catalytic Dehydrogenation of Methylcyclohexane (MCH) to Toluene in a Palladium/Alumina Hollow Fibre Membrane Reactor. *Procedia Engineering* 2013, *53*, 71-80.
93. Kluiters, S. Status review on membrane systems for hydrogen separation. *Energy Center of the Netherlands, Petten, The Netherlands* 2004.
94. Gallucci, F.; Fernandez, E.; Corengia, P.; van Sint Annaland, M. Recent advances on membranes and membrane reactors for hydrogen production. *Chemical Engineering Science* 2013, *92*, 40-66.
95. Adhikari, S.; Fernando, S. Hydrogen membrane separation techniques. *Ind Eng Chem Res* 2006, *45*, 875-881.

96. Rezac, M. E.; Koros, W. J.; Miller, S. J. Thermomechanical Stability of Polymer—Ceramic Composite Membranes. *Sep. Sci. Technol.* 1995, 30, 2159-2171.
97. Rezac, M. E.; Moore, N. S.; Back, A. Effect of Temperature on the Transport Properties and Morphology of Polymeric Asymmetric Membranes. *Sep. Sci. Technol.* 1997, 32, 505-525.
98. Zhu, L.; Swihart, M. T.; Lin, H. Tightening polybenzimidazole (PBI) nanostructure via chemical cross-linking for membrane H<sub>2</sub>/CO<sub>2</sub> separation. *J. Mater. Chem. A* 2017, 5, 19914-19923.
99. Vanherck, K.; Koeckelberghs, G.; Vankelecom, I. F. J. Crosslinking polyimides for membrane applications: A review. *Progress in Polymer Science* 2013, 38, 874-896.
100. Rezac, M. E.; Koros, W. J.; Miller, S. J. Membrane-Assisted Dehydrogenation of Normal Butane. *Ind Eng Chem Res* 1995, 34, 862-868.
101. Rezac, M. E.; Koros, W. J. Preparation of polymer—ceramic composite membranes with thin defect-free separating layers. *J Appl Polym Sci* 1992, 46, 1927-1938.
102. <https://www.chiyodacorp.com/jp/> Advanced Hydrogen Energy Chain Association for Technology Development.

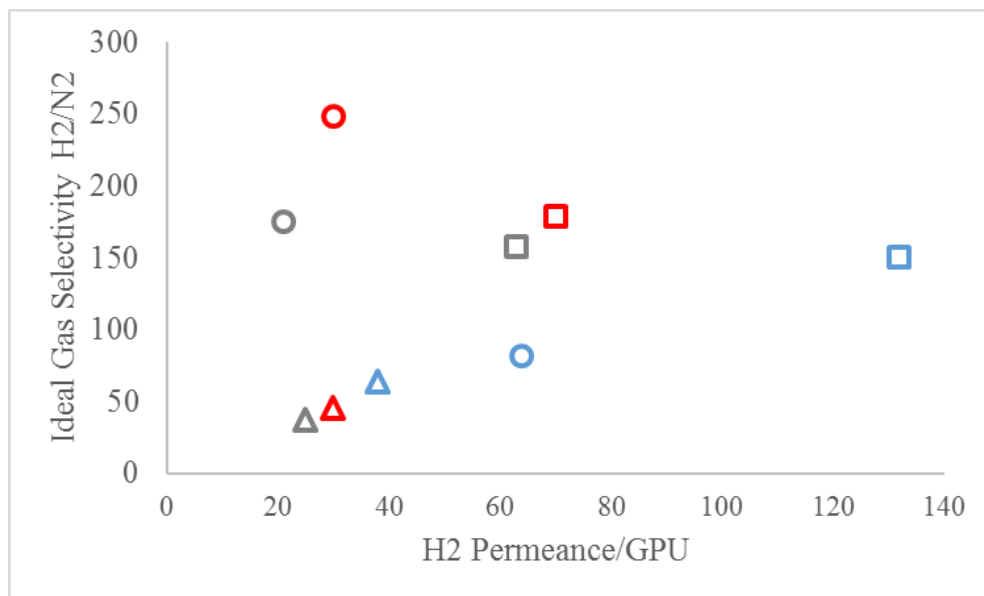
## Appendix A - Spin Coated PEI Membranes

Figure A-1 and A-2 show the transport properties of PEI membranes with catalyst spin-coated.

The membrane was spin-coated with  $\text{PdCl}_2$  solution and then reduced by  $\text{H}_2$ .



**Figure A-1 Change in Flux and H<sub>2</sub>/N<sub>2</sub> Selectivity of a PEI Membrane; Blue: Nascent Membrane, Grey: Spin Coated with PdCl<sub>2</sub>, Red: Reduced in H<sub>2</sub>**



**Figure A-2 Examples of Membranes with Catalyst Spin Coated. Different colors represent different stages of the membrane. Blue: nascent; grey: sputter-coated with catalyst Pd; red: Reduced in H<sub>2</sub> after coated with catalyst.**

## Appendix B - Calibration Curve

Figure C-1 show an example of a calibration curve based on the peak area of methylcyclohexane.

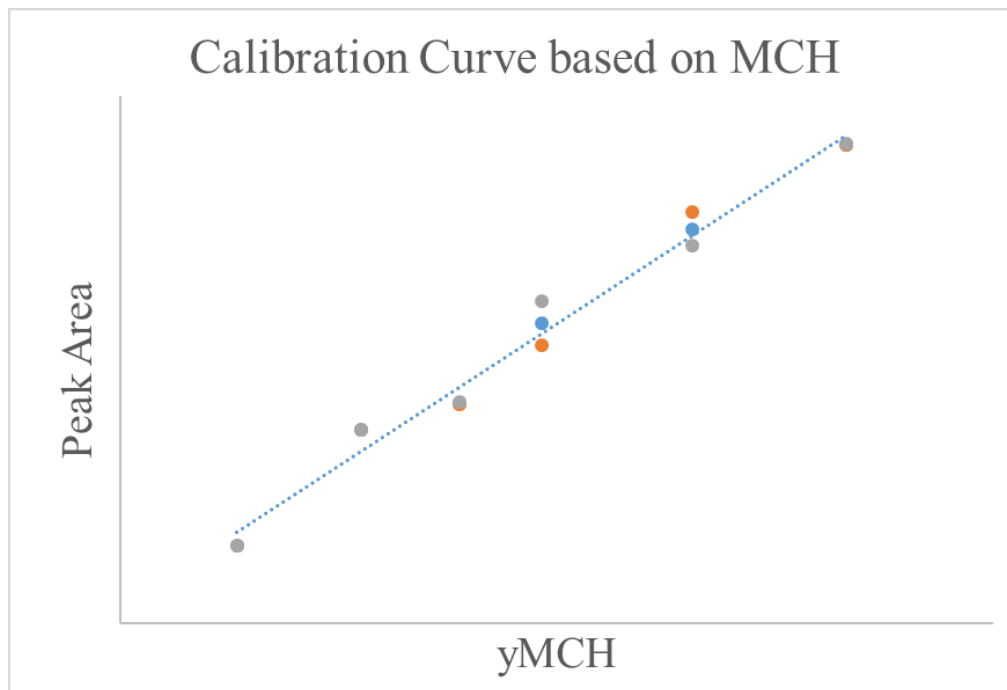


**Figure C-1 Calibration Curve**

## Appendix C - GC Spectra of Typical Product Composition in the Dehydrogenation of Methylcyclohexane



**Figure D-1 An Example of a GC Spectrum of a Sample Taken during the  
Dehydrogenation. Peak on left: Methylcyclohexane; Peak on right: Toluene**



## Appendix D – Conversion Factors for Gas Permeance

**Table F-1 Conversion Factors for Gas Permeance**<sup>42</sup>

Given a quantity in these units	Multiply by value below to convert to corresponding units					
	$1 \times 10^{-6} \text{ cm}^3(\text{STP})/\text{cm}^2 \cdot \text{s} \cdot \text{cmHg}$ (gpu)	L(STP)/m <sup>2</sup> · h · bar	cm <sup>3</sup> (STP)/cm <sup>2</sup> · min · bar	scf/m <sup>2</sup> · min · bar	mol/m <sup>2</sup> · s · Pa	mol/m <sup>2</sup> · h · bar
$1 \times 10^{-6} \text{ cm}^3(\text{STP})/\text{cm}^2 \cdot \text{s} \cdot \text{cmHg}$ (gpu)	1	2.7	$4.5 \times 10^{-3}$	$1.589 \times 10^{-3}$	$3.348 \times 10^{-10}$	0.1205
L(STP)/m <sup>2</sup> · h · bar	0.3703	1	$1.645 \times 10^{-3}$	$0.5808 \times 10^{-3}$	$1.224 \times 10^{-10}$	$4.404 \times 10^{-2}$
cm <sup>3</sup> (STP)/cm <sup>2</sup> · min · bar	$0.2222 \times 10^3$	$0.6079 \times 10^3$	1	0.3530	$0.7439 \times 10^{-7}$	26.78
scf/m <sup>2</sup> · min · bar	$6.293 \times 10^2$	$1.722 \times 10^3$	2.832	1	$2.107 \times 10^{-7}$	75.83
mol/m <sup>2</sup> · s · Pa	$0.2987 \times 10^{10}$	$0.8172 \times 10^{10}$	$1.344 \times 10^7$	$0.4746 \times 10^7$	1	$3.599 \times 10^8$
mol/m <sup>2</sup> · h · bar	8.299	22.71	$37.35 \times 10^{-3}$	$13.19 \times 10^{-3}$	$27.87 \times 10^{-10}$	1

A 1-μm-thick membrane having a permeability of 1 Barrer has a permeance of 1 gpu.

## Appendix E - Water Accumulation Rate during Bio-oil HDO Run

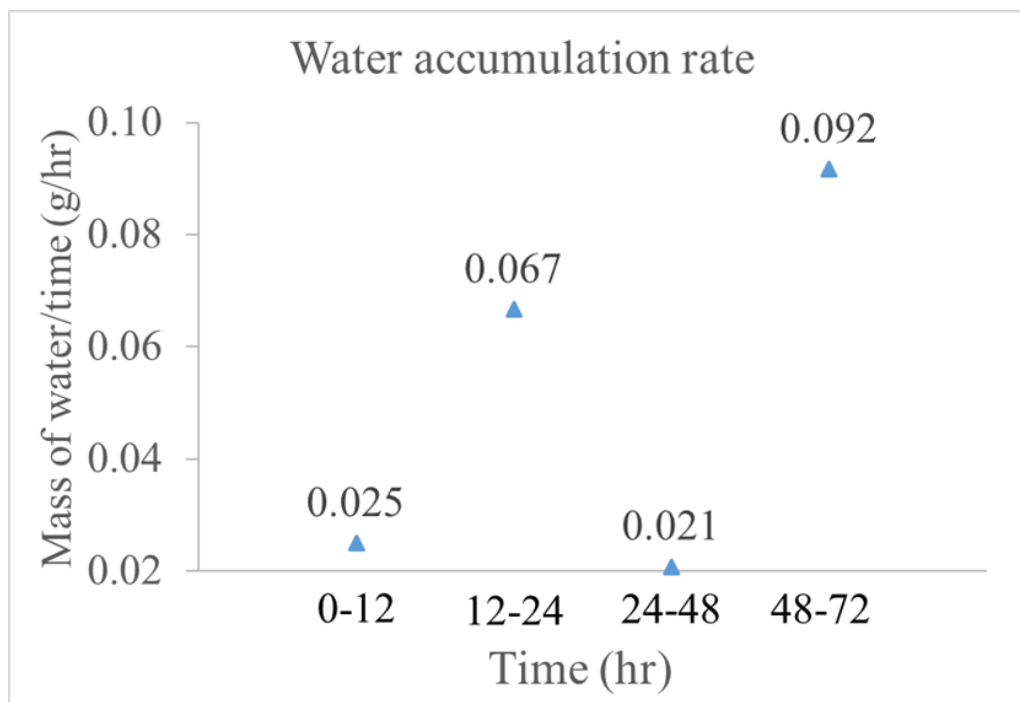


Figure H-1 Water Accumulation Rate during Bio-oil HDO Run